Microprocessor-controlled reluctance motor

MICROPROCESSOR-CONTROLLED RELUCTANCE MOTOR

J.C. Compter

MICROPROCESSOR-CONTROLLED RELUCTANCE MOTOR

J.C. Compter

Microprocessor-controlled reluctance motor

PROEFSCHRIFT

ter verkrijging van de graad van doctor in de technische wetenschappen aan de Technische Hogeschool Eindhoven, op gezag van de rector magnificus, prof. dr. S.T.M. Ackermans, voor een commissie aangewezen door het college van dekanen in het openbaar te verdedigen op vrijdag 4 mei 1984 te 16.00 uur.

door

Johan Cornelis Compter

geboren te 's-Gravenhage

DIT PROEFSCHRIFT IS GOEDGEKEURD
DOOR DE PROMOTOREN

Prof.dr.ir. A.J.C. Bakhuizen

en

Prof.dr.ir. J.G. Niesten

CIP-gegevens

Compter, Johan Cornelis

Microprocessor-controlled reluctance motor / Johan Cornelis Compter.
[S.l. : s.n.]. - Ill. fig., tab.
Proefschrift Eindhoven. - Met lit. opg., reg. ISBN 90-9000644-3
SISO 662.3 UDC 621.313.292 UGI 650
Trefw.: reluctantiemotoren.

Aan

Karin

Dankbetuiging

Bij deze wil ik mijn dank uitspreken aan allen die in welke vorm dan ook bijgedragen hebben aan de totstandkoming van dit proefschrift, in het bijzonder aan:

De directie van het Philips Natuurkundig Laboratorium voor de mogelijkheid die mij geboden is dit proefschrift te schrijven en voor al de faciliteiten, welke mij ter beschikking zijn gesteld om deze publicatie te verwezenlijken.

Ing. P. Heijmans voor het realiseren van de meetopstelling, het uitvoeren van de metingen en het opzetten van vele programma's voor de besturing van de motor.

De heer G. Luton voor het kritisch lezen van de engelse tekst.

Contents

Introduction

This study deals with a brushless electronically controlled single-phase reluctance motor. The motor has a high speed capability, due to its very robust rotor, and requires only one electronic power switch in its control circuitry. The latter feature considerably reduces the cost of production.
Research on polyphase reluctance motors has been done by Prof. Lawrenson et al. (see refs. [1], [2] and [3]). The polyphase operation of these motors, however, entails the use of many electronic power switches in the control circuitry and the cost of these switches is evidently an obstacle to the successful commercial use of polyphase motors in consumer products.
As our study is aimed particularly at the applicability of a reluctance motor in consumer products it concentrates on the single-phase reluctance motor. However the choice of a single-phase motor involves a starting problem and a strongly pulsating torque, which means that the motor is not suitable for applications that require constant torque or speed, as for example in video or audio equipment. Typical applications of this motor are to be found in domestic appliances, and in this area we consider this motor a serious competitor of the widely used A.C. series motor.
To solve the starting problem we use a microprocessor, which also facilitates control of the torque-speed curve over a wide range.

Chapter 1 begins with a qualitative description of the behaviour of the single-phase reluctance motor and discusses the additional components needed. An analytical and a numerical method that can be used to describe the motor are presented in chapter 2, and the results of these methods are compared with the results of the performance measurements on a prototype. Particulars of the control system are discussed in chapter 3. Because of the numerous measurements made necessary by the fact that many input parameters have to be independently varied, the test rig had to be automated, as described in chapter 4. Chapter 5 deals with the electronics of our experimental motors, and aspects of the design of a single-phase reluctance motor are described in chapter 6.

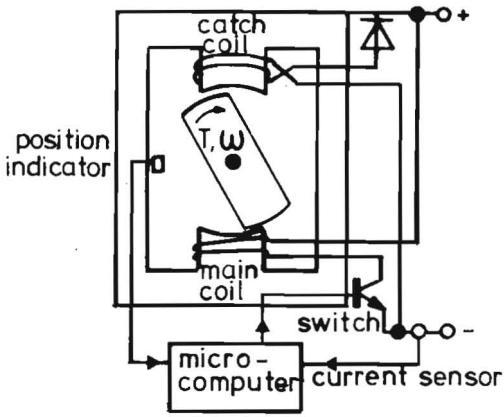

Fig. 1.1.1

Fig. 1.1.1. Principle of the motor and its control.

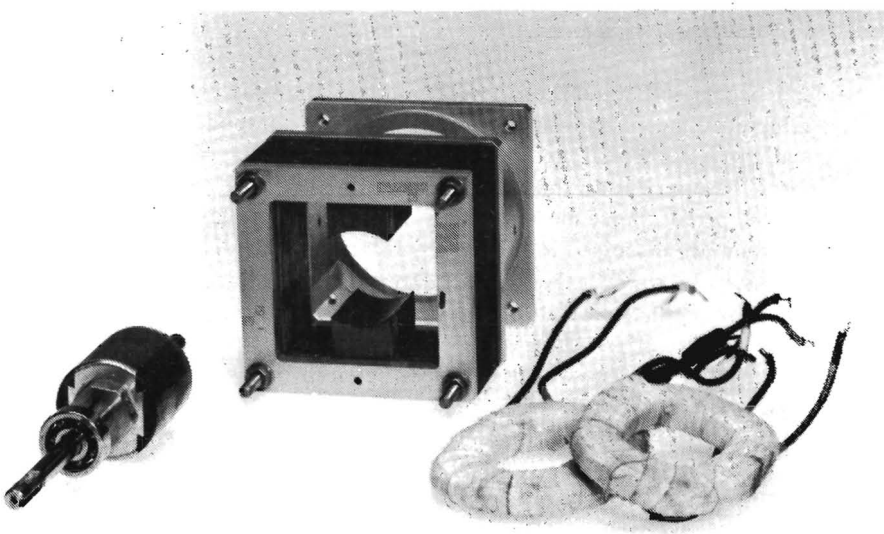

Fig. 1.1.2. The single-phase reluctance motor.

1. Qualitative description of the system

Compared with the A.C. series motor the single-phase reluctance motor has a number of disadvantages, in particular a starting problem and complex control electronics. In this section we give an account of the method used to eliminate the drawbacks.

Fig. 1.1.1 gives the configuration of a single-phase reluctance motor. The rotor consists of a stack of laminated iron, mounted on a shaft. The current through the coils is controlled by just one switch. If either one of the coils carries a current in the situation shown, a torque is developed in the positive direction, producing a motor action.
However when the rotor passes the vertical position, the torque becomes negative. To reduce this negative torque, the switch is opened before the rotor attains the vertical position. The switch is closed again when the rotor is near its horizontal position and so on. This switching action requires a rather sophisticated control system.
This motor unlike other motors requires no reversing of the current within one revolution, because its torque is independent of the polarity of the current. Owing to this characteristic just one switch suffices to control the motor.
It will be clear that torque production is heavily dependent on the rotor positions selected for closing or opening the switch; another important parameter in this respect is the angular velocity, as will be discussed in chapter 2. A switching action with satisfactory efficiency of the motor can be achieved by selecting optimum rotor positions for every torque/speed combination.
Therefore proper control requires accurate information on the position of the rotor at any given moment. This can be obtained from any suitable detector fitted to the shaft. In order to keep the cost of production as low as possible we use a very simple position sensor, which gives two pulses per revolution only. This simple sensor, however, requires some sophistication in the electronic equipment as will be discussed in chapter 3.
An important problem met in this type of motor is the start from standstill. For this purpose two permanent magnets are fitted to the stator, which give the rotor a favourable starting position under conditions we will discuss in chapter 6. Furthermore a special start procedure is implemented in the control unit.

Mainly for reasons of economy, as discussed in chapter 3, the control unit has been built around a microprocessor. For the processor we developed the software to fulfil the following tasks:

- to determine the moment for opening and closing the switch;
- to start the motor;
- to protect the electronic switch against excessively high currents.

The software is designed to work with the simple sensor, providing two pulses per revolution of the shaft.

2. Analysis of the single-phase reluctance motor

2.1. Analytical approach

An analytical description is usually a good way of getting a better understanding of a particular phenomenon.
In this chapter we analyse the electromechanical behaviour of the single-phase reluctance motor with the aim of finding relations between e.g. the average torque of the motor, the motor constants and the control parameters.
The conclusion of this chapter will be that an analytical approach leads to complicated equations, which can only be solved by numerical methods, even though many assumptions are made to simplify the equations. Considering their limited applicability and the existing more flexible, numerical methods, this line will not be pursued. Results of the analytical method, however, are to be used for the verification of subsequent calculations.

Fig. 2.1.1 shows a basic construction of the two-pole reluctance motor, which consists of the stator yoke with coil and the rotor. This system acts as a motor by energizing the coil in such a way that a positive mean value of torque is developed, the positive direction of the torque being defined in the same direction as that of the rotor angle.

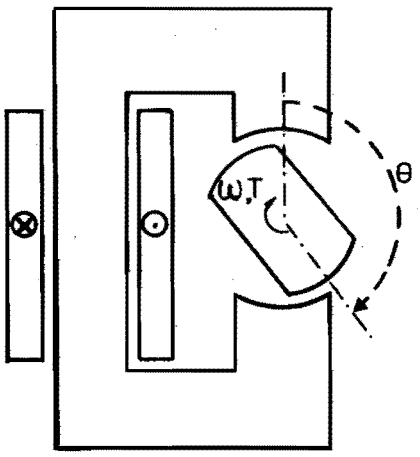

Fig. 2.1.1. Motor provided with one coil.

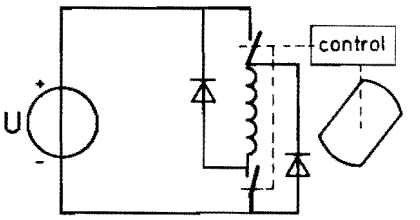

Fig. 2.1.2. The electronic circuit belonging to fig. 2.1.1.

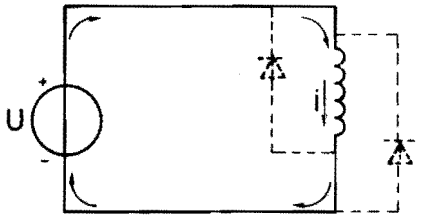

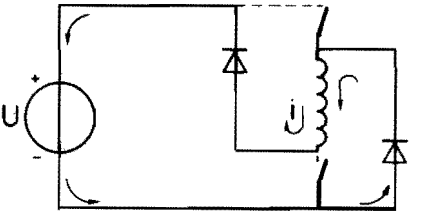

Fig. 2.1.3. Current path, switches closed. *Fig. 2.1.4. Current path, switches open.*

Fig. 2.1.2 shows a circuit that might be used to control the motor. Figs. 2.1.3 and 2.1.4 show the current paths when the switches are closed or open respectively. The main function of the two diodes is to recover the magnetic energy after the switches are opened. Fig. 2.1.5 shows a current versus time diagram.

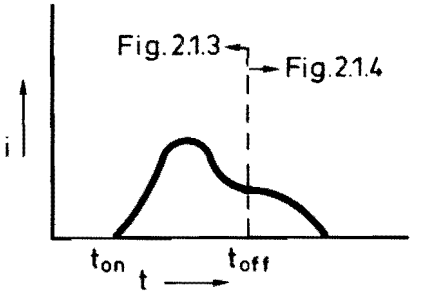

Fig. 2.1.5. The current as a function of time.

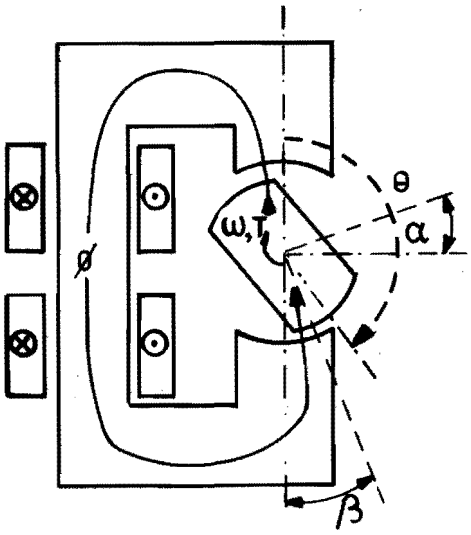

Fig. 2.1.6. The motor provided with two coils. Definition of the angles α and β.

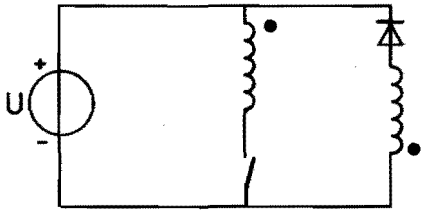

Fig. 2.1.7. The circuit belonging to fig. 2.1.6.

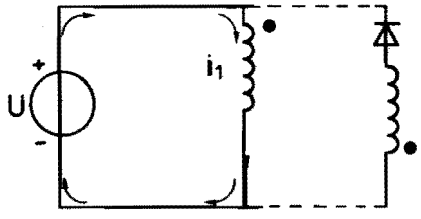

Fig. 2.1.8. Switch closed.

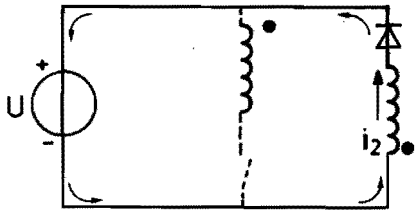

Fig. 2.1.9. Switch open.

An alternative way to control the current is presented by figs. 2.1.6 and 2.1.7. An advantage of this solution is that only one switch and one diode are required, but here we have to provide a second coil on the stator. We call this additional coil the catch coil and the other one the main coil. This catch coil permits the recovery of energy stored in the magnetic field after opening the switch.
The behaviour of both circuits (figs. 2.1.2 and 2.1.7) can be described with similar analytical equations. The following analysis will be based on figures 2.1.6 and 2.1.7. The voltages and currents are defined in figures 2.1.8 and 2.1.9.

In describing the second system we make the following assumptions:
- the rotational speed of the rotor is constant and clockwise;
- the currents carried by the main and the catch coil are periodic;
- there are no eddy currents in the rotor and stator;
- neither saturation nor hysteresis has to be reckoned with in the rotor- and stator iron;
- the two coils wound on the stator have the same number of turns;
- for the inductance of the coils a relation $L(\theta)$ is assumed to be known;
- the mutual inductance between the main and the catch coil is given by $\gamma L(\theta)$;
- the diode and the switch are ideal components.

The meaning of this last assumption is that the resistance of the component equals zero in the conducting state and infinity in the blocking state.

As mentioned before, the control circuit determines when the switch is opened or closed. In the following discussion it is assumed that the switch is closed when:

$$\theta = -\alpha - \pi/2 + k\pi \qquad 2.1.1$$

(see fig. 2.1.6) and opened when:

$$\theta = -\beta + k\pi. \qquad 2.1.2$$

As we are treating the steady-state behaviour of the motor it is sufficient to analyse the performance in the interval:

$$-\pi/2 - \alpha < \theta < \pi/2 - \alpha. \qquad 2.1.3$$

For further analysis we will require information about the initial values of the currents at the moment of the switching actions. At the moment t_{on}, where θ equals $\pi/2$-α, the switch is closed. Suppose that the current through the diode has a value

$$i_2(t_{on}) = i_{20}, \quad \text{with} \quad i_{20} > 0. \qquad 2.1.4$$

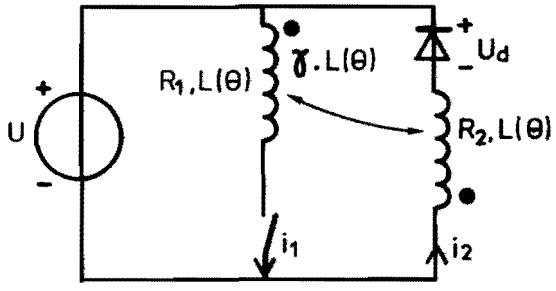

Fig. 2.1.10. The elements of the electrical circuit.

The voltage equations belonging to the network in fig. 2.1.10 are for $t = t_{on}$:

$$U = R_1 i_1 + \frac{d(L i_1)}{dt} + \frac{d(\gamma L i_2)}{dt} \qquad 2.1.5$$

$$U = -R_2 i_2 - \frac{d(L i_2)}{dt} - \frac{d(\gamma L i_1)}{dt} + U_d, \quad \text{with} \quad i_2 > 0. \qquad 2.1.6$$

It holds for $i_2 > 0$, that

$$U_d = 0 \qquad 2.1.7$$

on the assumption of ideal diode behaviour. We are interested in the phenomenon that occurs in the interval ΔT, just after the moment the switch closes. In this case we may write eqs. 2.1.5 and 2.1.6 as:

$$U = R_1 i_1 + \lim_{\Delta T \to 0} \frac{\Delta(L i_1 + \gamma L i_2)}{\Delta T} \qquad 2.1.8$$

$$U = -R_2 i_2 - \lim_{\Delta T \to 0} \frac{\Delta(L i_2 + \gamma L i_1)}{\Delta T}. \qquad 2.1.9$$

For a physical system we are allowed to assume finite values for the currents i_1 and i_2. With this assumption the last two equations give for $\Delta T \to 0$:

$$L i_1 + \gamma L i_2 = \text{continuous} \qquad 2.1.10$$

$$L i_2 + \gamma L i_1 = \text{continuous}. \qquad 2.1.11$$

Further we have:

$$L(t_{on}) = L(t_{on}^{+}) \quad \text{and} \quad i_1(t_{on}) = 0, \tag{2.1.12}$$

with $t_{on}^{+} = t_{on} + \Delta t$.
Combining eqs. 2.1.10 . . . 2.1.12 gives:

$$\gamma\, i_2(t_{on}) = i_1(t_{on}^{+}) + \gamma\, i_2(t_{on}^{+}) \rightarrow \gamma\, i_{20} = i_1(t_{on}^{+}) + \gamma\, i_2(t_{on}^{+}) \tag{2.1.13}$$

$$i_2(t_{on}) = i_2(t_{on}^{+}) + \gamma\, i_1(t_{on}^{+}) \rightarrow i_{20} = i_2(t_{on}^{+}) + \gamma\, i_1(t_{on}^{+}). \tag{2.1.14}$$

When we multiply 2.1.14 by γ, and subtract the result from 2.1.13 we get:

$$0 = i_1(t_{on}^{+}) - \gamma^2 i_1(t_{on}^{+}). \tag{2.1.15}$$

For $\gamma <> 0$ it holds that:

$$i_1(t_{on}^{+}) = 0 \quad \text{and} \quad i_2(t_{on}^{+}) = i_{20}. \tag{2.1.16}$$

Because of their bifilar winding, the two coils on the stator are assumed to be fully coupled magnetically, so in our case we have:

$$\gamma = 1. \tag{2.1.17}$$

A verification of eq. 2.1.17 is given in section 2.3. Addition of eqs. 2.1.8 and 2.1.9 gives:

$$2\,U = R_1\, i_1 - R_2\, i_2. \tag{2.1.18}$$

Together with eqs. 2.1.13 and 2.1.14 this yields:

$$i_1(t_{on}^{+}) = \frac{2\,U + R_2\, i_{20}}{R_1 + R_2} \tag{2.1.19}$$

$$i_2(t_{on}^{+}) = \frac{-2\,U + R_1\, i_{20}}{R_1 + R_2}. \tag{2.1.20}$$

The presence of the diode prevents the current i_2 from going negative. Inspection of eq. 2.1.20 shows that this occurs immediately after the moment the switch is closed, provided that the following condition is satisfied:

$$i_{20} < \frac{2\,U}{R_1}. \tag{2.1.21}$$

Eq. 2.1.13 gives for this case:

$$i_1(t_{on}^+) = i_{20}. \qquad 2.1.22$$

For the protection of the electronic equipment the control was made capable of limiting the currents to a safe value. This value was adjusted such that

$$0 \leqslant i_{20} < \frac{2U}{R_1}, \qquad 2.1.23$$

and consequently

$$i_2(t_{on}^+) = 0 \quad \text{and} \quad i_1(t_{on}^+) = i_{20}. \qquad 2.1.24$$

When the switch opens at t_{off}, following the same line of reasoning it can be shown that

$$i_2(t_{off}^+) = i_1(t_{off}) \qquad 2.1.25$$

and

$$i_1(t_{off}^+) = 0, \qquad 2.1.26$$

which is evident.

Now we know the behaviour of the currents at $t = t_{on}$ and $t = t_{off}$ respectively. This knowledge will be used in the following treatment, where the currents will be analysed for:

$$-\pi/2 - \alpha < \theta < -\beta \quad \text{and} \quad -\beta < \theta < \pi/2 - \alpha. \qquad 2.1.27$$

The switch closes when:

$$\theta = -\pi/2 - \alpha. \qquad 2.1.28$$

The initial condition for the flux linkage is given by

$$\Phi(-\pi/2 - \alpha) = L(-\pi/2 - \alpha)\, i_1(-\pi/2 - \alpha). \qquad 2.1.29$$

We have the following equation for the circuit in fig. 2.1.10 when the switch is closed:

$$U = R_1 i_1 + \frac{d\Phi}{dt}. \qquad 2.1.30$$

Introduction of

$$\omega = \frac{d\theta}{dt} \qquad 2.1.31$$

and

$$d\tau_1 = \frac{R_1}{\omega L}\, d\theta \qquad 2.1.32$$

leads to

$$\frac{U L}{R_1} = \Phi + \frac{d\Phi}{d\tau_1}. \qquad 2.1.33$$

The solution of eq. 2.1.33 is

$$\Phi(\tau_1) = \exp(-\tau_1) \int_0^{\tau_1} \frac{U L}{R_1} \exp(\tau_1')\, d\tau_1' + A \exp(-\tau_1). \qquad 2.1.34$$

Substitution of eq. 2.1.32 into eq. 2.1.34 and use of the initial condition of eq. 2.1.29 gives

$$L(\theta)\, i_1(\theta) = \frac{U}{\omega} \exp(-\tau_1) \int_{-\pi/2-\alpha}^{\theta} \exp(\tau_1(\theta'))\, d\theta' + \qquad 2.1.35$$

$$L(-\pi/2 - \alpha)\, i_1(-\pi/2 - \alpha) \exp(-\tau_1).$$

A good approximation for the inductance $L(\theta)$, based on measurements, is

$$L(\theta) = L_0 + L_2 \cos(2\theta), \quad \text{with} \quad L_2 < L_0. \qquad 2.1.36$$

To reduce the complexity of the following expressions we introduce the dimensionless variable

$$j_1(\theta) = \frac{R_1\, i_1(\theta)}{U} \qquad 2.1.37$$

and the dimensionless parameters

$$r_1 = \frac{R_1}{\omega L_0} \qquad 2.1.38$$

$$g = \frac{L_2}{L_0} \qquad 2.1.39$$

$$\sigma_1(\theta) = \frac{r_1}{(1 - g^2)^{1/2}} \arctan\left\{\left(\frac{1 - g}{1 + g}\right)^{1/2} \tan(\theta)\right\}. \qquad 2.1.40$$

Now eq. 2.1.32 can be written in another form:

$$\tau_1(\theta) = r_1 \int_{-\pi/2-\alpha}^{\theta} \frac{1}{1 + g\cos(2\theta')}\, d\theta' \qquad 2.1.41$$

$$\tau_1(\theta) = \sigma_1(\theta) - \sigma_1(-\pi/2 - \alpha). \qquad 2.1.42$$

Substitution of eq. 2.1.36 into eq. 2.1.35 leads to

$$j_1(\theta) = \frac{r_1 \exp(-\sigma_1(\theta))}{1 + g\cos(2\theta)} \int_{-\pi/2-\alpha}^{\theta} \exp(\sigma_1(\theta'))\, d\theta' + \qquad 2.1.43$$

$$\frac{1 - g\cos(2\alpha)}{1 + g\cos(2\theta)}\, j_1(-\pi/2 - \alpha) \exp(-\tau_1(\theta)).$$

Equation 2.1.43 applies for:

$$-\pi/2 - \alpha < \theta < -\beta. \qquad 2.1.44$$

The same procedure can be followed to obtain the formula for the current i_2. Introduction of

$$j_2(\theta) = \frac{R_2\, i_2(\theta)}{U} \qquad 2.1.45$$

$$r_2 = \frac{R_2}{\omega L} \qquad 2.1.46$$

$$\sigma_2(\theta) = \frac{r_2}{(1 - g^2)^{1/2}} \arctan\left\{\left(\frac{1 - g}{1 + g}\right)^{1/2} \tan(\theta)\right\} \qquad 2.1.47$$

$$\tau_2(\theta) = \sigma_2(\theta) - \sigma_2(-\beta) \qquad 2.1.48$$

leads to

$$j_2(\theta) = -\frac{r_2 \exp(-\sigma_2(\theta))}{1 + g\cos(2\theta)} \int_{-\beta}^{\theta} \exp(\sigma_2(\theta'))\, d\theta' + \exp(-\tau_2(\theta)) * \qquad 2.1.49$$

$$\left\{ \frac{r_1 \exp(-\sigma_1(-\beta))}{1 + g\cos(2\theta)} \int_{-\pi/2-\alpha}^{-\beta} \exp(\sigma_1(\theta'))\, d\theta' + \right.$$

$$\left. \frac{1 - g\cos(2\alpha)}{1 + g\cos(2\theta)}\, j_1(-\pi/2 - \alpha) \exp(-\tau_1(-\beta)) \right\},$$

where the assumptions are made that

$$j_2(-\beta + \Delta) = j_1(-\beta - \Delta) \quad \text{with} \quad \Delta \to 0 \qquad 2.1.50$$

and

$$-\beta < \theta < \pi/2 - \alpha. \qquad 2.1.51$$

As we are dealing with the steady-state behaviour of the motor we can write

$$j_2(\pi/2 - \alpha - \Delta) = j_1(\pi/2 - \alpha + \Delta) = j_2(-\pi/2 - \alpha - \Delta) \quad \text{with} \quad \Delta \to 0. \qquad 2.1.52$$

Combination of equations 2.1.43, 2.1.49 and 2.1.52 leads to

$$j_2(-\pi/2 - \alpha) = \left\{ r_1 \exp(-\sigma_1(-\beta) - \tau_2(-\pi/2 - \alpha)) \int_{-\pi/2-\alpha}^{-\beta} \exp(\sigma_1(\theta'))\, d\theta' - \right. \qquad 2.1.53$$

$$\left. r_2 \exp(-\sigma_2(-\pi/2 - \alpha)) \int_{-\beta}^{\pi/2-\alpha} \exp(\sigma_2(\theta'))\, d\theta' \right\} *$$

$$[\{1 - g\cos(2\alpha)\}\{1 - \exp(-\tau_1(-\beta) - \tau_2(\pi/2 - \alpha))\}]^{-1}.$$

With eqs. 2.1.43, 2.1.49 and 2.1.53 the currents are given for

$$j_2(-\pi/2 - \alpha) > 0. \qquad 2.1.54$$

If $j_2(-\pi/2-\alpha)$ equals zero, eqs. 2.1.43 and 2.1.49 become by substitution of $j_2(-\pi/2-\alpha)=0$:

$$j_1(\theta) = \frac{r_1 \exp(-\sigma_1(\theta))}{1 + g\cos(2\theta)} \int_{-\pi/2-\alpha}^{\theta} \exp(\sigma_1(\theta'))\, d\theta' \qquad 2.1.55$$

and

$$j_2(\theta) = \left\{ r_1 \exp(-\sigma_1(-\beta) - \tau_2(\theta)) \int_{-\pi/2-\alpha}^{-\beta} \exp(\sigma_1(\theta'))\, d\theta' - \right. \qquad 2.1.56$$

$$\left. r_2 \exp(-\sigma_2(\theta)) \int_{-\beta}^{\theta} \exp(\sigma_2(\theta'))\, d\theta' \right\} / \{1 + g\cos(2\theta)\}$$

Whether eq. 2.1.54 is fulfilled or not depends largely on the values of α and β. To express this condition in an analytical form we use the following line of reasoning:
If $j_2(\theta)$ equals zero for $\theta=-\pi/2-\alpha$ then i_2 can already reach zero for $\theta=\theta_z$, with

$$-\beta < \theta_z < \pi/2 - \alpha. \qquad 2.1.57$$

Then eq. 2.1.56 gives

$$r_1 \exp(-\sigma_1(-\beta) - \tau_2(\theta_z)) \int_{-\pi/2-\alpha}^{-\beta} \exp(\sigma_1(\theta'))\, d\theta' = \qquad 2.1.58$$

$$r_2 \exp(-\sigma_2(\theta_z)) \int_{-\beta}^{\theta_z} \exp(\sigma_2(\theta'))\, d\theta'.$$

The unknown value of θ_z can be determined by means of a numerical scanning procedure.

In the foregoing we have found expressions for the currents through the motor coils. The validity of the expressions 2.1.43, 2.1.49 and 2.1.53 depends on the condition of eq. 2.1.54. If this is not valid, eqs. 2.1.55 and 2.1.56 have to be used as long as $j_2(\theta)>0$.

The mean torque $\bar{T}$ of the motor is given by

$$\bar{T} = \frac{1}{\pi}\left\{\int_{-\pi/2-\alpha}^{-\beta} \tfrac{1}{2} i_1^2 \frac{dL}{d\theta'}\, d\theta' + \int_{-\beta}^{\pi/2-\alpha} \tfrac{1}{2} i_2^2 \frac{dL}{d\theta}\, d\theta'\right\}. \qquad 2.1.59$$

Evaluation of the analytical equations

Our intention is to analyse the electromechanical behaviour of the motor in order to show the influence of the control variables α and β on the torque and the efficiency of the motor.

To simplify the equations we have introduced many assumptions as mentioned at the beginning of this section. Nevertheless the equations remain too complex to be solved solely by analytical means; in solving the equations a computer has to be used.

With a computer, however, there are more straightforward ways of calculating motor performance. Moreover a number of assumptions can then be discarded, leading to a more realistic model. We propose the application of a completely numerical method, which makes it possible to introduce a non-sinusoidal relation between the inductance L and the rotor position θ and to allow for saturation in the magnetic circuit.

The analytical method of description developed in this section will be used as a test of the following numerical approach.

2.2. Numerical approach

To arrive at a more general method of describing the steady-state behaviour of the single-phase reluctance motor we treat in this section a method based on the time discretization of the differential equations.

As will be shown, the resulting formulas allow us to make calculations with a non-sinusoidal relation between the inductance of the stator winding and the rotor position. Some examples will be given to demonstrate the influence of the control variables and conclusions will be drawn concerning an ideal reluctance motor. In section 2.3 we also introduce magnetic saturation and for the description we use formulas partly based on the expressions given in this section.

Fig. 2.2.1 shows the electrical diagram of the motor. In this section we assume that magnetic saturation, hysteresis and eddy currents are absent. To make the formulas valid for the time interval the switch is closed and open, we introduce the variables a and R_a with the following characteristics:

$$-\pi/2 - \alpha + k\pi \leqslant \theta < -\beta + k\pi \rightarrow a = 1,\ R_a = R_1 \qquad 2.2.1$$

corresponding to a closed switch and

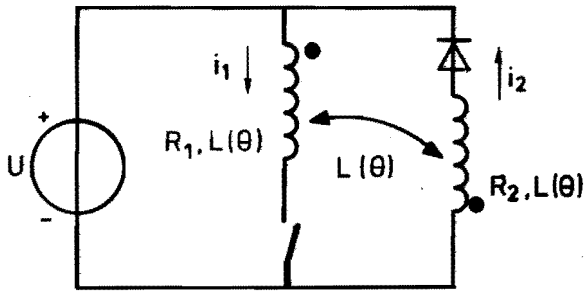

Fig. 2.2.1. The electrical circuit, assuming that the two coils are fully magnetically coupled.

$$-\beta + k\pi \leqslant \theta < \pi/2 - \alpha + k\pi \rightarrow a = -1, R_a = R_2 \qquad 2.2.2$$

corresponding to an open switch.

The equations belonging to the circuit, using the variables a and R_a, are:

$$a\,U = R_a\,i + \frac{d(L\,i)}{dt} \qquad 2.2.3$$

$$T = \tfrac{1}{2}\,i^2\,\frac{dL}{d\theta}\,. \qquad 2.2.4$$

In fact eq. 2.2.3 belongs to the circuit in fig. 2.1.3. But it also suits the circuit in fig. 2.2.1 provided that the current i_2 equals zero if the switch is closed and that the current i_1 equals zero if the switch is open.

Further we have:

$$i \geqslant 0 \qquad 2.2.5$$

$$L = L(\theta) \qquad 2.2.6$$

$$\theta(t) = \theta(t_i) + \int_{t_i}^{t} \omega\,.\,dt = \theta(t_i) + \omega(t - t_i). \qquad 2.2.7$$

The relation 2.2.6 has to be specified in the program.

A Runge-Kutta procedure can be used to evaluate eq. 2.2.3 and 2.2.4 in combination with eqs. 2.2.1 and 2.2.2, but numerical instability might then occur

if the differential equations are stiff (see ref. [4]). Since in the following section the motor will be described for the case where magnetic saturation is present, the differential equations will indeed be stiff. Another problem connected with available Runge-Kutta procedures is the required format of the input data. In section 2.3 we represent the flux linked with the coils as a function of the current and the rotor position by means of an array $\Phi(i_x,\theta_y)$, with a suitable number x of current values and rotor positions y. Available Runge-Kutta procedures are not well suited to this kind of input, because they require an analytical expression for the linked flux.
To achieve uniformity in sections 2.2 and 2.3 we want to use one procedure to find the solution of the differential equations in the more complicated situations as well. In the following we write the differential equations as a set of difference equations and solve these equations as a function of time.

To arrive at a set of difference equations we introduce:

$$\Delta T = t_{i+1} - t_i \qquad 2.2.8$$

$$I_i = i(t_i) \qquad 2.2.9$$

$$\Delta I_i = I_{i+1} - I_i \qquad 2.2.10$$

$$L_i = L(t_i) \qquad 2.2.11$$

$$L_i' = \frac{dL}{d\theta}\bigg|_{t=t_i} \qquad 2.2.12$$

$$L_i'' = \frac{dL}{d\theta}\bigg|_{t=t_{i+1}} - \frac{dL}{d\theta}\bigg|_{t=t_i} \qquad 2.2.13$$

$$\theta_i = \theta(t_i) \qquad 2.2.14$$

$$\theta_{i+1} = \theta_i + \omega\,\Delta T. \qquad 2.2.15$$

We assume that the following condition holds:

$$t_i \leqslant t \leqslant t_{i+1} \qquad 2.2.16$$

Then we are allowed to use as an approximation:

$$L(t) = L_i + \omega(t - t_i)\,.\,L_i' + \tfrac{1}{2}\omega\,\frac{(t - t_i)^2}{\Delta T}\,.\,L_i''. \qquad 2.2.17$$

$$i(t) = I_i + \frac{t - t_i}{\Delta T}\,\Delta I_i. \qquad 2.2.18$$

Equation 2.2.17 is equivalent to

$$L(\theta) = L_i + (\theta - \theta_i) \,.\, L_i' + \tfrac{1}{2} \frac{(\theta - \theta_i)^2}{\theta_{i+1} - \theta_i} \,.\, L_i''. \qquad 2.2.19$$

To build up the difference equations we use the following algorithm:

$$f_1(t) = f_2(t) \rightarrow \frac{1}{\Delta T} \int_{t_i}^{t_{i+1}} f_1(t')\, dt' = \frac{1}{\Delta T} \int_{t_i}^{t_{i+1}} f_2(t')\, dt'. \qquad 2.2.20$$

Eq. 2.2.3 becomes

$$\int_{t_i}^{t_{i+1}} a\, U\, dt = \int_{t_i}^{t_{i+1}} \left\{ R_a\, i + \frac{d(L\, i)}{dt'} \right\} dt'. \qquad 2.2.21$$

Substitution of eq. 2.2.17 and 2.2.18 into 2.2.21 leads to

$$a\, U = I_i(R_a + \omega\, L_i' + \tfrac{1}{2}\omega\, L_i'') + \Delta I_i \left(\frac{L_i}{\Delta T} + \omega\, L_i' + \tfrac{1}{2}\omega\, L_i'' + \tfrac{1}{2} R_a \right). \qquad 2.2.22$$

The current ΔI_i is the only unknown, which becomes after rearranging:

$$\Delta I_i = \frac{a\, U - I_i(R_a + \omega\, L_i' + \tfrac{1}{2}\omega\, L_i'')}{\dfrac{L_i}{\Delta T} + \omega\, L_i' + \tfrac{1}{2}\omega\, L_i'' + \tfrac{1}{2} R_a}. \qquad 2.2.23$$

The mean torque within the time interval $t_i \ldots t_{i+1}$ is given by

$$\bar{T}_i = \frac{1}{\Delta T} \int_{t_i}^{t_{i+1}} \tfrac{1}{2} \left(I_i + \frac{t' - t_i}{\Delta T} \Delta I_i \right)^2 \left(L_i' + L_i'' \frac{(t' - t_i)}{\Delta T} \right) dt' \qquad 2.2.24$$

or

$$\bar{T}_i = \tfrac{1}{2} (I_i^2 + \Delta I_i \,.\, I_i + \tfrac{1}{3} \Delta I_i^2)\, L_i' + (\tfrac{1}{4} I_i^2 + \tfrac{1}{3} \Delta I_i \,.\, I_i + \tfrac{1}{8} \Delta I_i^2)\, L_i''. \qquad 2.2.25$$

To have a simple accuracy check we introduce the following energy relations:

$$W_{diss,i} = W_{diss,i-1} + \int_{t_i}^{t_{i+1}} i^2\, R_a\, dt = \sum_{j=0}^{i} R_a (I_j^2 + \Delta I_j \,.\, I_j + \tfrac{1}{3} \Delta I_j^2)\, \Delta T \qquad 2.2.26$$

$$W_{mech,i} = W_{mech,i-1} + \int_{t_i}^{t_{i+1}} \omega\, T\, dt = \sum_{j=0}^{i} \omega\, \bar{T}_j\, \Delta T \qquad 2.2.27$$

$$W_{in,i} = W_{in,i-1} + \int_{t_i}^{t_{i+1}} a\, U\, i(t')\, dt' = \sum_{j=0}^{i} a_j\, U(I_j + \tfrac{1}{2}\Delta I_j)\, \Delta T \qquad 2.2.28$$

$$W_{magn,i} = \tfrac{1}{2} L_{i+1} I_{i+1}^2. \qquad 2.2.29$$

The variable a_j has the value of a at $t = t_j$. The calculation starts with $t = t_0$ and we assume that the calculation ends at $t = t_n$. The energy balance at time t_n is:

$$\tfrac{1}{2} L_0 I_0^2 + W_{in,n} = W_{magn,n} + W_{diss,n} + W_{mech,n} + \Delta W_n. \qquad 2.2.30$$

The variable ΔW_n represents the error due to the method used after n time steps. To get an indication of the accuracy of the calculation we introduce

$$\varepsilon = \frac{\Delta W_n}{W_{in,n}}. \qquad 2.2.31$$

The value of this variable increases with increasing time step ΔT. The time steps have to be shortened if the error is unacceptable.

With the expressions found we can analyse the influence of the control variables α and β by means of computer calculations. Fig. 2.2.2 gives the flow chart of the program.
Before the calculation starts for $t = t_0$ we have to give the initial conditions at $t = t_0$, namely the rotor position and the current. We use as initial rotor position $\theta = -\pi/2 - \alpha$, where the switch is closed. It is assumed in the program that the current in the catch coil might not be zero at the moment the switch closes. Whether this is the case depends on the values of the control variables α and β, the speed and the motor constants.
If the inductance is given by eq. 2.1.36, then eq. 2.1.58 can be used to determine whether the current i_2 equals zero or not just before the moment the switch closes. If not, eq. 2.1.53 gives us the right value of i_2 at $t = t_{on}$.
Knowing the initial value of the current, it is sufficient to solve the equations for the interval

$$-\pi/2 - \alpha \leqslant \theta < \pi/2 - \alpha \qquad 2.2.32$$

to get the mean torque and the efficiency, which is defined as:

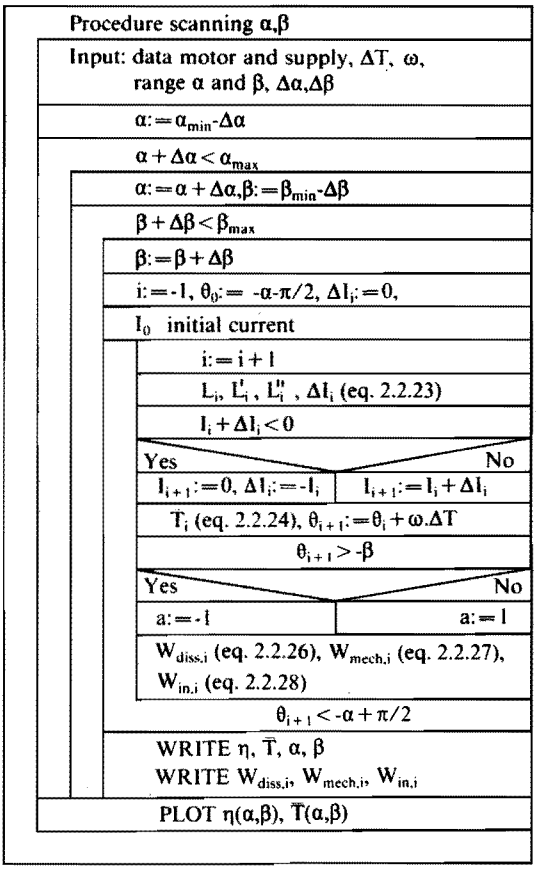

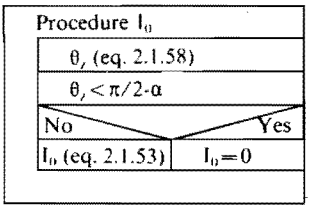

Fig. 2.2.2. The flowchart of a numerical program that solves the equations belonging to the idealized reluctance motor.

$$\eta = \frac{W_{mech,n}}{W_{in,n}}, \qquad 2.2.33$$

where the index n means that at $t = t_{n+1}$ the rotor position θ has passed $\pi/2-\alpha$. If the inductance of the stator coil is not the same function as eq. 2.1.36 another procedure should be followed. The current should be given an initial value and the calculation of the current should be repeated until an acceptable small difference exists between the calculated currents at $-\pi/2-\alpha+k\pi$ and $-\pi/2-\alpha+(k+1)\pi$.

It is possible to verify the formulas developed in this section by comparing the results of the analytical formulas described in section 2.1 with the results of the computer procedure of this section. The analytical expressions belonging to the currents are eqs. 2.1.43 and 2.1.49; the mean torque is given by eq. 2.1.59. These latter equations are solved by means of a numerical integration procedure available for the computer used.
The input data used are:

$$R_1 = 4.275\ \Omega \qquad R_2 = 4.275\ \Omega \qquad 2.2.34$$

$$L(\theta) = 0.102 + 0.0856\cos(2\theta)\ H \qquad 2.2.35$$

$$U = 120\ V \qquad 2.2.36$$

$$\omega = 1571\ rad/s. \qquad 2.2.37$$

Table 2.2.1 gives the results, which show fair agreement. The existing deviations can be reduced by demanding a higher accuracy in the numerical programs.

		section 2.1		section 2.2	
α (rad)	β (rad)	torque (mNm)	eff. (%)	torque (mNm)	eff. (%)
0.0	0.0	1.36	61.4	1.36	61.3
0.0	0.3	8.83	94.8	8.83	94.8
0.0	0.6	8.35	95.9	8.35	95.9
0.3	0.0	70.26	34.7	70.10	34.6
0.3	0.3	20.71	92.7	20.71	92.7
0.3	0.6	21.42	93.8	21.42	93.8
0.6	0.0	38.87	6.5	38.66	6.4
0.6	0.3	137.4	49.9	137.4	49.9
0.6	0.6	37.33	90.8	37.33	90.8

Table 2.2.1

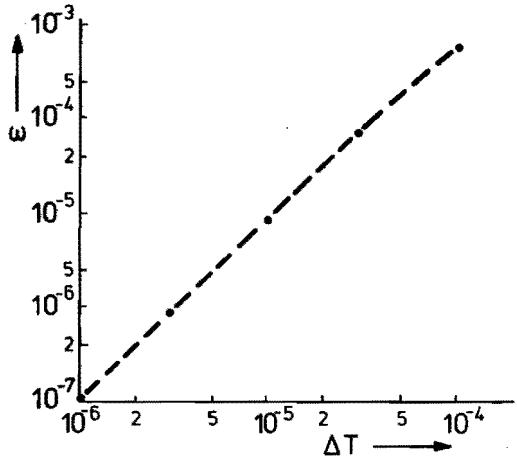

Fig. 2.2.3. The behaviour of the relative error ε of the energy balance as a function of the time step ΔT.

Fig. 2.2.3 shows the behaviour of eq. 2.2.31 as a function of the time step ΔT. We consider the results presented in table 2.2.1 and fig. 2.2.3 to be an indication of the correctness of the program. A proof that the method followed is suitable for our purpose is given in section 2.3, where the method is extended to include magnetic saturation and where the results of the new method are compared with the results of measurements.

To show the influence of the control variables α and β we use the parameters of the experimental motor as input for the program in fig. 2.2.2. We note that the results are of limited value, because eddy currents, hysteresis and saturation in the magnetic circuit are not included in this numerical procedure.

In the program the following constants and relations are used:

$$R_1 = 4.35\ \Omega \qquad R_2 = 4.35\ \Omega \tag{2.2.38}$$

$$L(\theta) = 0.102 + 0.0856\cos(2\theta)\ \text{H} \tag{2.2.39}$$

$$U = 220\ \text{V} \tag{2.2.40}$$

$$\omega = 1571\ \text{rad/s} \tag{2.2.41}$$

$$\Delta T = 0.015/\omega\ \text{s} \tag{2.2.42}$$

$$-\pi/2 - \alpha \leqslant \theta < \pi/2 - \alpha. \tag{2.2.43}$$

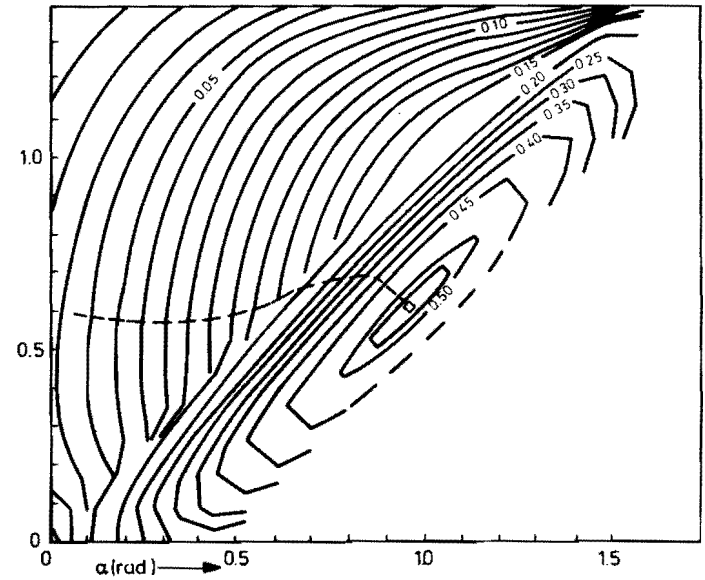

Fig. 2.2.4a. Calculated torque at 15 000 r.p.m. The torque depends on the angles α and β, which are defined in fig. 2.1.6.

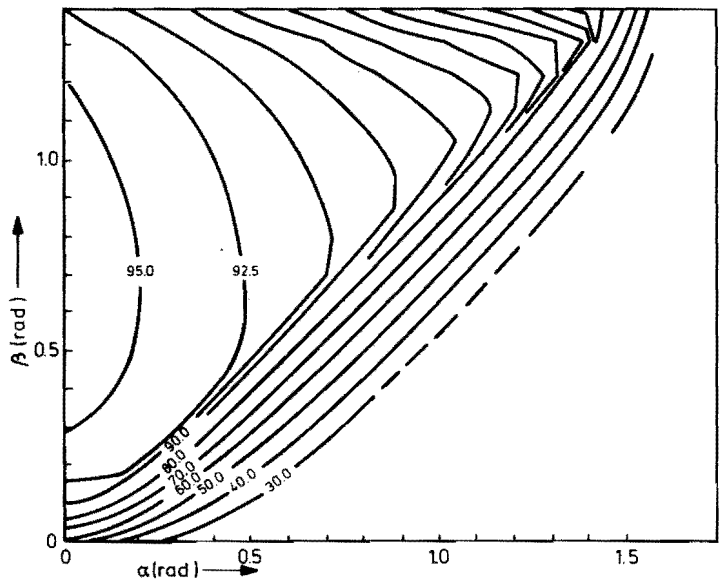

Fig. 2.2.4b. Calculated efficiency. The dashed curve connects the sets of α and β that give a maximum obtainable efficiency for every occurring value of the torque.

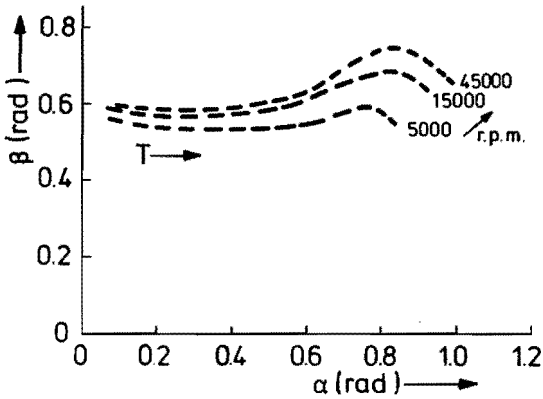

Fig. 2.2.5a. Optimum sets of α and β for different speeds.

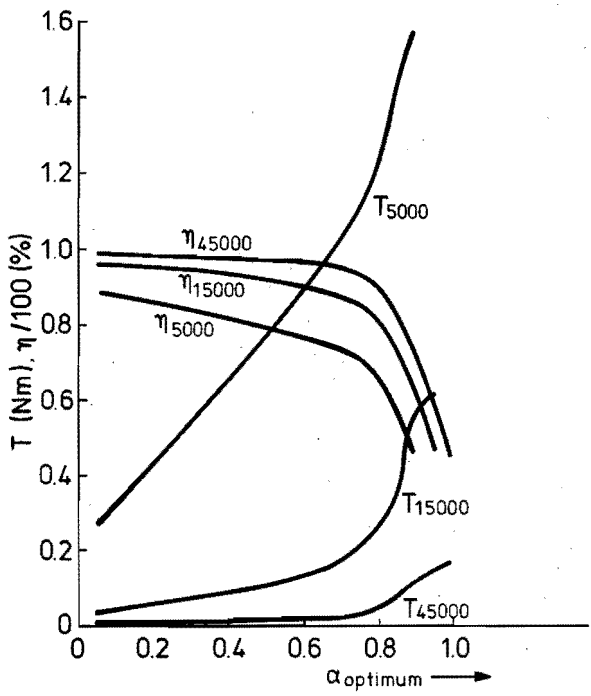

Fig. 2.2.5b. Efficiency and torque related to the curves in fig. 2.2.5a.

We have used fig. 2.2.3. to obtain a value for the time step ΔT that gives an acceptable error in the energy balance. We regard an energy balance error of less than 0.1 % as acceptable, because the measuring error in the test rig will be larger.

Fig. 2.2.4 gives the curves with a constant torque ($\overline{T}$) and a constant efficiency (η) as a function of the control variables. The dashed curve connects the points where a maximum efficiency is found for a certain value of the torque. In fig. 2.2.5a these curves are given for other velocities.
It appears that steep gradients of both torque and efficiency are related to the situation where $i_2 > 0$ at $t = t_{on}$.
From these curves the following conclusions are drawn:

- For every angular velocity ω and applied torque one set of values for α and β gives a maximum efficiency.
- The value of β is near 0.6 for these optimum combinations at the three selected speeds.
- It is mainly the variable α that determines the value of the torque.
- If the value of the control variable α increases, a point is reached where the current in the motor windings becomes continuous. In that situation the torque assumes larger values, but efficiency decreases considerably (see fig.2.2.5b). Apparently the continuous current is favourable for the torque production. At the same time, however, the dissipation increases very fast. This is caused by the presence of the current during the time the term $dL/d\theta$ is negative in eq. 2.2.4. Its influence grows rapidly when α increases.

2.3. Analysis including saturation

In the preceding section the electromechanical behaviour of the motor was described under the assumption of negligible saturation. In practice saturation will be present, as shown in fig. 2.3.1, where the measured flux in our experimental motors is given as a function of the rotor position and the current. Each mark represents a measured flux value. These data were obtained in an array $\Phi(i_x,\theta_y)$ and will be used as input for the program that will be described in this section. With this program the behaviour of the motor as a function of the variables α and β can be obtained in a shorter time than by measuring the behaviour in the test rig, even in our case where the measurements are automated.

The following assumptions are made:

- eddy currents and hysteresis are negligible.
- the electronic components are ideal.
- the angular velocity ω is constant.
- the main coil and catch coil on the stator are magnetically fully coupled, have the same number of turns and their resistances remain constant.

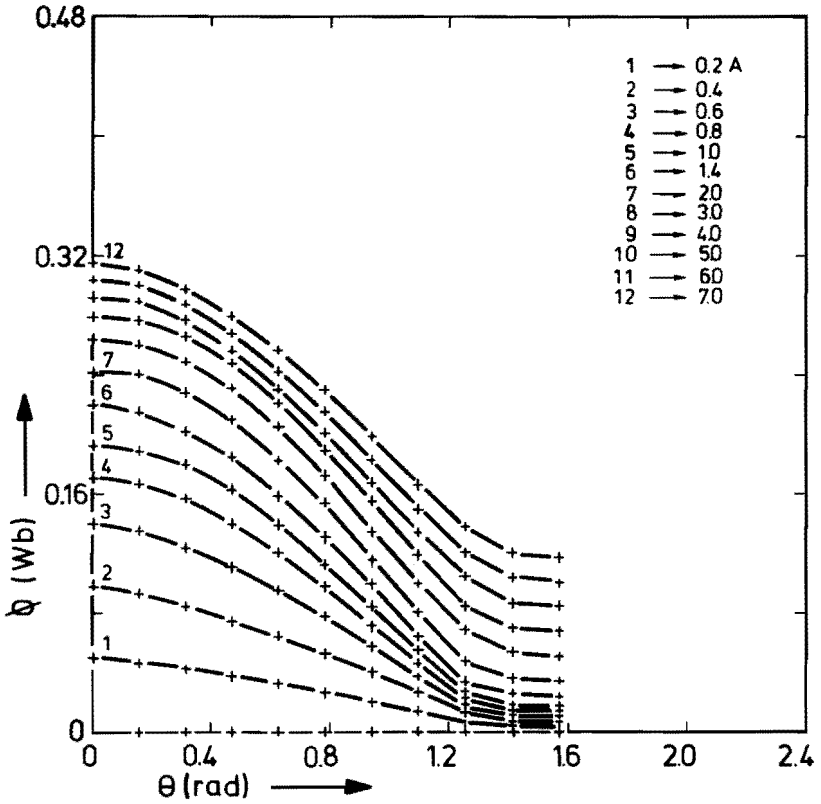

Fig. 2.3.1. The marks give the measured value of the flux related to a certain current and rotor position.

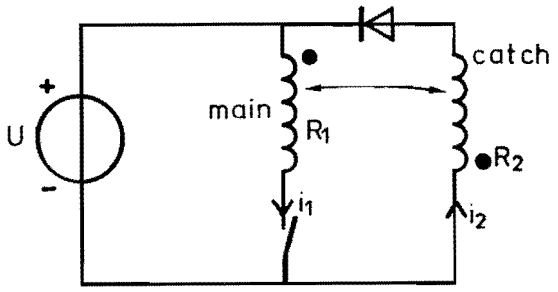

Fig. 2.3.2. The electrical circuit for the motor when magnetic saturation is involved.

Figure 2.3.2 gives the following network equations:

$$U = R_1 i_1 + \omega \frac{\partial \Phi}{\partial \theta} + \frac{\partial \Phi}{\partial i_1} \frac{di_1}{dt} \qquad 2.3.1$$

if the switch is closed, and

$$-U = R_2 i_2 + \omega \frac{\partial \Phi}{\partial \theta} + \frac{\partial \Phi}{\partial i_2} \frac{di_2}{dt} \qquad 2.3.2$$

if the switch is open and $i_2 > 0$.
This includes the assumption that no current passes the catch coil if the switch is closed (see the discussion in section 2.1).
The torque will be computed by way of the magnetic co-energy W_{co} (ref. [5]), using the expression:

$$T = \frac{\partial W_{co}}{\partial \theta}, \qquad 2.3.3$$

where the co-energy is defined as:

$$W_{co} = \int_0^i \Phi \, di \Big|_{\theta = \text{constant}}. \qquad 2.3.4$$

Inspection of the preceding equations shows that for every occurring combination of the rotor position θ and current i the values of $\partial\Phi/\partial i$, $\partial\Phi/\partial\theta$ and $\partial W_{co}/\partial\theta$ should be available.
To get these function values use is made of a cubic spline interpolation (see ref. [6]) to interpolate the data of the flux measurements (see fig. 2.3.1) for both the current and the rotor position in order to refine the grid θ,i. The refined grid is given by:

$$0 \leqslant \theta \leqslant \pi/2, \qquad \Delta\theta = \pi/60 \qquad 2.3.5$$

and

$$0 \leqslant i \leqslant 7, \qquad \Delta i = 0.2\,. \qquad 2.3.6$$

In this grid the required functions are calculated at every nodal point and these data are used in the program that solves the equations belonging to the motor. For every combination of θ,i the above-mentioned functions are calculated by means of a six-point interpolation of the function values at the surrounding nodal points.
To analyse the behaviour of the torque and efficiency of the motor as a function of the control variables α and β with a numerical program the equations 2.3.1 and 2.3.2 have to be written in a time-discrete form, in accordance with the examples given in the preceding sections.

First we reduce eqs. 2.3.1 and 2.3.2 to

$$a\,U = R_a\,i + \omega\,\frac{\partial\Phi}{\partial\theta} + \frac{\partial\Phi}{\partial i}\,\frac{di}{dt} \qquad 2.3.7$$

with

$$a = 1, \quad R_a = R_1 \quad \text{and} \quad i = i_1 \qquad 2.3.8$$

if the switch is closed and with

$$a = -1, \quad R_a = R_2 \quad \text{and} \quad i = i_2 \qquad 2.3.9$$

if it is open. The calculation of the current will start at $t = t_{on}$, where the initial conditions are:

$$i = 0 \qquad 2.3.10$$

$$\theta = -\pi/2 - \alpha \qquad 2.3.11$$

$$a = 1 \qquad 2.3.12$$

$$\omega = \omega_0. \qquad 2.3.13$$

Using the algorithm of eq. 2.2.20 on eq. 2.3.7, we get

$$\int_{t_i}^{t_{i+1}} a\,U\,dt = \int_{t_i}^{t_{i+1}} \left\{ R_a\,i + \omega\,\frac{\partial\Phi}{\partial\theta} + \frac{\partial\Phi}{\partial i}\,\frac{di}{dt} \right\} dt. \qquad 2.3.14$$

We assume that for the small interval ΔT we have

$$a = \text{constant}. \qquad 2.3.15$$

To obtain an approximated value of $\partial\Phi/\partial\theta$ and $\partial\Phi/\partial i$, the value of the current should be predicted for $t > t_i$. We will use as extrapolation:

$$i(t) = I_i + (I_i - I_{i-1})\,\frac{t - t_i}{\Delta T}. \qquad 2.3.16$$

We define I_{sugg} as:

$$I_{sugg} = 2\,I_i - I_{i-1}. \qquad 2.3.17$$

The rotor position θ_{i+1} is given by:

$$\theta_{i+1} = \theta_i + \omega\,.\,\Delta T \qquad 2.3.18$$

according to the assumption that the angular velocity is constant. On the basis of the last equations the terms $\partial\Phi/\partial\theta$ and $\partial\Phi/\partial i$ will be:

$$\frac{\partial\Phi}{\partial\theta} = \frac{\partial\Phi}{\partial\theta}\Big|_{\theta_i,I_i} + \left(\frac{\partial\Phi}{\partial\theta}\Big|_{\theta_{i+1},I_{sugg}} - \frac{\partial\Phi}{\partial\theta}\Big|_{\theta_i,I_i}\right)\frac{t - t_i}{\Delta T} \qquad 2.3.19$$

$$\frac{\partial\Phi}{\partial i} = \frac{\partial\Phi}{\partial i}\Big|_{\theta_i,I_i} + \left(\frac{\partial\Phi}{\partial i}\Big|_{\theta_{i+1},I_{sugg}} - \frac{\partial\Phi}{\partial i}\Big|_{\theta_i,I_i}\right)\frac{t - t_i}{\Delta T}. \qquad 2.3.20$$

Substitution into 2.3.14 leads to

$$a\,U = R_a(I_i + \tfrac{1}{2}\Delta I_i) + \tfrac{1}{2}\omega\left(\frac{\partial\Phi}{\partial\theta}\Big|_{\theta_i,I_i} + \frac{\partial\Phi}{\partial\theta}\Big|_{\theta_{i+1},I_{sugg}}\right) + \qquad 2.3.21$$

$$\tfrac{1}{2}\frac{\Delta I_i}{\Delta T}\left(\frac{\partial\Phi}{\partial i}\Big|_{\theta_i,I_i} + \frac{\partial\Phi}{\partial i}\Big|_{\theta_{i+1},I_{sugg}}\right).$$

The unknown current change ΔI_i becomes:

$$\Delta I_i = 2\,\frac{a\,U - R_a\,I_i - \tfrac{1}{2}\omega\left(\frac{\partial\Phi}{\partial\theta}\Big|_{\theta_i,I_i} + \frac{\partial\Phi}{\partial\theta}\Big|_{\theta_{i+1},I_{sugg}}\right)}{R_a + \left(\frac{\partial\Phi}{\partial i}\Big|_{\theta_i,I_i} + \frac{\partial\Phi}{\partial i}\Big|_{\theta_{i+1},I_{sugg}}\right)/\Delta T}. \qquad 2.3.22$$

Under the constraint $\Delta T \to 0$ we assume that it holds that:

$$T = \frac{\partial W_{co}}{\partial\theta}\Big|_{\theta_i,I_i} + \left(\frac{\partial W_{co}}{\partial\theta}\Big|_{\theta_{i+1},I_{i+1}} - \frac{\partial W_{co}}{\partial\theta}\Big|_{\theta_i,I_i}\right)\frac{t - t_i}{\Delta T}. \qquad 2.3.23$$

The mean torque over the interval $t_i < t < t_{i+1}$ becomes

$$\bar{T}_i = \tfrac{1}{2}\left(\frac{\partial W_{co}}{\partial\theta}\Big|_{\theta_i,I_i} + \frac{\partial W_{co}}{\partial\theta}\Big|_{\theta_{i+1},I_{i+1}}\right). \qquad 2.3.24$$

The mean value of the torque and the efficiency over the interval $t_0 \ldots t_n$ are given respectively by

$$\bar{T} = \frac{1}{n}\sum_{j=0}^{n-1}\bar{T}_j \qquad 2.3.25$$

and

$$\eta = \frac{1}{n} \sum_{j=0}^{n-1} \frac{\bar{T}_j}{a_j U(I_j + I_{j+1})/2}, \qquad 2.3.26$$

where a_j means the value of a over the interval $t_j \ldots t_{j+1}$. The steady-state behaviour can be described by repeating the calculation of equations 2.3.22 and 2.3.24 during the time that the rotor position is given by:

$$-\pi/2 - \alpha \leqslant \theta \leqslant \pi/2 - \alpha. \qquad 2.3.27$$

If the current I is unequal to zero just for the moment $t = t_{on}$, the calculation should be repeated until:

$$I\Big|_{\theta = -\alpha + \pi/2 + k\pi} = I\Big|_{\theta = -\alpha + \pi/2 + (k+1)\pi} + \varepsilon, \qquad 2.3.28$$

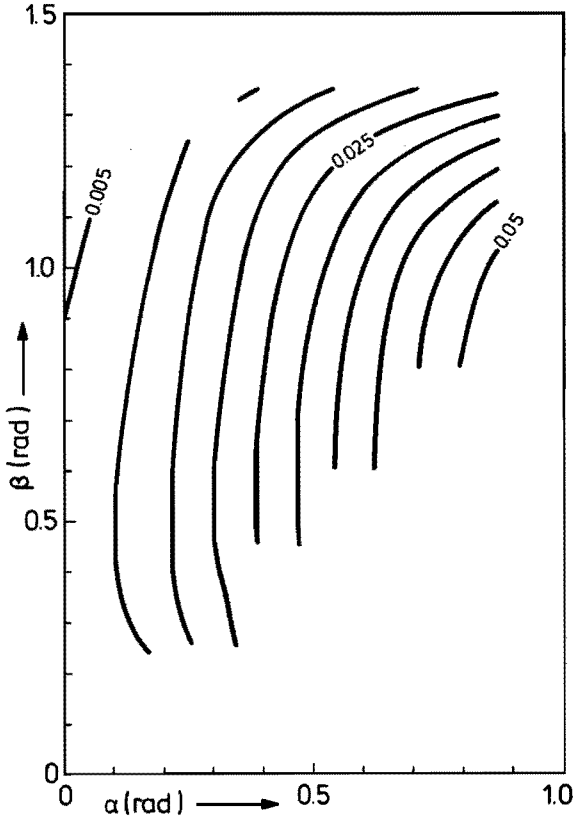

Fig. 2.3.3. The measured torque at 15 000 r.p.m.

where the variable ε represents an acceptable error. Here the steady-state mean torque and efficiency should be calculated by using the results over the last iteration, given by:

$$-\alpha + \pi/2 + k\pi \leqslant \theta \leqslant -\alpha + \pi/2 + (k+1)\pi. \qquad 2.3.29$$

We are not interested in the case $I > 0$ at $t = t_{on}$, because the efficiency will be less than we will accept for the applications we have mentioned in the introduction. The efficiency should be better than 60 %.
Fig. 2.3.3 and fig. 2.3.4 present the measured torque and efficiency of our experimental motors as a function of the control variables α and β. The measurement equipment is described in chapter 4 and the dimensions of the motor are given in chapter 6. We note that we have measured the torque by

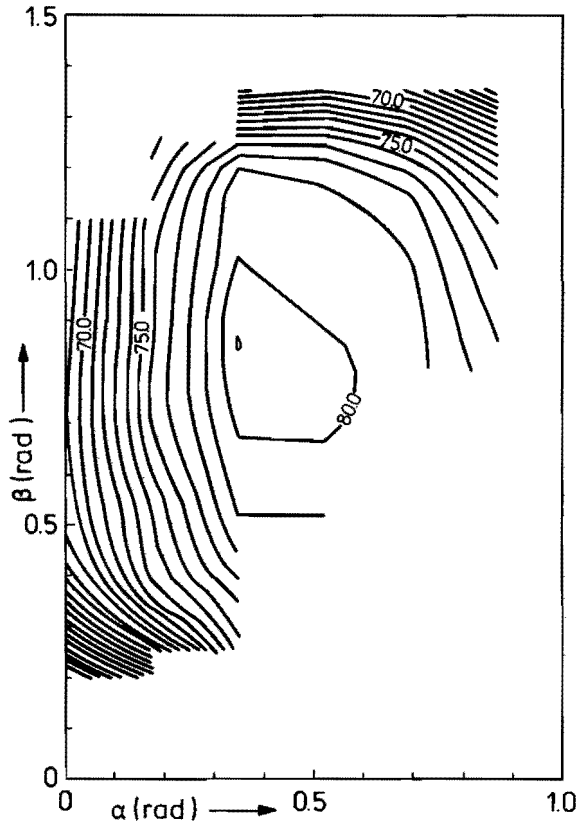

Fig. 2.3.4. The measured efficiency at 15 000 r.p.m.

means of the reaction torque on the stator. The results of the program based on the method described in this section are given in fig. 2.3.5 and fig. 2.3.6.
A fair agreement exists between figures 2.3.3 and 2.3.5, representing respectively the measured and calculated torque. On the other hand, there is a great discrepancy between the efficiency curves in figures 2.3.4 and 2.3.6. We note a lower efficiency for all combinations of α and β and the shape of the curves is different.

The following effects may contribute to this discrepancy:
- losses in the iron;
- non-ideal behaviour of the electronic components;
- increased resistance of the coils owing to temperature rise;
- increased resistance owing to high-frequency effects;
- faulty assumptions concerning the linkage of the catch and main coils.

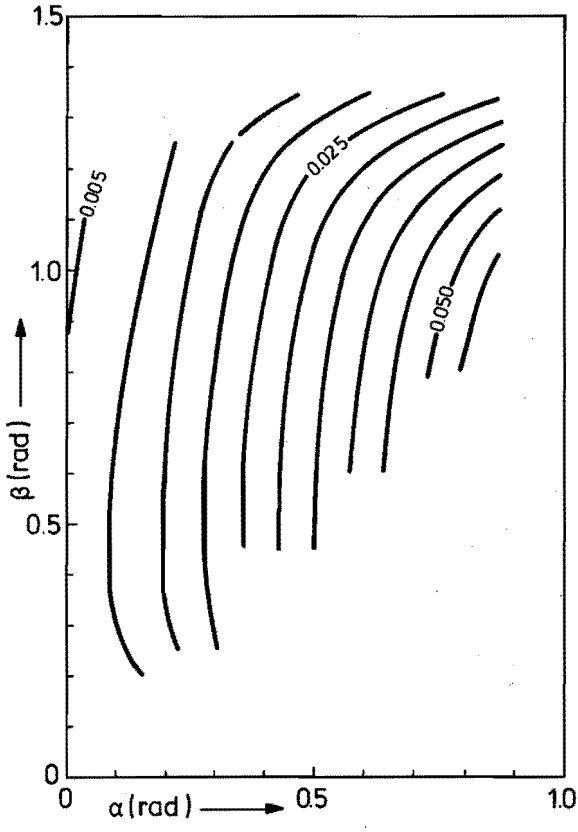

Fig. 2.3.5. Calculated torque at 15 000 r.p.m. (including saturation). This figure should be compared with fig. 2.3.3.

To check the last-mentioned possibility we have connected the coils in series and in such a manner that the direction of the current of the main coil is opposite to the current carried by the catch coil. A full coupling should lead to a purely resistive and frequency-independent character of the impedance of the two coils connected in series. It is only at frequencies higher than 5 kHz that a change of the impedance occurs greater than the measurement errors. The switching frequency, which corresponds to the speed of 15 000 r.p.m., used for the measurements, equals 500 Hz. Comparing this frequency with 5 kHz, we reject the possibility of non-ideally coupled coils.

We assumed the resistance of the coils to be constant, so we neglected an increase due to temperature rise and current displacement. The occurrence of the latter effect is possible, but cannot explain the strong increase of the losses, taking into account the wire thickness (0.5 mm) and a basic frequency of 500 Hz.

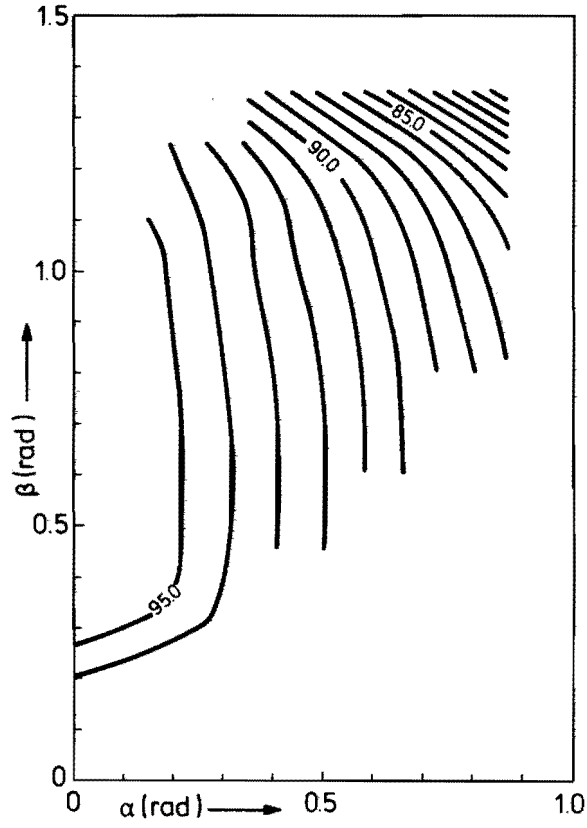

Fig. 2.3.6. Calculated efficiency at 15 000 r.p.m. (including saturation). Related measurement given in fig. 2.3.4.

Introducing in the program the changing resistance of the coils due to the temperature rise and the non-ideal behaviour of the electronic switch and the diode leads to the results shown in figs. 2.3.7 and 2.3.8. Comparing figs. 2.3.6 and 2.3.8 we see a decrease of the efficiency of between 1 % and 3 %; there remains a remarkable difference between the measured and the calculated efficiency (figs. 2.3.4 and 2.3.8 respectively).

There remain the losses due to the eddy currents and the hysteresis in the magnetic material used in the stator and rotor.
The nature of these losses is rather complicated. We point out that the flux does not vary sinusoidally with time, that the distribution of the flux in the rotor and the stator poles is not uniform and that the direction of the magnetic field with respect to the rotor changes with time. So specifications given by the producer of the lamination are not suitable to be used as data for a calculation. Numerical

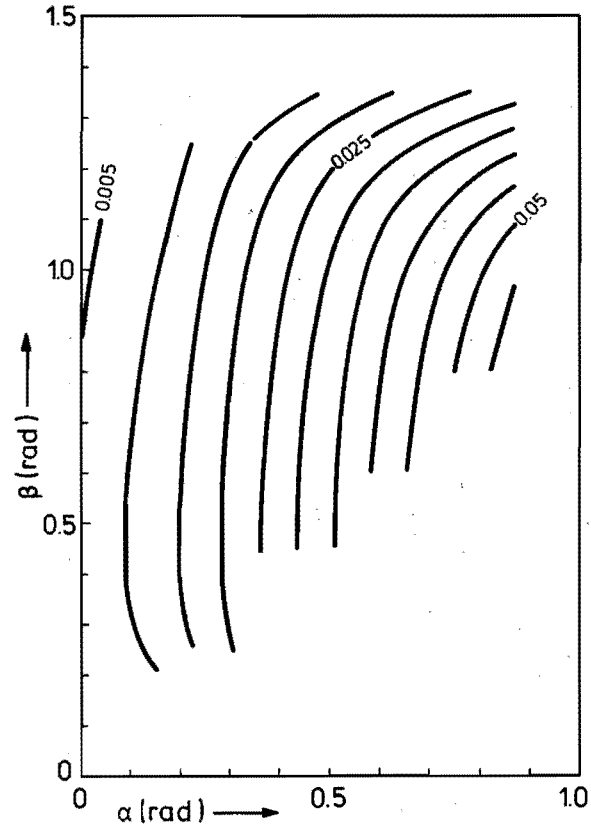

Fig. 2.3.7. The calculated torque after a correction for the temperature dependence of the coil resistance and the losses in the power electronics. Related measurement given in fig. 2.3.3.

programs suitable for calculating iron losses under the conditions mentioned above are not yet available as far as we know, and it is beyond the scope of this study to develop such a program.

Conventional calculations using the specifications of the lamination will not be reliable. Such conventional calculations lead to the efficiency curves shown in fig. 2.3.9. We consider the result to be an improvement of the shape of the curve, but still not satisfactory.

We have used a lamination with a resistivity of 70 μΩcm and a thickness of 0.35 mm. The resistivity is high compared with the usual value for silicon steel of 50 μΩcm. A further reduction of the eddy current losses can be achieved by using a magnetic circuit made of a lamination with a thickness of 0.1 mm instead of 0.35 mm.

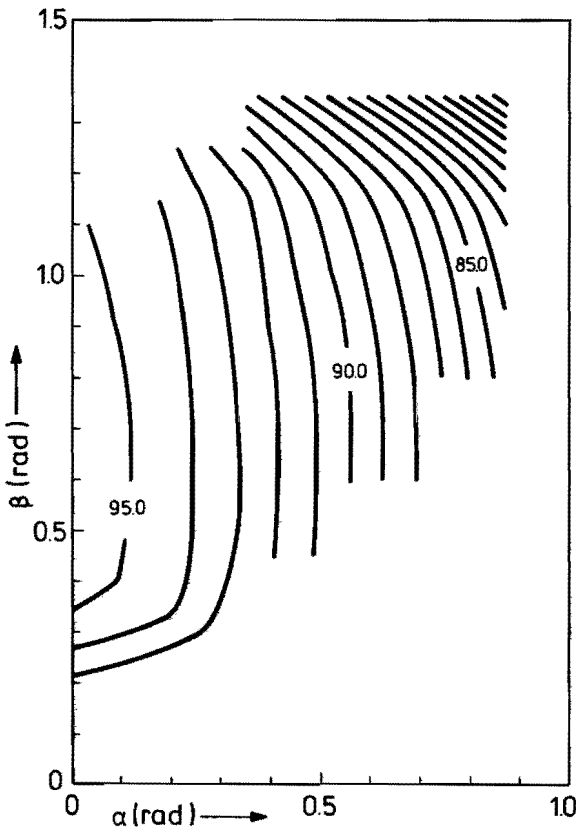

Fig. 2.3.8. The calculated efficiency after the correction. Related measurement given in fig. 2.3.4.

The improvement of the torque calculations obtained with the more complicated model can be seen by comparing figs. 2.3.5 and 2.3.10. The latter figure shows the results of the method described in section 2, where the following input is used:

$$R_1 = 4.8\ \Omega, \qquad R_2 = 4.5\ \Omega \tag{2.3.30}$$

$$L(\theta) = 0.1058 + 0.0901 \cos(2\theta)\ \text{H} \tag{2.3.31}$$

$$U = 120\ \text{V} \tag{2.3.32}$$

$$\omega = 1571\ \text{rad/s}. \tag{2.3.33}$$

The maximum and minimum inductances in eq. 2.3.31 correspond to the maximum and minimum flux of the experimental motor measured with a current of 1 A.

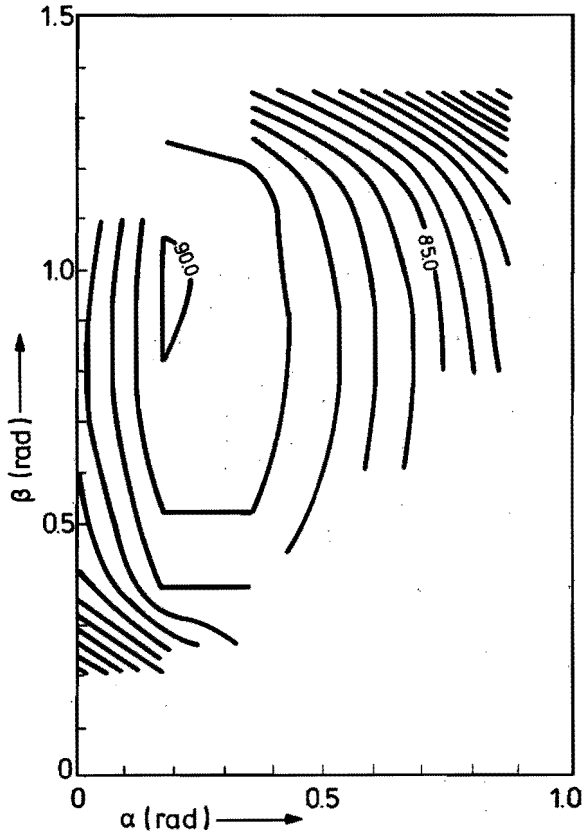

Fig. 2.3.9. The calculated efficiency when the temperature rise of the coils, losses in the power electronics, eddy current losses in the lamination and hysteresis losses in the lamination are included.

2.4 Conclusions

With a more sophisticated numerical model developed for describing the electromechanical behaviour of the motor it is found that the calculated torque as a function of the switch-on and switch-off time agrees well with the results of the measurements.

The efficiency as a function of the same variables does not agree with the measurements, most probably owing to eddy current and hysteresis losses in the stator and rotor iron. An accurate calculation for the losses related to eddy currents and hysteresis by analytical means is difficult, because the flux distribution is not uniform and does not change sinusoidally in time and the calculation has to include the rotation of the rotor in the pulsating field. As far as we know, no numerical programs exist that can solve this problem and we consider the development of such a program to be outside the scope of this study. The consequence is that the efficiency of the motor should be obtained by measurement.

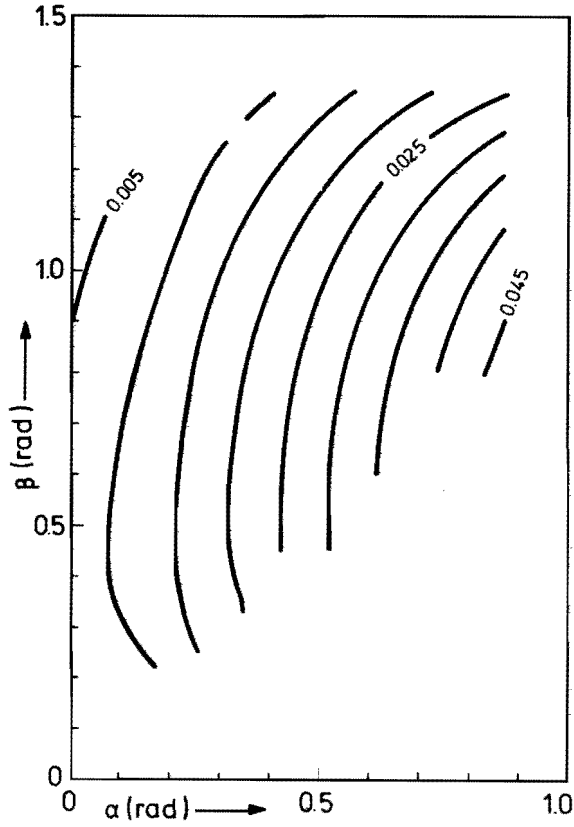

Fig. 2.3.10. This figure gives the torque when the linear model given in Ch. 2.2 is used.

3. Motor control

3.1. Selection of the control

In the preceding chapter we saw that the behaviour of the motor is to a large extent determined by the values of the control variables α and β. For every speed a certain combination of α and β can be found that gives a maximum efficiency for the required torque at that speed. Now we have to decide on the control of the motor and on the way in which to implement a mechanism that selects these optimum values.
Due to the characteristics of the motor an unusual procedure has to be applied to start it. This procedure too, which we discuss later on, has to be incorporated in the control.
Another important aspect of the control is the protection of the power electronics against too high currents.

Signals that have to be available for the control are the ON/OFF signal (given by the user), the rotor position signal and a signal indicating whether the current exceeds the maximum value or not.
From the rotor position signal the speed is obtained by measuring the time the rotor needs to rotate over a certain angle. Assuming a constant rotor speed this angle might be e.g. 180 degrees. We choose this angle because a simple and relatively cheap sensor can be used to get a pulse signal every 180 degrees. This gives the control the additional task of measuring the time between two successive sensor signals to determine the speed.
The current in the coils of the motor is determined by measuring the voltage drop across two resistors connected in series with the two coils of the motor (see fig. 3.1.1). The current in both coils has to be sensed, because due to a negative value of $\partial\Phi/\partial\theta$ the current in the catch coil can rise above values allowed by the switch. The switch should not be closed when this occurs.

We propose the use of a microprocessor because it offers the following advantages compared with other solutions such as discrete electronics, or analog and digital integrated circuits:

- small size;
- low energy consumption (hence a small power supply);
- flexibility during the experimental phase (no new wiring when changes are necessary);
- complicated algorithms and features are easily introduced.

When the decision is made to use a processor, a member of a particular family of processors has to be chosen. General considerations are:

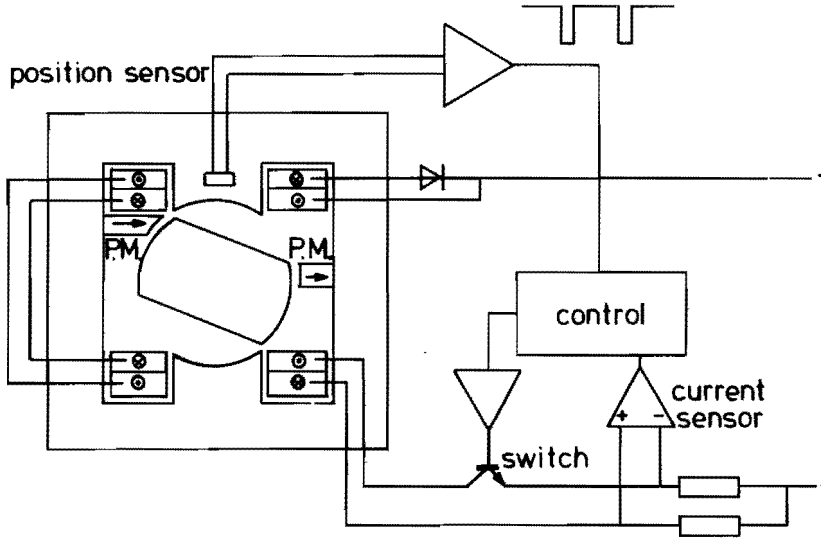

Fig. 3.1.1. Motor control.

- cost;
- more than one producer;
- available facilities to make and test the program (assembler and in-circuit emulator available?);
- knowledge and experience with a certain processor;
- are there alternatives (within the chosen family) with higher capabilities to prevent the rewriting of an important part of the developed software and to avoid the purchase of a new microprocessor development system when the processor does not fit if more functions than just the motor control have to be implemented?
- required number of external integrated circuits (e.g. for the clock, timers and communication with other parts of the system).

Of more technical interest are the following topics:

- size of on-board RAM and ROM;
- addressable external memory;
- separate address and data bus;
- interrupt mechanism used (single level or vectored interrupt?);
- word length (4,8,16 or 32 bits);
- stack mechanism used (hardware or pointer-stack);
- number of timers;
- speed of the processor and power of the instruction set high enough in order to reach the required execution times?
- supply voltages required.

To determine the power of the instruction set important matters to be considered are:

- the available ways of addressing a memory location (direct, indirect, relative and indexed)?
- types of jumps;
- bit manipulation;
- ck operations;
- arithmetic instructions (double precision?).

We selected the type 8048, a single-chip processor, because it meets all the general questions mentioned above (see ref. [7]). When the type 8048 is compared with other processors, however, it is seen to have a number of limitations (such as speed, instruction set, stack and interrupt mechanism, memory size and number of timers). If this processor is not suitable for applications of the motor that require the implementation of other functions, a more powerful member of the same family (e.g. the 8051) might be used.

3.2. Description of the control program

The information required for controlling the switch comprises the signals of the position sensor and the current sensor. In this section we discuss how this information is used, without going into the details of the program. At the end we give a comparison between the time diagram for the processor used and the diagram that would apply if the 8051 were used.

Input signals

The sensor for the rotor position gives a signal every 180 degrees. The processor has to acknowledge this signal immediately, because it contains the essential information of the speed and the rotor position. From this information the correct moment to open or close the electronic switch has to be determined, for which purpose we connect the signal with the interrupt input of the processor. To record the time between two interrupts, which is related to the actual speed, we use the 8-bit timer of the processor.

A signal will be given by the current sensor when the current approaches the maximum allowable value for the power electronics. This signal has a high priority, because to ignore it would lead to damage. Owing to the lack of a second interrupt input this signal has to be fed to another input port or be mixed with the signal of the position sensor. In the latter case an additional signal has to be added to give the processor the information that the pending interrupt is caused by the current detection. Because of the inductive character of the motor the current cannot rise to unacceptable values within e.g. 20 μs, and this allows us to connect the current detector with an input port of the processor. This means that the program should verify whether or not the current exceeds the maximum value by a repetitive check of this port. In our program this is done every 25 μs.

When the user wants to start the motor, the processor is reset for a short time and connected with the clock. When the reset is ended the processor starts the control program. The program is stopped by resetting the processor and by disconnecting the processor and clock.

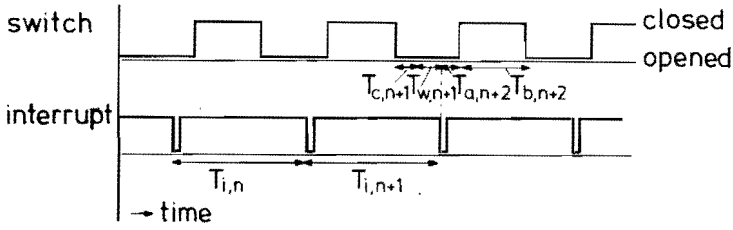

Fig. 3.2.1. Principle of control.

Steady state

The basic idea of the control is given in fig. 3.2.1, starting with the closing of the switch. It is assumed here that the speed is more than 11 720 r.p.m.

The measured time between the two preceding signals of the sensor ($T_{i,n}$) is used within the time $T_{c,n+1}$ to determine the new values of the time intervals $T_{a,n+2}$ and $T_{b,n+2}$; this is done every 32 interrupt pulses. Later in this section we will discuss the reason for taking this number. The relations between the angles α and β, defined in the preceding chapter, and the times T_a and T_b are:

$$T_a = \frac{\pi/2 - \alpha}{\omega} \qquad 3.2.1$$

$$T_b = \frac{\pi/2 + \alpha - \beta}{\omega}. \qquad 3.2.2$$

When a new signal is received from the sensor ($T_{w,n+1}$) the control program waits for the time $T_{a,n+2}$, closes the switch and opens it again after the time $T_{b,n+2}$.

A software timer is required to realize the times T_a and T_b, because the type 8048 processor contains only one on-board timer and it is the task of this timer to measure the time between the interrupt signals. We have developed for this purpose a procedure whose execution time is adjustable by means of the value of a variable.

In this procedure a regular check is made to determine whether the current exceeds the maximum allowable value and, if it does, the switch is opened for a short time.

The new values of T_a and T_b are calculated within the time between the opening of the switch and the reception of a new interrupt, because here the processor has no other tasks, as shown in fig. 3.2.2.

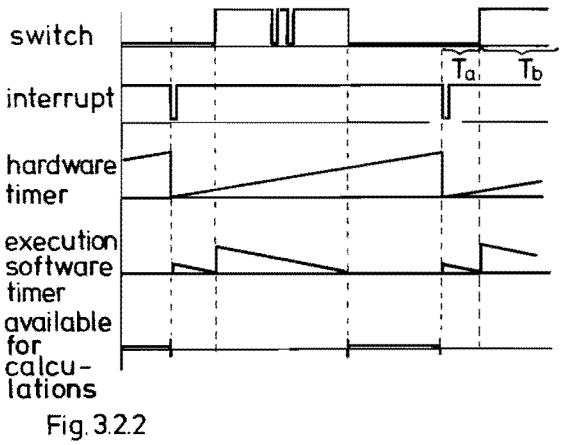

Fig. 3.2.2. Time available for calculations.

Start procedure

We now turn to the starting of the motor. Let us suppose that the rotor is in line with the stator poles at standstill. Excitation of the coils is of no use, because the rotor will remain in line and will not rotate. To ensure that this situation does not occur we propose placing two permanent magnets in the stator bore, which give the rotor a defined position at standstill, as shown in fig. 3.1.1. Excitation of the coils at standstill will always produce an initial rotation clockwise. It will be the task of the start procedure to accomplish a good start, a good start meaning that the rotor starts rotating in the desired direction from the very first moment.

After the command to start the motor the program has to check whether the rotor is rotating. If it is, then the speed has to be determined by measuring the time between two successive interrupt pulses and a jump has to be made to the part of the program pertaining to this speed (see fig. 3.2.3). This check is necessary because the rotor position will be unknown, which means that the behaviour of the motor will be unpredictable when the procedure for a start from standstill is used in the case of a rotating rotor.

When no rotation is found, a number of required variables, e.g. $T_{b,1}$, $T_{a,2}$ and $T_{b,2}$, are given their initial values and the switch is closed for the time $T_{b,1}$ (see fig. 3.2.4). The time intervals mentioned above are values found from experiment, which result in a maximum acceleration for the motor used. In chapter 6 we give a description of the experiments leading to a maximum acceleration.

The switch will be opened a short time if the current exceeds the maximum allowable value. The value of $T_{b,1}$ is such that in practice the rotor has reached the position where the sensor produces an interrupt when the interval $T_{b,1}$ is

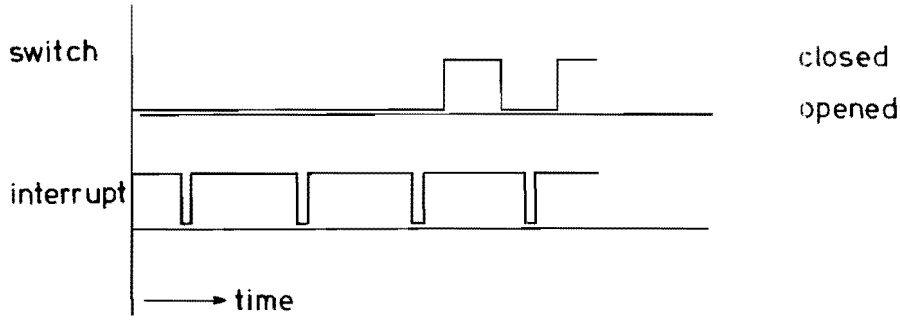

Fig. 3.2.3. Rotating rotor at the start.

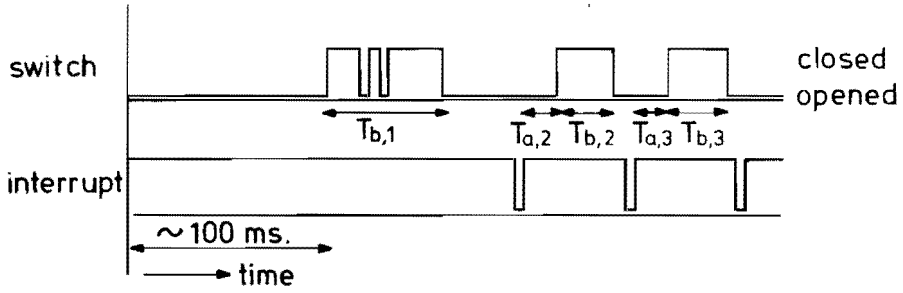

Fig. 3.2.4. Start from standstill.

passed. Once the interrupt is received, then the switch remains open for the time $T_{a,2}$ and is closed again for the time $T_{b,2}$.
The same time values are used again after the reception of the second interrupt ($T_{a,3} = T_{a,2}$ and $T_{b,3} = T_{b,2}$). After the third pulse a "table look-up" procedure is used to obtain new values for T_a and T_b by means of the measured time between the preceding interrupts. This will be repeated every five interrupt pulses until the time interval is less than 2.56 ms (corresponding speed: 11 720 r.p.m.).

Supposing a very fast acceleration of the rotor in the case of a small load torque, the interrupt will occur at an earlier moment than expected by the program, e.g. in the time interval with a closed switch or within the time taken to calculate new values of T_a and T_b. We distinguish between two situations, namely when this phenomenon occurs during the two start pulses and when it occurs in the time afterwards.

$T_{b,1}$: open switch, replacement of the predefined $T_{a,2}$ by $T'_{a,2} = T_{a,2}$-1.28 ms and $T'_{b,2} = T_i/2$ (see fig. 3.2.5).

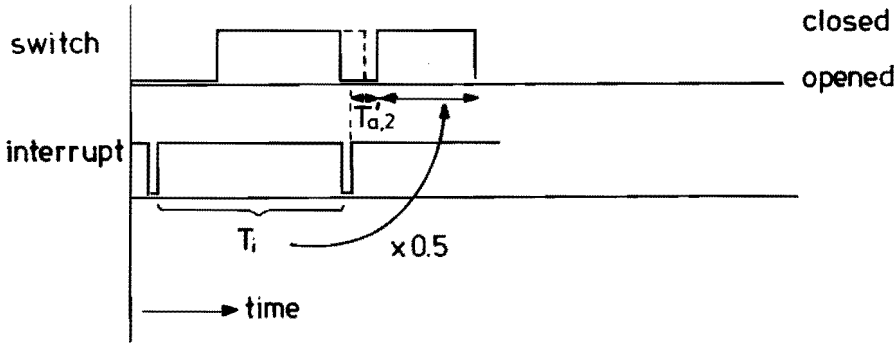

Fig. 3.2.5. Reception of an interrupt within the time interval $T_{b,1}$.

$T_{b,2}$: open switch, replacement of the predefined $T_{a,3}$ by $T'_{a,3} = T_{a,3}$-1.28 ms and $T'_{b,3} = T_i/2$.

$T_{c,1}$: open switch, replacement of the predefined $T_{a,2}$ by $T'_{a,2} = T_{a,2}$-1.28 ms and $T'_{b,2} = T_i/2$.

During the start we cannot afford the loss of a pulse for the electronic switch, because this increases the risk of a stillstanding rotor. The control program has to obtain new values of T_a and T_b by using the available information and this has to be realized in a minimum of time, because the processor has also the task of guarding the T_a by means of a software timer. So a calculation requiring a long execution time is not possible.
As the speed is higher than expected, the new time interval T_a has to be smaller than the predefined value; the same argument holds for the pulse width. The actions mentioned above are crude, but they require a minimum of time.

When an interrupt occurs within the following intervals the program proceeds to:

$T_{b,n}$: open switch and
for $T_{a,n} > 2.56$ ms - $T_{a,n+1} = T_{a,n}$-1.28 ms, $T_{b,n+1} = T_i/2$
for $T_{a,n} < 2.56$ ms - new calculation for $T_{a,n+1}$ and $T_{b,n+1}$

$T_{c,n}$: new calculation of $T_{a,n+1}$ and $T_{b,n+1}$ (see fig. 3.2.6).

The aim of these procedures is to ensure that the interrupt is not received at a wrong moment a second time.

It is possible that the first pulse will not start the motor properly. To increase the certainty that the motor will start, the first pulse is repeated when the time between the first closing of the switch and the reception of an interrupt exceeds a

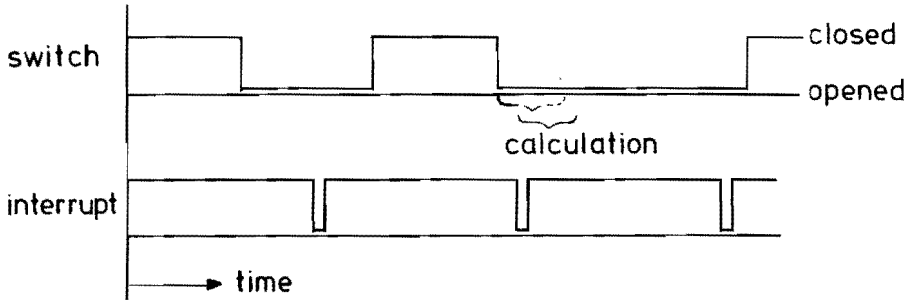

Fig. 3.2.6. Reception of an interrupt within the time taken up by calculations.

maximum value. The start pulse is also given when the time between successive interrupts exceeds that value. This check is built into the timer overflow routine, which will be discussed later on in this section.

Speeding-up

Adaptation of T_a and T_b, instead of after every five pulses, takes place every 32 pulses when the time between the two preceding interrupts is less than 2.56 ms. The reason for this number of 32 pulses is that the microprocessor requires more time than is available for the execution of the "table look-up" procedure at very high speeds (e.g. 60 000 r.p.m.). When in this case the interrupt is received during the determination of T_a and T_b, the switch remains open until a new interrupt is received. Meanwhile the "table look-up" procedure is executed (see fig. 3.2.6.), so one pulse in 32 might be absent.

Adaptation every 32 pulses gives rise to a delay time in the control loop, because the actual values of T_a and T_b belong to the speed measured between 2 and 33 interrupt pulses ago. An increase in delay time in a control loop leads to unstable behaviour. The critical value of the delay time depends on the transfer function of the other components in the loop (see ref. [8]). We found by experiment that the number of pulses should not be higher than 32 for our motor and control program.

Timer

The on-board timer of the processor has the task of measuring the time that elapses between two successive interrupts. The content of this timer is increased automatically one step every n cycles of an oscillator connected with the processor. The number of cycles is determined by some hardware components connected with the processor. Starting and stopping of the timer are coupled with the reception of an interrupt by means of some instructions in the program. An overflow of this 8-bit timer sets the timer overflow flag and creates a timer overflow interrupt. When this interrupt is acknowledged the flag will be reset and

a subroutine will be executed, which increases a variable (the overflow counter) by one step. So the time between two interrupts is found by reading the contents of the timer, the overflow counter and the timer overflow flag. The flag has to be tested, because the timer overflow interrupt is not acknowledged under all conditions. In this way the 8-bit timer is extended to a 16-bit timer, which offers sufficient resolution at high speeds and with a range which is also suited to the low speeds at the start. When an overflow occurs a check is made to determine whether the number of the overflows received exceeds a maximum allowable value. Assuming that the rotor stands still when this last value is passed, the program begins again with a new start pulse.

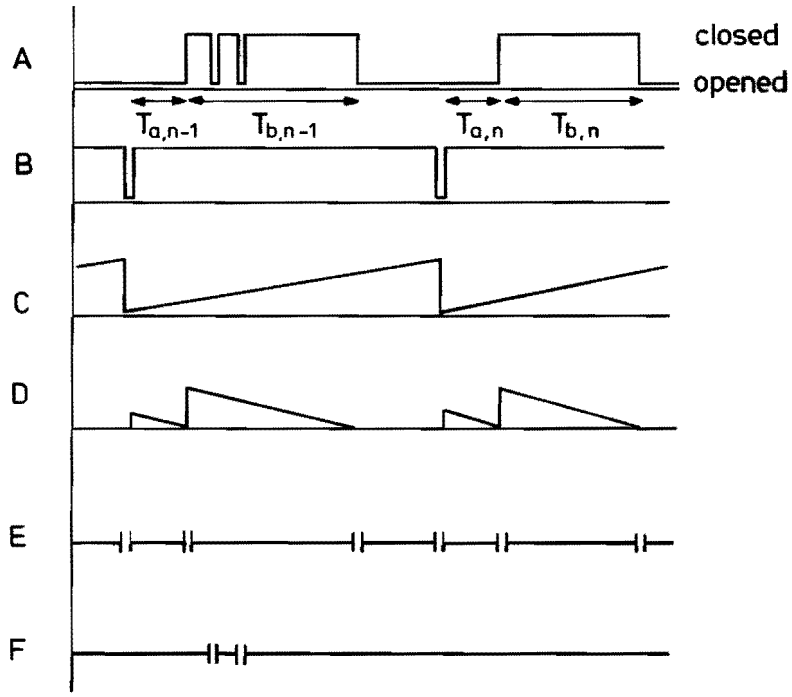

A : switch
B : interrupt
C : timer 1
D : timer 2
E : time taken for servicing counter and switch
F : time taken for current protection

Fig. 3.2.7. Time available for calculations when the 8051 is applied.

8051 versus 8048

The more recent type 8051 processor has two 16-bit timers and two external interrupt inputs; the use of this processor would result in a time diagram as shown in fig. 3.2.7, which should be compared with the time diagram of the 8048 given in fig. 3.2.2. With the 8051 far more time remains available for determining T_a and T_b, because the task of guarding the times T_a and T_b is performed by the second timer. The signal of the current sensor might be connected with the second interrupt input. In that case the time given by || is claimed by the motor control. Therefore when more functions have to be implemented (e.g. for a display or other control functions) we advise the use of this processor. Since our aim up to now is simply to control the motor, we use the 8048 processor, especially because it costs about 70 % less to produce than the 8051.

3.3. Program

This section gives a detailed description of the control program for the 8048. To control the motor we need integer variables with a range from 0 to 65535, which in terms of a microprocessor means 16-bit variables. The 8048 is an 8-bit processor and to get 16-bit numbers we had to split the numbers into two parts, e.g. $T_a(1)$, $T_a(2)$ and $T_b(1)$, $T_b(2)$. Each second term represents the most significant part.

The following relations exist between the variables used in the preceding section and the variables we will introduce now:

$$\{T_a(1) + 256\,T_a(2)\} * 5\,\mu s = T_a \qquad 3.3.1$$

$$\{T_b(1) + 256\,T_b(2)\} * 5\,\mu s = T_b \qquad 3.3.2$$

$$\{T(1) + 256\,T(2)\} * 10\,\mu s = T_i. \qquad 3.3.3$$

Figs. 3.3.1 ... 3.3.6 present the flowchart of the program and fig. 3.3.7 gives the list of symbols used. Two timers are used in the program, namely the hardware timer of the microprocessor and a program loop (WAIT procedure). The time measured by the hardware timer is given by:

$$\{(\text{timer}) + 256\,(\text{OVF} + \text{TF})\} * 10\,\mu s, \qquad 3.3.4$$

where (timer) means the contents of the 8-bit timer, OVF the contents of the 8-bit extension and TF the timer overflow flag (see section 3.2). It is the divider, placed between the clock and the timer input of the processor, that determines the time 10 μs (see chapter 5). The execution time of the WAIT procedure is:

$$\{T(1) + 256\,T(2)\} * 5\,\mu s. \qquad 3.3.5$$

0003	JUMP INT	external interrupt
0007	JUMP TOF	timer overflow

Fig. 3.3.1. Interrupt table.

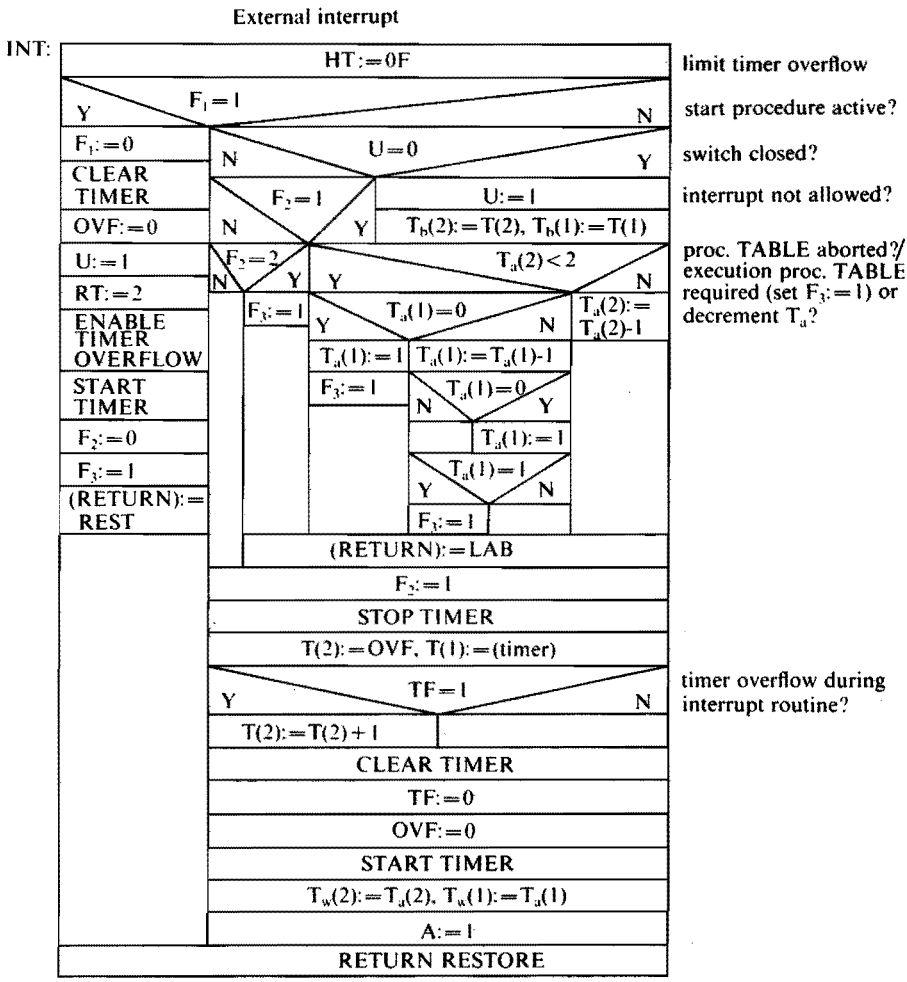

Fig. 3.3.2. External interrupt routine.

We start with the external interrupt and the timer overflow interrupt. The microprocessor is allowed to acknowledge an interrupt when this interrupt is enabled and the instruction in progress does not belong to an interrupt service routine. Once the interrupt is acknowledged, then the processor will stop the program under execution, store on the stack the address of the next instruction and make a call to location 0003 for an external interrupt and to 0007 for a timer overflow interrupt (see fig. 3.3.1). On these addresses the service routines start. These routines have to be terminated with a RETURN RESTORE to indicate the end of the service routine, which means that new interrupts might be acknowledged and the interrupted program has to be continued.
For our application we need the facility that the program continues at a different location when errors occur , e.g. when the external interrupt is received with a closed switch. This is possible by changing the stored address on the stack, which is indicated in the flow chart with: (RETURN):= .... (see ref. [9]).

Due to the interrupt mechanism of the processor used the pulse length of the interrupt should be longer than the time taken to execute the timer overflow routine. The background of this requirement is that the processor does not acknowledge an external interrupt received during the execution of the timer overflow routine. Further the length should be shorter than the execution time of the interrupt service routine. If it is not, the still pending interrupt signal will be interpreted as a new interrupt when the execution of the interrupt service routine is ended. This will lead to a wrong measurement of the speed of the motor.

Starting with the external interrupt routine INT (fig. 3.3.2), we meet the statement: HT = 0F. This means that when 15 timer overflows occur before a new interrupt is received, the program has to be restarted at BEG in the Main program (see fig. 3.3.3 and 3.3.4), because the velocity of the rotor is too low.

When the flag F_1 equals one, an external interrupt is received in the observation time of 100 ms (see Main program), which means that the rotor is already moving at the start of the program. In this case the timer is started from zero, and $F_2 := 0$ and $F_3 := 1$ indicate that the TABLE procedure has to be executed after the reception of a new external interrupt to get the proper values for T_a and T_b belonging to the actual speed.
If the flag F_1 equals zero, then the state of the switch is tested by means of the variable U. If the switch is open ($U = 1$) and the external interrupt is expected by the program ($F_2 = 0$), then the interrupted program will be continued after storage of the value of the timer, the variable OVF and a test of the overflow flag TF. Otherwise something was wrong and after the execution of RETURN RESTORE the processor has to continue with the instructions, starting at LAB.
The following errors are possible:

- interrupt while the switch was closed ($U = 0$);
- interrupt within the time T_a ($F_2 = 1$);
- interrupt during execution of the TABLE routine ($F_2 = 2$).

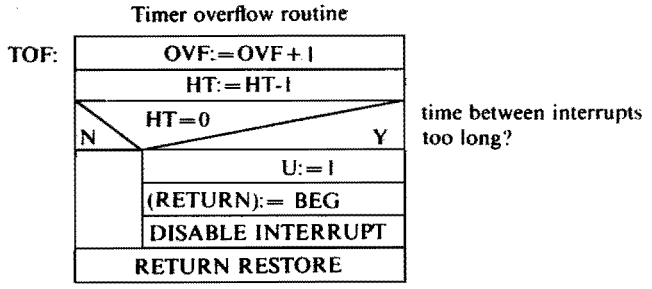

Fig. 3.3.3. Timer overflow routine.

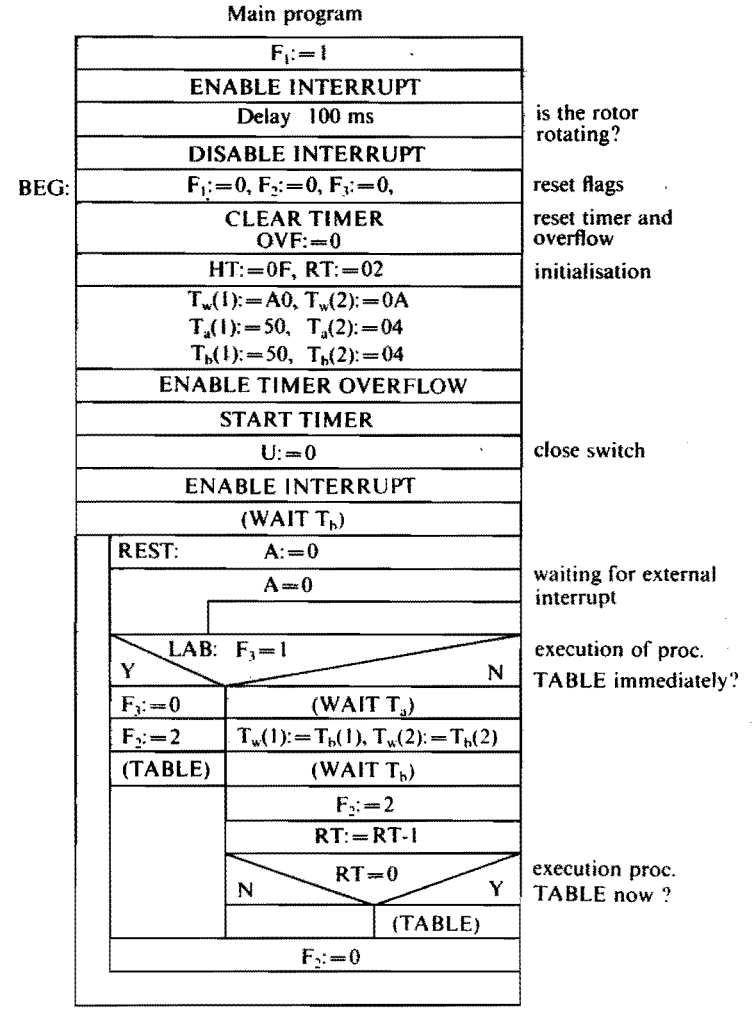

Fig. 3.3.4. Main program.

In the flowchart the corrections belonging to a certain error are given. The flag F_3 is set to one when a decrease of T_a only is supposed not to be sufficient.
For the case $F_3 = 0$ the elements of T_w are given the correct values, which determine the time between the interrupt and the closing of the switch. When $F_3 = 1$, then T_w gets the final values in the TABLE procedure.

We draw attention to the statement A:=1 at the end of the external interrupt routine, because this statement will be important when the instruction (RETURN):=LAB is not executed, which means that no error is found. This will be treated later on.

The main program starts with a delay of 100 ms to see if the rotor is moving. If no external interrupt (the signal from the sensor) is received, the processor continues with the initiation of some variables. RT=02 means that after every two interrupts the TABLE routine has to be executed to get new values for T_a and T_b. The length of the first pulse T_w, the time between the first interrupt and the second pulse (T_a) and the length of the second pulse (T_b) are set. Sequentially the timer is started, the switch closed and the WAIT routine executed during the time interval T_w. In the latter routine the current overload protection is implemented, which opens the switch when the current is too high. At the end of the WAIT routine the switch is opened.
Returning to REST, the processor waits for an external interrupt by repeating a short loop, which tests whether the variable A equals zero.
This loop is left for a short time after the reception of an external interrupt, because the processor has to execute the external interrupt routine. In this routine the value of A is changed to one, as mentioned before. Returning from the service routine it is found that A=1 and the loop is left.
The program waits for the time given by T_a and sequentially the switch is closed for a time given by the new values of T_b. Depending on the decremented value of RT, the TABLE routine is executed before the processor continues the program with the instructions starting at REST.

If the interrupt is received e.g. while the switch is closed, the program will be continued at LAB also. In this case the flag F_3 equals one when correct values for T_a and T_b are not available and then the TABLE routine will be executed.

RT determines the number of external interrupts that has to be passed before a new combination of T_a and T_b is calculated. The value of RT at the start was two. This variable becomes five the first time the TABLE routine is executed and finally, when no timer overflow occurs, the value is changed to 32 (=&H20).

The task of the TABLE routine is to get proper values for T_a and T_b, belonging to the actual values of T(1) and T(2), which are related to the speed. If no timer overflow has occurred (T(2)=0), two elements of the TAB array are selected. If T(2)<>0 then four values are selected and transferred to the elements of T_a and T_b.

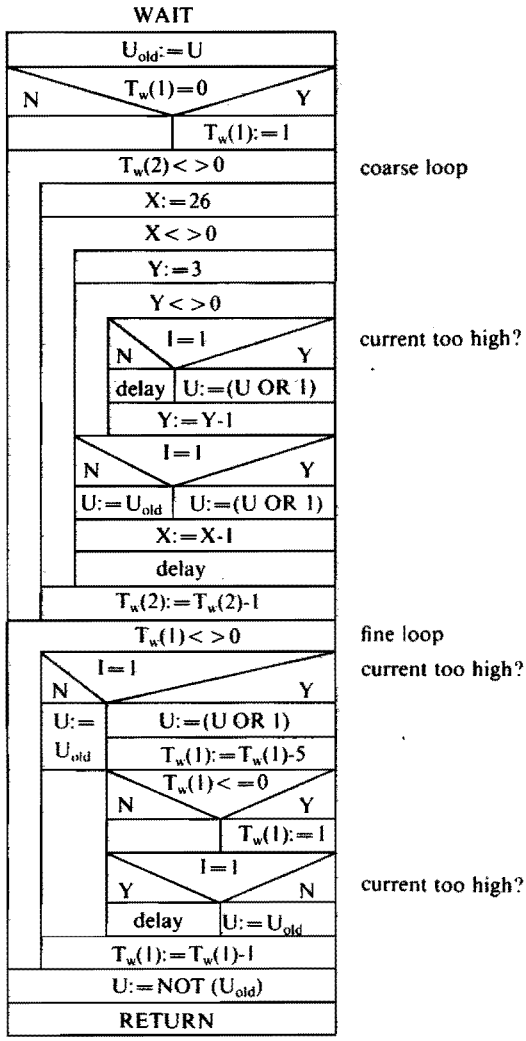

Fig. 3.3.5. ***Wait procedure.***

With the contents of the TAB array the torque-speed relation of the motor is determined. Additional arrays have to be added to the program if an application requires several torque-speed relations. A particular torque-speed curve can be selected in this casse by placing a certain value on an input port, which has to be read by some additional instructions in the TABLE routine to select the correct array.

TABLE

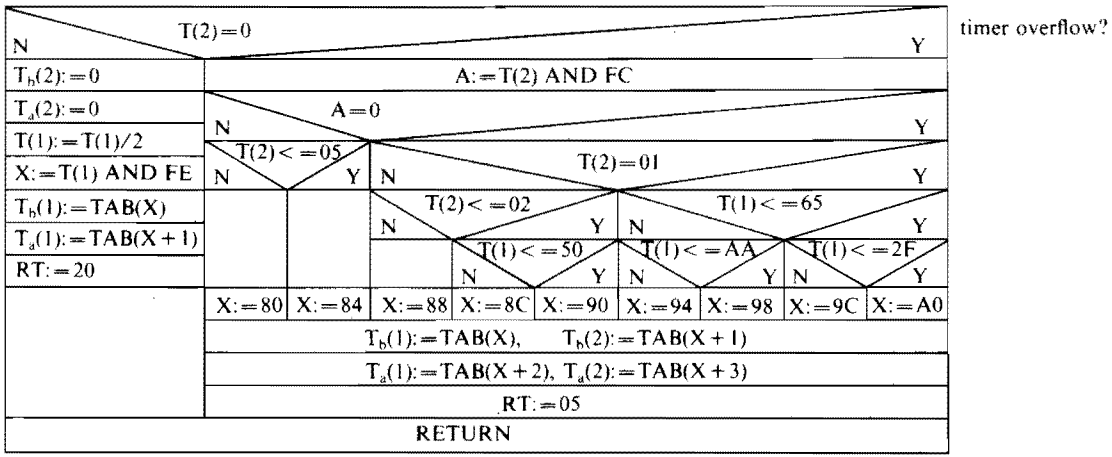

Fig. 3.3.6. Table procedure.

3.4. Conclusions

The program described in this chapter performs the following tasks: it determines the correct moment for opening and closing the electronic switch;

- it accomplishes a start from standstill and a good restart when the rotor is still rotating;
- it protects the power electronics against too high currents.

The program developed allows the use of a sensor that gives just two pulses per revolution, and if an application requires another torque versus speed curve than the one implemented, it is only necessary to reprogram a table stored in the processor.

As a concession to the program, we had to add to the motor two permanent magnets to give the rotor a well-known position at standstill to accomplish a good start.

Symbols		
		Condition
Flags:	$F_1 = 0$	Start from standstill
	$F_1 = 1$	Start with moving rotor
	$F_2 = 0$	Interrupt allowed
	$F_2 = 1$	Interrupt not allowed
	$F_2 = 2$	Interrupt during execution of TABLE subroutine
	$F_3 = 1$	Execute TABLE subroutine
	TF = 1	Pending timer overflow
Input:	I = 1	Current exceeds maximum value
Output:	U = 0	Switch closed
	U = 1	Switch opened
Variables:	X,Y,A	Temporary variables
	TAB	Array, stored values of T_a and T_b
	T	Array, time between interrupts
	T_w	Array, used for WAIT subroutine
	T_a	Array, switch-on time
	T_b	Array, pulse width
	OVF	Counter, number of timer overflow
	HT	Counter, guards OVF
	RT	Counter, number of interrupts to be passed before adaptation of T_a and T_b in the TABLE subroutine
	U_{old}	Temporary variable

Fig. 3.3.7. Symbols used in control program.

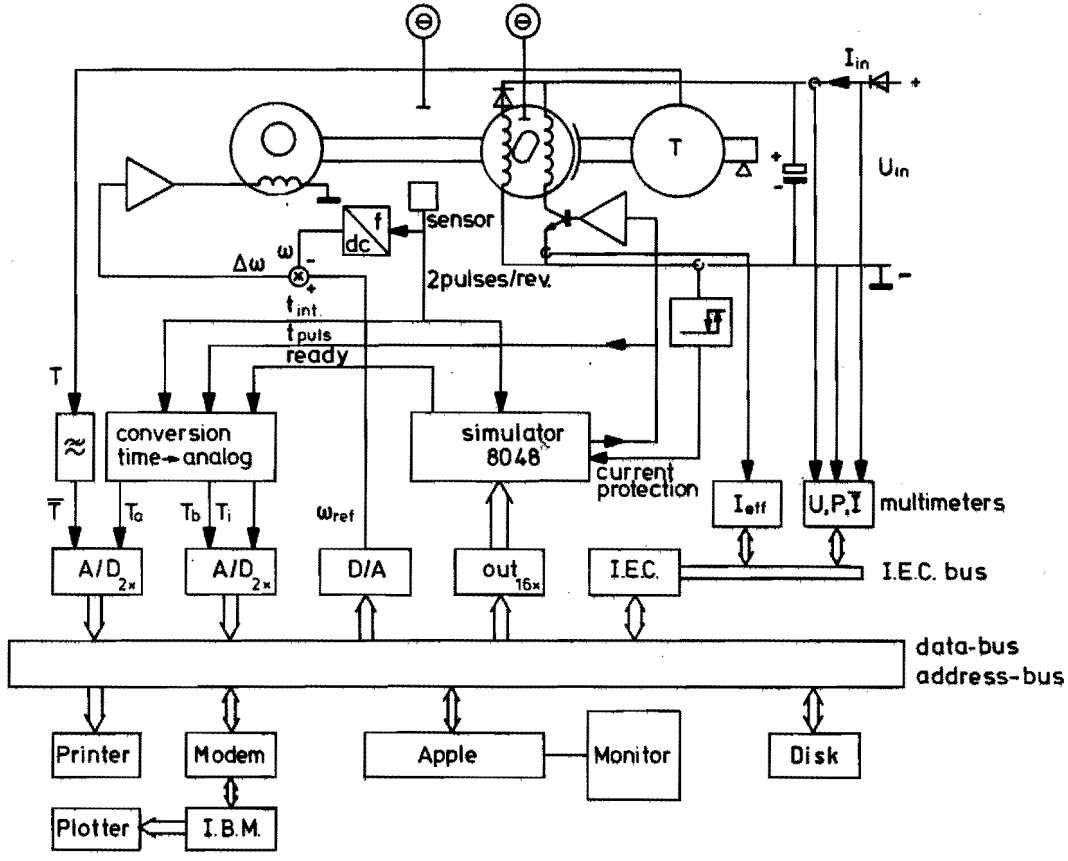

Fig. 4.1.1. Automated test rig.

4. Measuring equipment

In chapter 2 we used a method of calculation to describe the influence of the control variables α and β on the torque and efficiency of a reluctance motor and we compared this influence with the results of measurements.
This chapter deals with the equipment used.

The purpose of the measuring equipment is to measure the torque and efficiency of a single-phase reluctance motor at a fixed speed, fixed supply voltage and at a number of switch-on and switch-off angles. Changing these variables leads to a large number of measurements and data. We have automated the whole test procedure and the processing of the results to reduce the time required for the measurements and thus bring forward the moment when figures become available which describe the behaviour of the motor, and also to minimize the chance of measurement errors.

Fig. 4.1.1 shows the complete measuring equipment, in which a microcomputer accomplishes the tasks of general controller and administrator. We chose an Apple II computer, because the required hardware, e.g. digital-to-analog and analog-to-digital converters and parallel input/output ports , were available for this computer. All the measured data are stored on a magnetic disk and when a measurement at a certain motor speed is finished the data are sent to another computer (in our case an I.B.M. computer). On this computer the software package G.P.C.P. (General Purpose Contouring Program from Calcomp) is used to make plots as given in fig. 2.3.3, which give a good impression of the behaviour of the motor at the actual speed and supply voltage.

For the microcomputer we developed a program which controls the measurements. When the required speed of the motor and the required combinations of switch-on and switch-off angles are given, the program calculates the required set-point for the speed control of the eddy current brake and calculates the width of the pulses and the length of time between the signal of the rotor position sensor and the next pulse. We will call the latter time the triggering moment. The triggering moment and the pulse width are transferred to a simulator for the processor, which contains a program similar to the motor control program described in chapter 3. A distinction has to be made between the ways in which the pulse width and the triggering moment are obtained. Instead of using a "table look-up" procedure, here we use the data placed on the input port coupled with the microcomputer.
When the control program has accepted the new pulse width and triggering moment, it sends a "ready" signal to an electronic circuit to start the conversion of the measured time between two sensor pulses (T_i), the measured pulse width (T_b) and the measured triggering moment (T_a) into analog signals. The microcomputer reads these signals by means of three 10-bit A/D converters.

The microcomputer gives the calculated set-point to the eddy current brake control when the ready signal is sent. The brake causes the reluctance motor to have the required speed by changing the braking torque. The set-point is adjusted if the measured time T_i does not agree within 1 %.

The torque of the motor is measured by means of the reaction torque on the stator to eliminate the influence of the friction of the rotor bearings. We use a torque measurement system made by Staiger-Mohilo. A low-pass filter is placed between the torque meter and the related A/D converter to obtain the mean value of the torque.
Two electronic multimeters are connected with the microcomputer by means of an I.E.C. bus, a standardized form of communication which enables the computer to select one of the functions of the multimeter and to choose the right sensitivity.

The microcomputer stores the triggering moment and pulse width, the related switch-on and switch-off angles, the measured time T_i, the mean value of the electromagnetic torque $\overline{T}$, the supply voltage U_{in}, the mean value of the supply current $\overline{I_{in}}$, the input power P, the effective current through the main coil I_{eff} and, if required, the temperature θ of the motor windings and the ambient temperature.

Subsequently the whole range of required values of α and β is scanned. When all measurements are completed, the data might be transferred to a printer to obtain a list of the data or transferred to an I.B.M. computer via a modem to get a plot of the torque and efficiency as a function of α and β for the speed and supply voltage used.

Conclusions
The equipment described in this chapter measures automatically the steady-state behaviour of the single-phase reluctance motor at a fixed speed and for a required number of switch-on and switch-off angles.
The automated measurement method used reduces the chance of errors caused by erroneous registration, and leads quite quickly to a graphical presentation that gives a good impression of the behaviour of the motor. As we have seen in chapter 2, there is a non-negligible difference between the measured and the calculated efficiency of the motor. For this reason a test rig is required to determine accurately the efficiency of the motor.

5. Electronics

We deal in this chapter with the electronic part of the motor control. In the preceding chapter we have seen that the control procedures are embodied in the program for the processor. The input necessary for this program to control the motor properly is information about the rotor position, the current through the coils and an ON/OFF signal. The output of the program is a signal to an electronic switch to open or close.
The electronic circuits we will consider in this chapter are the interfaces between the processor on the one hand and the sensors, the ON/OFF switch and the electronic switch on the other.

Fig. 5.1.1 shows the digital electronics required to start and stop the motor. The electronic switch always has to receive the command to open the switch when the motor has to be stopped. This is realized by a RESET command to the processor during more than 50 ms. Within this time the processor reaches its initial state, which includes a command to the switch to open.

The command ON also results in a RESET command during 50 ms. For our application it is important that the processor starts from its well-defined initial state with the execution of the first instruction of the program when the RESET command is stopped. In fig. 5.1.2 the signals RESET and XTAL are given when the command OFF or ON is received, as the case may be.

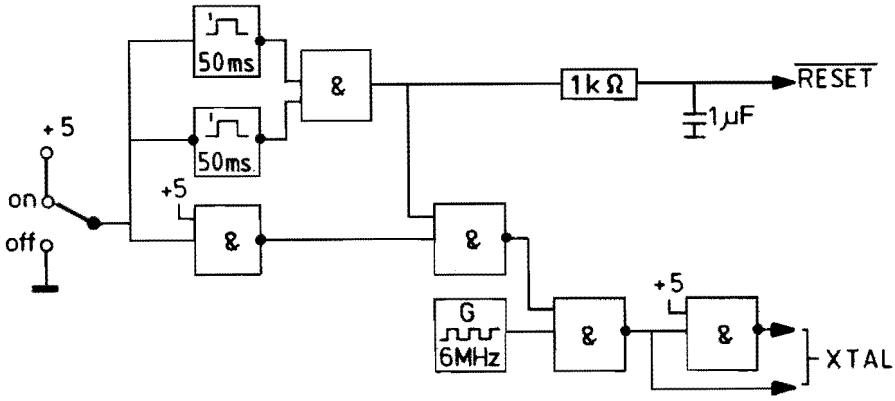

Fig. 5.1.1. ON/OFF circuit.

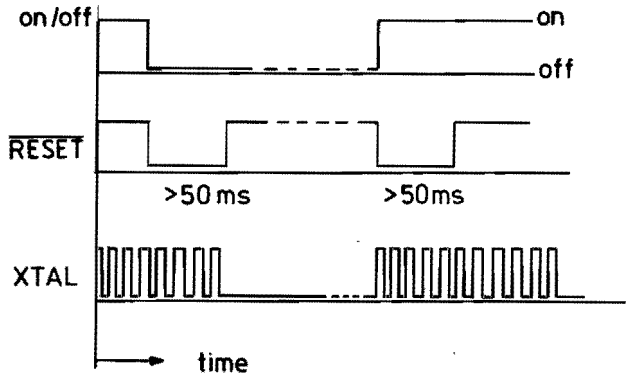

Fig. 5.1.2. The signals XTAL and RESET.

Information about the rotor position can be obtained by means, for example, of an optical sensor and a two-slotted disc mounted on the shaft, as shown in fig. 5.1.3. The given electronic circuitry produces the required number of two pulses per revolution as discussed in the preceding chapter.
An alternative sensor is a Hall element in combination with a permanent magnet (see fig. 5.1.4). This sensor is less sensitive to dust and soiling and is cheaper, but it involves accepting reduced accuracy in the position detection. For this reason we use an optical sensor in our test rig. The use of a two-pole magnet entails that on the negative and positive going edge of the sensor signal a pulse must be created by means of single-shot circuits.

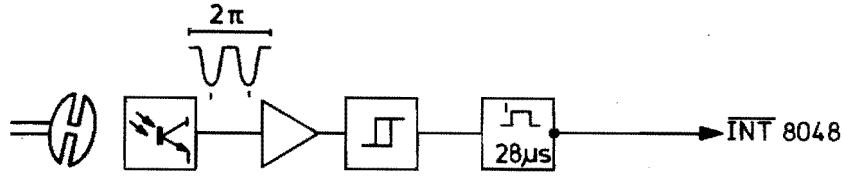

Fig. 5.1.3. Circuit for an optical sensor.

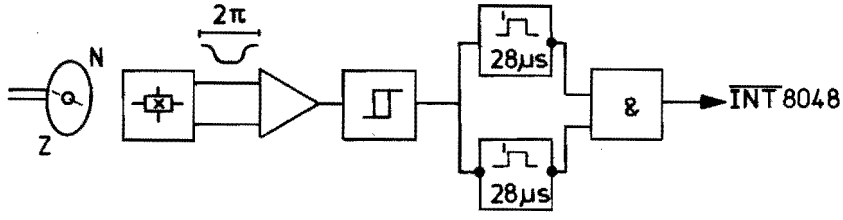

Fig. 5.1.4. Circuit for a Hall element.

The output of the sensor electronics is connected with the interrupt input of the processor. We have chosen a pulse width of 28 μs because the width has to be longer than the execution time of the timer overflow routine and shorter than the execution time of the interrupt service routine, as discussed in section 3.3.

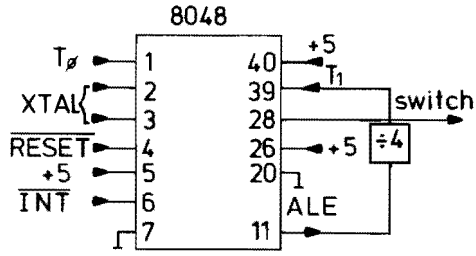

Fig. 5.1.5. The connections with the microprocessor.

The internal counter of the processor is used to measure the time between the interrupt pulses. In fact the number of pulses received on pin T1 is counted (see fig. 5.1.5) and by connecting this pin with a signal of fixed frequency we ensure that the contents of the counter will be related to the time elapsed between two interrupts. The frequency is obtained by dividing the clock frequency by 60. On the pin ALE is found the clock frequency divided by 15 and an external circuit divides this signal by 4, leading to the factor 60. Thus the counter is incremented every 10 μs with the clock frequency of 6 Mhz.

The output of the processor is the command to open or close the electronic switch. One of the pins of the data bus (pin P11) is used as output for this signal. The signal is transmitted to the power electronics part of the system by means of a pulse transformer, as shown in fig. 5.1.6. The output of the transformer consists of small pulses and positive feedback is used to ensure that these small signals lead to an open or closed switch.

A snubber circuit is connected with the collector of the power transistor to prevent damage from high transient voltages occurring during the opening of the switch. The power supply for the motor comes from the rectified mains voltage (220 V A.C.). Because of the characteristics of the circuit (see fig. 5.1.7), the power transistor should be suitable for more than twice the rectified voltage.

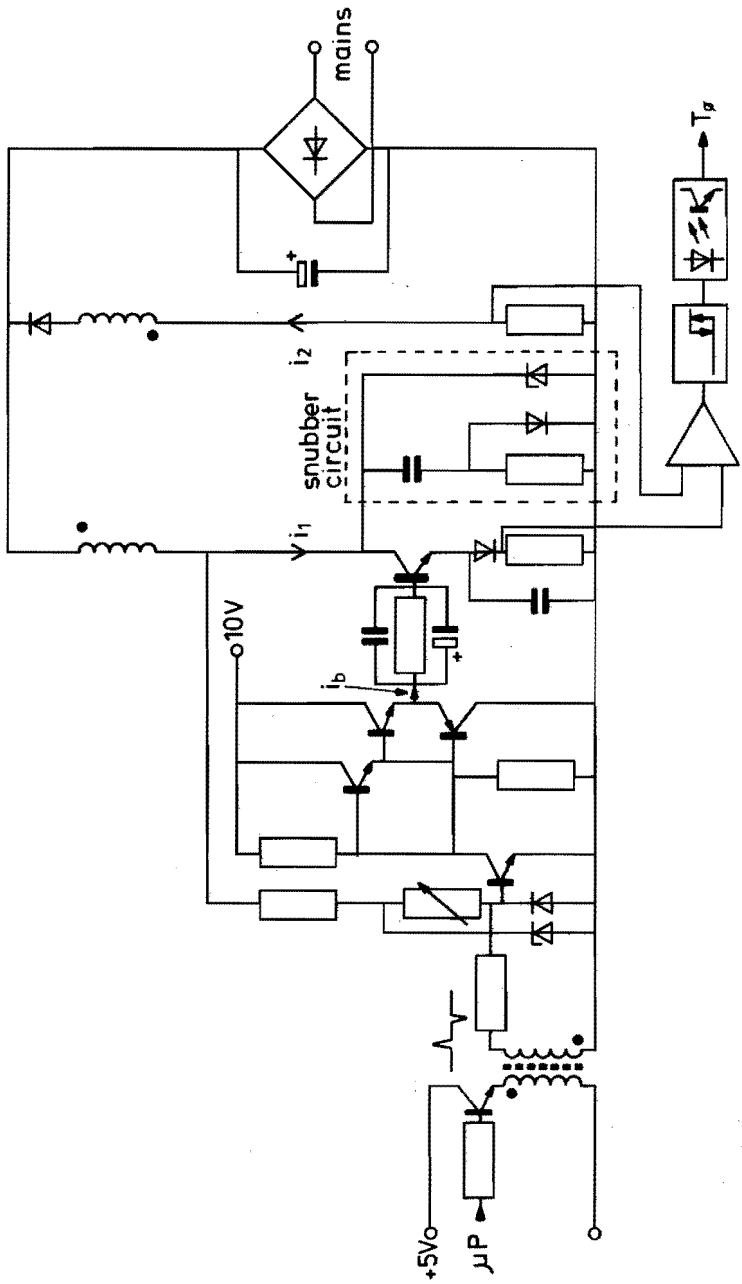

Fig. 5.1.6. The electronic power switch.

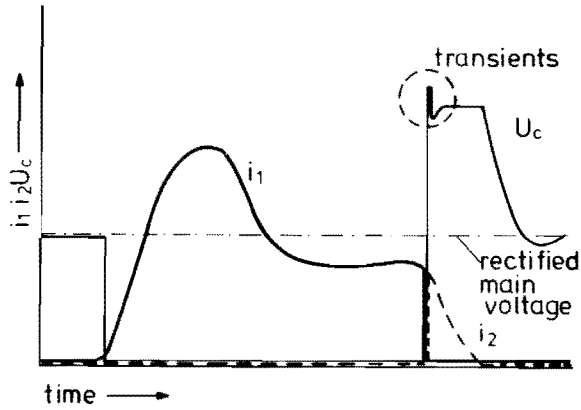

Fig. 5.1.7. The collector-emitter voltage and the currents carried by the main and catch coil.

A current sensor has been added to prevent excessively high currents through the electronic switch. Placed in series with the two coils of the motor are two resistors to measure the current. The voltage drop across these resistors is amplified and used as input for a comparator with an adjustable hysteresis. The base current of the power transistor flows through the resistor connected with the emitter of the power transistor. This current introduces an additional voltage drop. For correct operation of the current overload protection the hysteresis should have the same value as this additional voltage drop.
Pin T0 is connected with the output of the comparator and by reading the signal on this pin the processor receives an indication when the current passes the maximum allowable value for the electronic switch. The program will give the command to open the switch when this occurs. The switch will be closed again when the output of the comparator is inverted and when a time interval is passed which is determined by the control software.

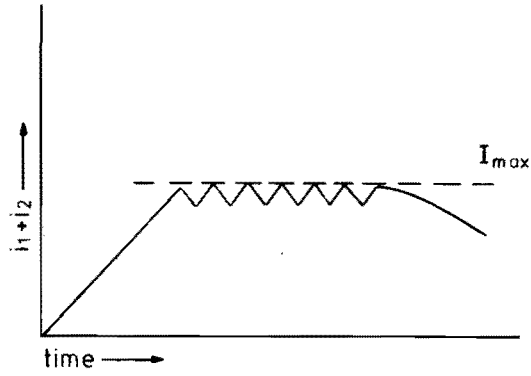

Fig. 5.1.8. The signal seen by the current overload protection.

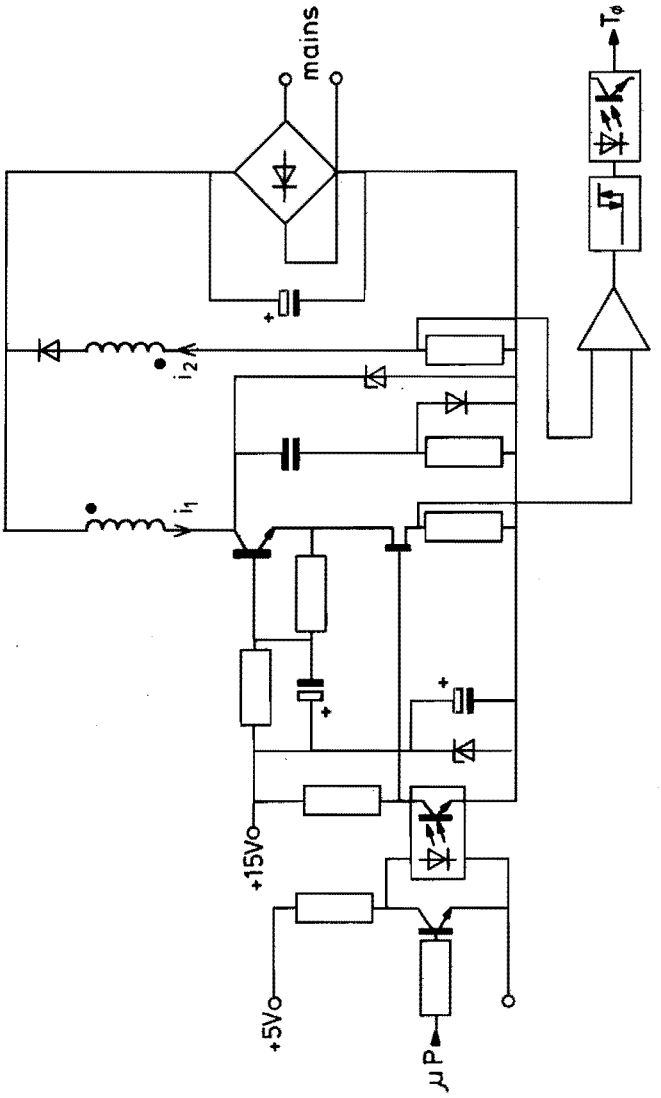

Fig. 5.1.9. The electronic power switch, using a FET.

From fig. 5.1.8 it will be clear that the chopper frequency depends only on the time interval of the control, assuming that the hysteresis of the comparator is equal to the voltage drop introduced by the base current. A smaller time interval gives a higher chopper frequency and therefore leads to higher losses in the electronic switch, due to the non-ideal behaviour of the switch, and to higher losses in the snubber circuit. These losses limit the allowable chopper frequency.

An alternative circuit for the electronic switch is given in fig. 5.1.9, where a field effect transistor (FET) is used to drive the power transistor. Fewer components are required, but it depends especially on the cost of producing the FET whether this solution is more economical. The circuits in figs. 5.1.6 and 5.1.9 require a second supply to deliver the base current of the power transistor. With a view to further development it is advisable to consider the use of a Darlington transistor as a switch to achieve a more economical control circuit without a second low voltage supply.
For domestic appliances a filter will probably have to be added behind the rectifier to prevent mains interference.

Figs. 5.1.10 and 5.1.11 give an example of the current carried by the main coil and catch coil respectively. The switch voltage waveform is given by fig. 5.1.12.

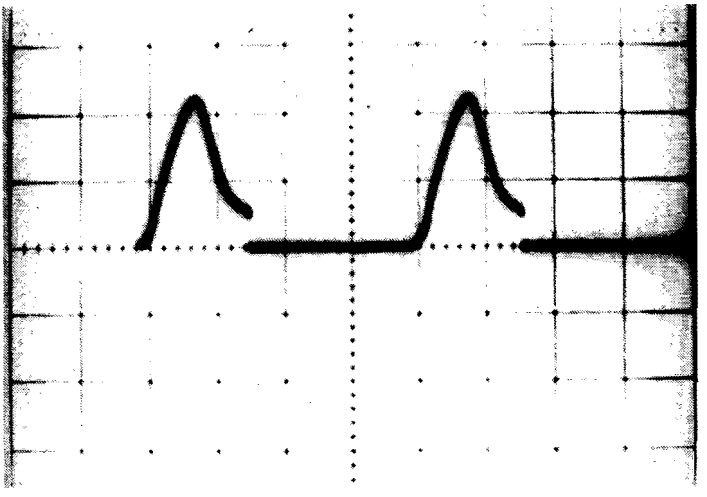

Fig. 5.1.10. Main coil current at 14 500 r.p.m., 120 V, $\alpha = 0.62$ rad and $\beta = 1.02$ rad.
Calibrations: 1.25 A/div, 0.5 ms/div.

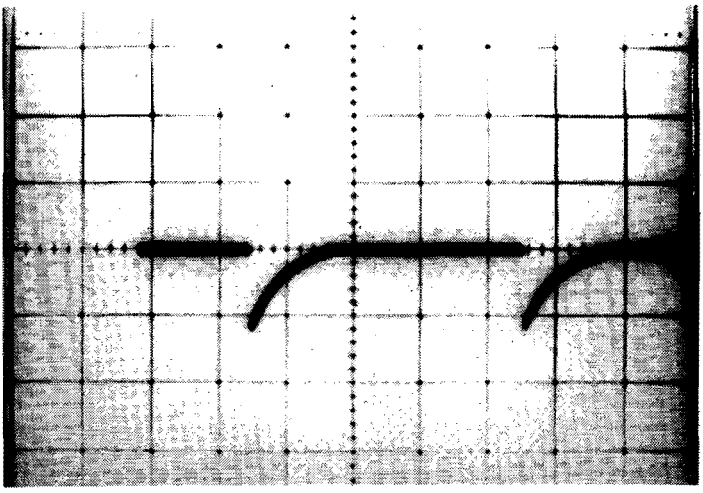

Fig. 5.1.11. Catch coil current.
Calibrations: 0.5 A/div, 0.5 ms/div.

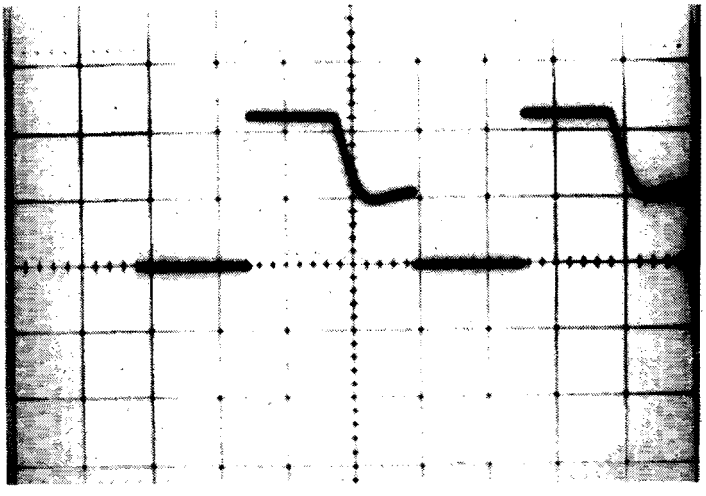

Fig. 5.1.12. Switch voltage waveform.
Calibrations: 100 V/div, 0.5 ms/div.

Conclusions

The electronics necessary to control the motor are, besides the microprocessor:

- the electronic switch;
- a circuit for the position sensor;
- a circuit for the current sensor;
- an ON/OFF circuit for the processor.

A 5 V supply is used for the digital electronics and it depends on the electronic switch used whether a second low voltage supply is required.

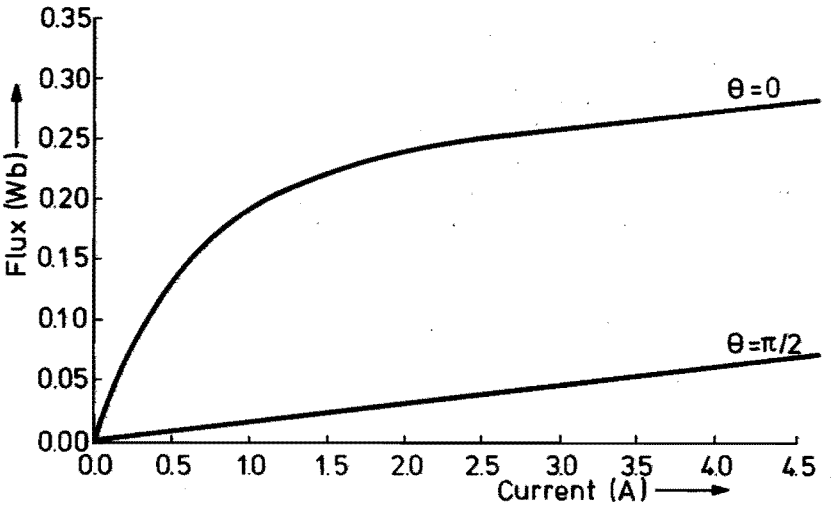

Fig. 6.1.1. Measured flux at $\theta=0$ and $\theta=\pi/2$.

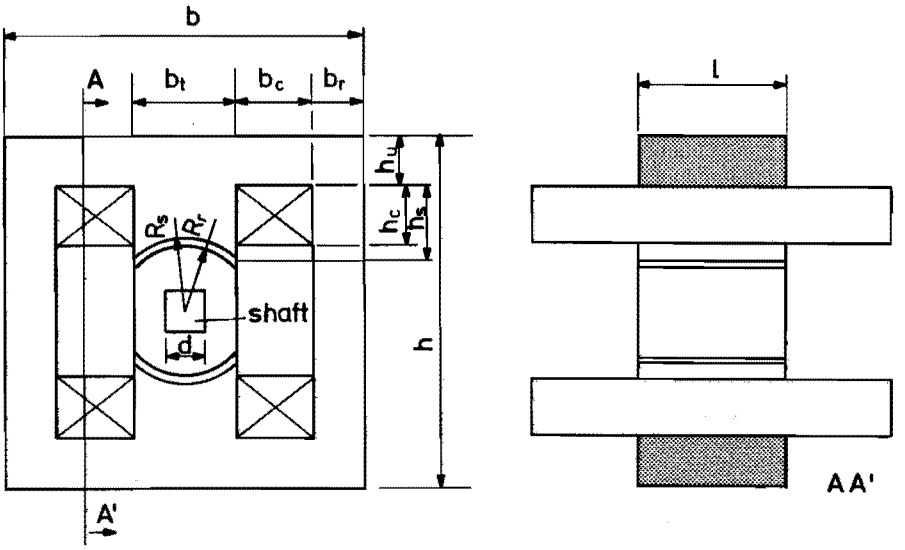

Fig. 6.1.2. Dimensions of the motor in mm.

$b=70$, $b_t=18.1$, $b_c=15$, $b_r=11$, $h_u=10$, $h_c=10$, $h_s=13$, $h=70$, $l=29.5$, $d=8$, $R_s=15.00$, $R_r=14.90$.
Number of turns of the main and catch coil: 314.
Wire diameter: 0.5.

6. Design aspects

In this chapter we will discuss a number of aspects related to the design and the control of a single-phase reluctance motor. We will not deal here with the optimization of the motor, because this depends to a great extent on the application and on the weight factor of e.g. the costs. We consider that an optimization, due to its complexity (see e.g. ref.[10]) is a separate study in itself.

The first section deals with the parameters governing the performance of the motor, in particular the flux linked with the coils and the resistance of the coils. In the second section we describe the influence of the permanent magnets. The third section presents a procedure leading to the optimum length of the first and the second pulse for the electronic switch and the optimum moment of triggering the second pulse, which largely determine the starting behaviour of the motor. The last section deals with the supply voltage.

6.1. Flux and resistance

The performance of the single-phase reluctance motor is mainly determined by the flux linked with the coils as a function of the angular position of the rotor and the current. To implement the method given in section 2.3. we need the flux for a limited number of rotor positions and current values. The required number and the values depend on the shape of the function $\Phi(i,\theta)$.
Fig. 2.3.1 shows the flux linkage of one of our experimental motors. It is obvious that a set of sinusoidal functions, depending on the rotor position, might be used as a good approximation for the linked flux. Each function is related to a fixed value of the current. We suggest the following function:

$$\Phi(\theta)\Big|_{i=\text{constant}} = \Phi_0 + \Phi_2 \cos(2\theta), \qquad 6.1.1$$

in which the values of the unknown components Φ_0 and Φ_2 depend on the value of the current. In order to obtain these unknown components we need to know the minimum and maximum value of the flux for every relevant current.

Fig. 6.1.1 shows the linked flux at $\theta = 0$ and $\theta = \pi/2$ as a function of the current measured in the motor shown in fig. 6.1.2.

The maximum values are measured for the rotor position $\theta = 0$ and we remark that the non-linearity of the relation between the flux and current is caused by the characteristics of the iron parts of the motor, namely the stator and rotor lamination and the shaft. It is interesting to note the almost linear relation between the flux and the current when the rotor stands at $\theta = \pi/2$. In order to explain this we use the equivalent magnetic network for the motor given in fig. 6.1.3. The flux linked with the two coils connected in series is given by:

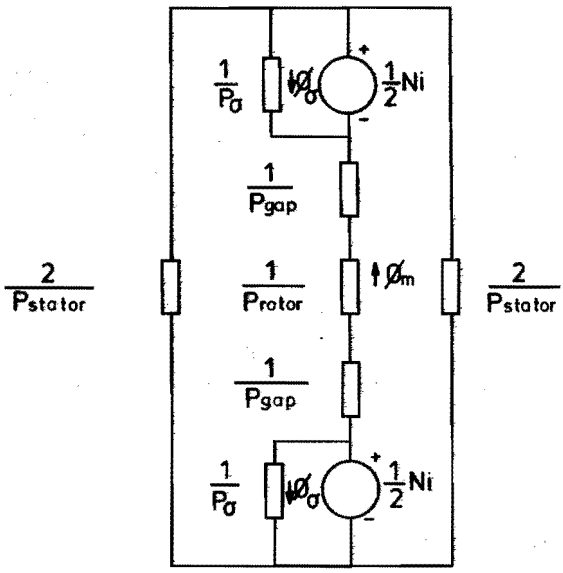

Fig. 6.1.3. Equivalent magnetic network. The coil overhang and slot leakage are represented by P_σ.

$$\Phi = 2 \cdot \tfrac{1}{2} N(\Phi_m + \Phi_\sigma) = N^2 \left(\frac{1}{\frac{2}{P_{gap}} + \frac{1}{P_{rotor}} + \frac{1}{P_{stator}}} + \tfrac{1}{2} P_\sigma \right) i. \qquad 6.1.2$$

The magnetic permeance of the two airgaps is much smaller than the permeance of the iron parts for $\theta = 0$ and the currents used (and related flux densities). This leads to the fairly linear behaviour noted.

In the following we will discuss the calculation of the flux linkage, starting with the situation $\theta = 0$. A uniform flux density in the lamination, gap and shaft is assumed and we will neglect the leakage fields (coil-overhang and slot leakage) and fringing. The calculation will show that the two assumptions lead to deviations which are acceptable for a design procedure.

Looking at fig. 6.1.2 it is obvious that the influence of the shaft should not be disregarded. We determined the permeance of the lamination on the basis of the initial magnetization curve, which we obtained by means of a ring of the laminated iron used, as shown in fig. 6.1.4. The initial B-H curve of the shaft is measured with a permeameter. The flux linked with the motor coils, calculated by means of fig. 6.1.3, is shown in fig. 6.1.5.

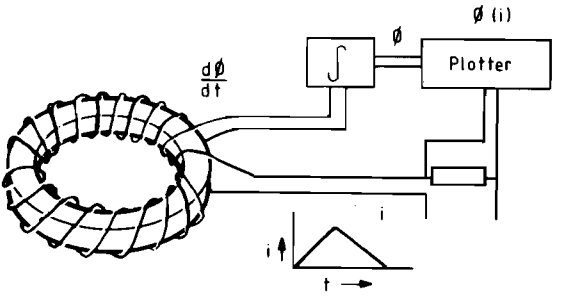

Fig. 6.1.4. Determination of the B-H curve.

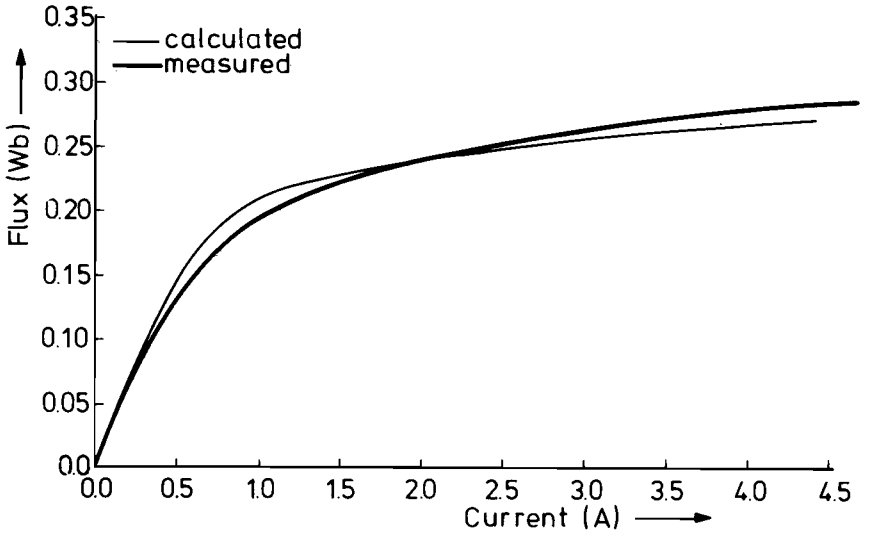

Fig. 6.1.5. Measured and calculated relation between the flux and current at $\theta = 0$.

The discrepancy at currents higher than 2 A is caused by leaving out of account the leakage fields and fringing, whose influence grows when the iron parts of the magnetic circuit are saturated. At currents lower than 2 A the discrepancy is probably caused by an unknown clearance between the shaft and the rotor lamination (see fig. 6.1.6).

We have to accept the introduction of a mechanical clearance when the material is stamped, and furthermore the clearance is increased by the manual removal of the sharp edges caused by the stamping. Supposing the respective clearances to be 40 μm and 100 μm, we get the flux curves given in fig. 6.1.7, where it can be seen that a fair agreement is found for a calculation with the latter value. It is not

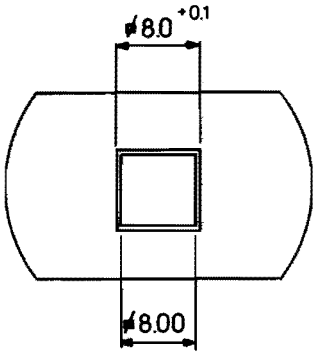

Fig. 6.1.6. The clearance between the shaft and the rotor lamination.

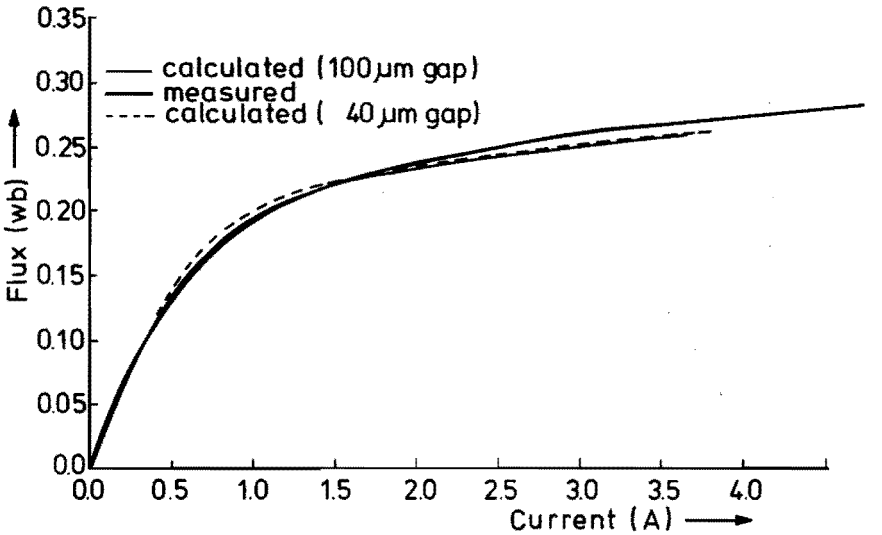

Fig. 6.1.7. The relation between the flux and the current at $\theta = 0$ after a correction for the gap (see fig. 6.1.6).

possible to measure the clearance without damaging the rotor. With another rotor we found a clearance up to 300 μm, so it is reasonable to take 100 μm as a realistic value for the mechanical clearance introduced.
We consider this method of calculation to be satisfactory for a design procedure because the discrepancy between the result of the measurement and the calculation is less than 5 % for a current higher than 2 A.

For the situation $\theta = \pi/2$ we take the permeance of the iron parts of the circuit to be much higher than the permeance of the airgap. When we split the magnetic field outside the iron parts into separate areas as shown in fig. 6.1.8 the permeance for area 1, using the symbols in fig. 6.1.9, is given by:

$$P_l = \int_{-b_t/2}^{b_t/2} \frac{\mu_0 l}{(R_s^2 - x^2)^{1/2} - b_t/2}\,dx = \qquad 6.1.3$$

$$2\mu_0 l\left[\arcsin\left(\frac{b_t}{2R_s}\right) - \frac{b_t}{2R_s}\left\{1 - \left(\frac{b_t}{2R_s}\right)^2\right\}^{-1/2}\log\left\{\left(1 - \left(\frac{b_t}{2R_s}\right)^2\right)^{1/2} - \frac{b_t}{2R_s}\right\}\right] =$$

$1.4\ 10^{-7}$ Wb/A,

assuming parallel field lines.

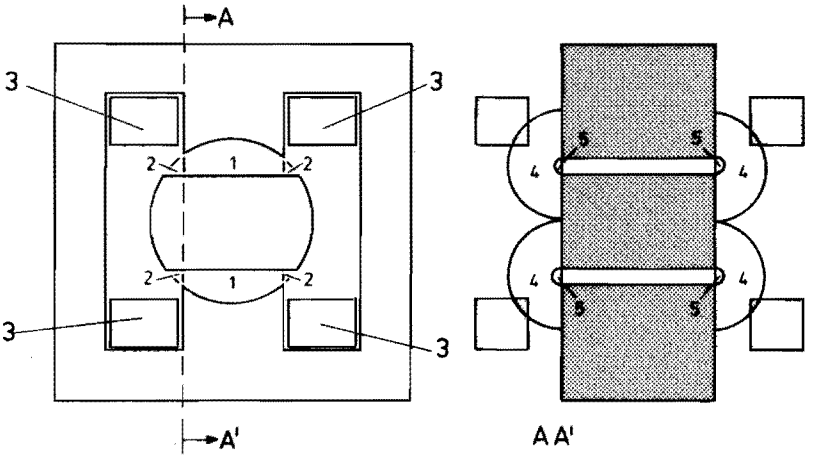

Fig. 6.1.8. Flux paths.

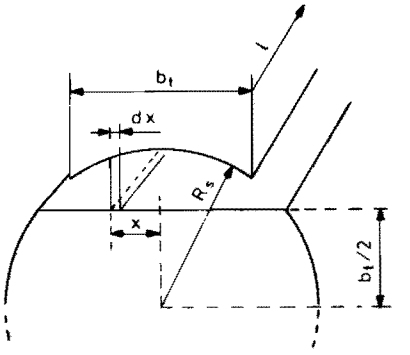

Fig. 6.1.9. Permeance calculation (eq. 6.1.3).

For area 2 we find in ref. [11], p. 134, eq. 11:

$$P_2 = 0.52\,\mu_o l = 0.193\,10^{-7}\ \text{Wb/A}. \qquad 6.1.4$$

The slot leakage in area 3 is given by (ref. [12]):

$$P_3 = \left(\frac{h_c}{3b_c} + \frac{h_s - h_c}{b_c}\right)\mu_o l = 0.1565\,10^{-7}\ \text{Wb/A}. \qquad 6.1.5$$

The inductance so far is given by:

$$L = N^2(\tfrac{1}{2}P_1 + P_2 + P_3) = 10.4\ \text{mH}. \qquad 6.1.6$$

The use of a two-dimensional field program such as MAGGY (see ref. [13]) leads to 10.8 mH. We therefore consider eqs. 6.1.3 . . . 6.1.5 satisfactory for our purpose. The areas 4 and 5 are related to the third dimension, and the permeances for these areas are as follows:

Area 4 (ref. [11], p. 132, eq. 8a and fig. 6.1.10):

$$P_4 = \int_{-b_t/2}^{b_t/2} \frac{0.64\,\mu_o}{\dfrac{(R_s^2 - x^2)^{1/2} - b_t/2}{b_t/2} + 1}\,dx = 0.64\,\mu_o b_t \arcsin\left(\frac{b_t}{2R_s}\right) = 0.09\,10^{-7}\ \text{Wb/A}. \qquad 6.1.7$$

Area 5 (ref. [11], p. 132, eq. 7):

$$P_5 = 0.26\,\mu_o\, b_t = 0.059\,10^{-7}\ \text{Wb/A}. \qquad 6.1.8$$

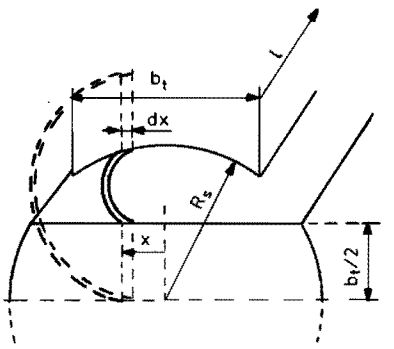

Fig. 6.1.10. Permeance calculation (eq. 6.1.7).

We were unable to find in the literature any analytical method or tables for the coil-overhang leakage in a configuration similar to our reluctance motor.
To show the importance of the coil-overhang leakage we note that eqs. 6.1.3 . . . 6.1.7 give for the inductance

$$L = N^2(\tfrac{1}{2}P_1 + P_2 + P_3 + P_4 + P_5) = 11.8\,\text{mH}. \qquad 6.1.9$$

However a measurement gives 15.7 mH. Attempts to find methods giving an upper and lower limit for the coil-overhang leakage required a large number of assumptions in order to arrive at solvable analytical equations. However the assumptions tended to increase the unreliableness of the results (see also ref. [14]) and we conclude that a reliable determination of the inductance at $\pi = \theta/2$ is only possible by using a numerical field program such as e.g. PADDY (see ref. [15]), which gave us an inductance of 15.6 mH.

Summarizing, we see that a simple method can be used to obtain the flux for $\theta = 0$. However a three-dimensional numerical field calculation program has to be used to obtain the flux at $\theta = \pi/2$. One calculation with such a program is sufficient, because of the almost linear relation between the flux and current at $\theta = \pi/2$.
The results of these calculations can be used in the program described in section 2.3 to determine the torque production of the motor in relation to the speed, supply voltage and the value of the control variables α and β.
When a final design is obtained (e.g. optimized for an acceptable combination of cost, mechanical output power and dimensions) the flux as a function of the current and rotor position can be verified by means of a three-dimensional field calculation program, such as PADDY. We advise a three-dimensional program because the neglected coil-overhang leakage and the fringing are essentially a three-dimensional field problem, as mentioned in connection with the flux determination at $\theta = \pi/2$.

An equal flux density in all the iron parts at $\theta = 0$ is used as the starting point for designing the cross-section of the yoke, stator poles and rotor. Mechanical clearances and the available stamping tools introduce small deviations.
The flux in the rotor is assumed to be carried by the shaft as well (see fig. 6.1.7), and of course one has to take into consideration that this leads to losses due to eddy currents in the solid iron shaft. We therefore consider the rotor given in fig. 6.1.11 a better design, because less flux will be carried by the shaft, entailing lower losses. The wider rotor also reduces the influence of the unknown mechanical clearance between the rotor lamination and the shaft.
As a compromise we have to accept an increase of the inductance at $\theta = \pi/2$. For this rotor we measured an inductance of 17 mH, whereas the original rotor gave 15.7 mH, an increase of approximately 10 %. As a consequence the slope of the flux line at $\theta = \pi/2$ in fig. 6.1.1 will also increase, which means a decrease of

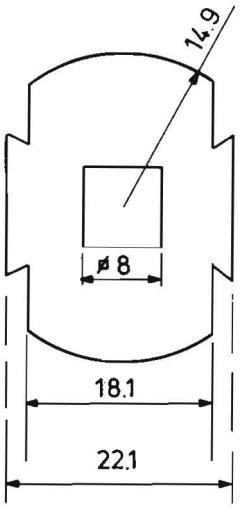

Fig. 6.1.11a. Dimensions of the wider rotor.

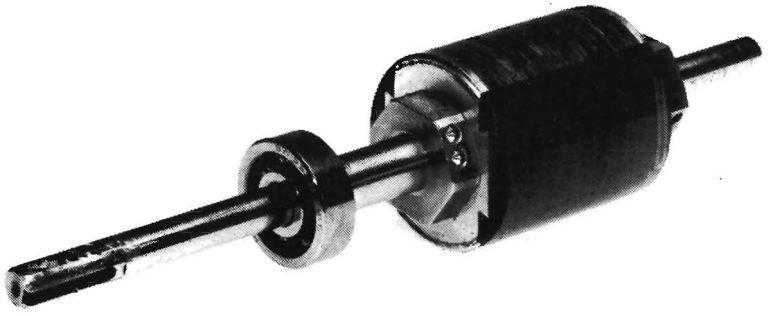

Fig. 6.1.11b. The wider rotor.

approximately 2 % for the maximum obtainable mechanical output power of the motor.
Only experiments with different rotors will provide an answer to the question of which cross-section of the rotor is optimal for a given cross-section of the shaft, because the losses in the shaft cannot easily be calculated (see the discussion at the end of section 2.3).

The airgap between the rotor and stator poles is 100 μm. A decrease of the gap will give a faster rise from $i = 0$ for the Φ line at $\theta = 0$ in fig. 6.1.1. The area between the two Φ lines increases, leading to a higher value of the maximum obtainable mechanical output power. However one should find an optimum between the price to be paid for the decreased clearance and the increased output power.
- We note that the influence of the decreased gap diminishes when saturation occurs in the iron parts of the circuit, because then the magnetic resistance of the iron will dominate.

In our design we have chosen the same width for the rotor and the stator poles (18 mm). The result in our configuration is a fairly sinusoidal relation between the flux and the rotor position at a fixed current. We note that this relation mainly determines the torque production and the current carried by the coils as a function of time.
In our motor the value of the tooth-width/tooth-pitch ratio is 0.38. In ref. [16] a ratio of 0.35 . . . 0.42 is given as optimum for the torque production. However these values relate to the static torque production in stepping motors, which have a large number of teeth per pole. As far as we know, nothing has been reported in the literature on the optimum relation between the flux linkage, rotor position and current with respect to the torque production and efficiency of the reluctance motor. A further study of this aspect is desirable.

In the reluctance motor we distinguish the bifilar-wound main and catch coils; the coils have the same number of windings and their resistances are inversely proportional to the copper cross-section. Choosing the same copper cross-section for the wire of both coils is not the optimum if we consider the dissipation. Assuming a fixed copper cross-section available for two coils, we have (see fig. 6.1.12):

$$A_{cu} = A_{cu,m} + A_{cu,c} = \alpha A_{cu} + (1 - \alpha) A_{cu}. \qquad 6.1.10$$

For the sake of simplicity we have drawn two separate coils to represent the bifilar-wound coils. Let the effective current for the main coil be I_m and for the catch coil I_c, then the dissipation is given by:

$$P(:) \frac{I_m^2}{A_{cu,m}} + \frac{I_c^2}{A_{cu,c}} \qquad 6.1.11$$

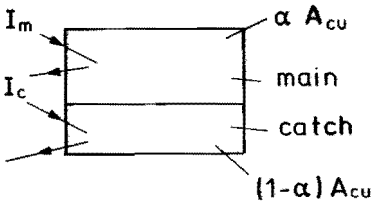

Fig. 6.1.12. Cross-section of the coils.

$N_{main} = N_{catch}$

or

$$P(:) \frac{I_m^2}{\alpha A_{cu}} + \frac{I_c^2}{(1-\alpha) A_{cu}}. \qquad 6.1.12$$

For a minimum total dissipation the ratio between the copper cross-sections is then given by:

$$\frac{dP}{d\alpha} = 0 \rightarrow \frac{A_{cu,c}}{A_{cu,m}} = \frac{I_c}{I_m}. \qquad 6.1.13$$

The result is the same current density in the wires of both coils. Looking at our experimental motor with bifilar-wound main and catch coils, we observe the effective current through the main coil to be much higher (note that the ratio also depends on the control variables and a realistic value is 5). With eq. 6.1.13 an optimum ratio of 5 is found between the cross-sections of both wires, and the theoretical decrease of the copper losses should be 31 % compared to the case with equal wires.
For the production of bifilar-wound coils a ratio of 2 is the maximum allowable value. A higher ratio will involve problems during the winding of the coils and for this reason we cannot select the optimum cross-section ratio.

For further development we suggest experiments with two coils as shown in fig. 6.1.13. These coils can be wound separately and the use of the optimum wire size ratio is possible. One should pay attention here, however, to the flux linkage between the main and catch coils, since a decreased linkage will increase the dissipation in the snubber circuit of the power electronics (see fig. 5.1.6).

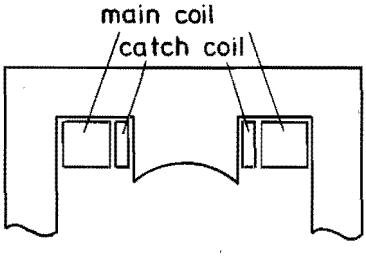

Fig. 6.1.13. Separate coils.

6.2 The permanent magnets

As has been discussed in section 3.1, we had to place two permanent magnets in the stator bore to obtain an advantageous starting position for the rotor.

Fig. 6.2.1 gives the construction with permanent magnets which we found suitable for a load with low friction at standstill (less than 5 mNm). The field of the magnets generates a torque acting on the rotor that depends on the angular position as shown in fig. 6.2.2.

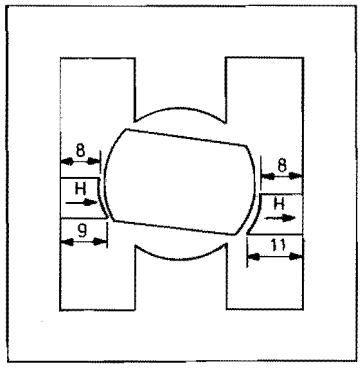

Fig. 6.2.1. Dimensions of the magnets.

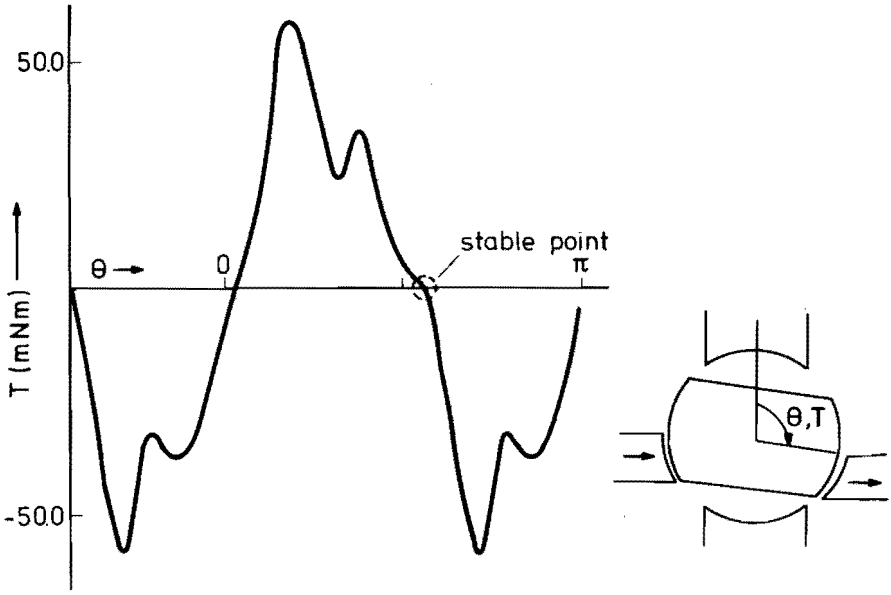

Fig. 6.2.2. The measured torque.

When a maximum speed is required after the first pulse given by the control circuitry the rotor position θ should be slightly higher than $\pi/2$, because the maximum amount of energy can then be transferred to the mechanical part when the pulse ends at $\theta = \pi$.
However a magnet configuration that leads to this starting position entails a high sensitivity to friction torques, because the friction might cause a rotor position slightly smaller than $\pi/2$, which leads to a wrong initial rotation of the rotor. Furthermore we note that the torque production of the motor is low when the rotor position is near $\pi/2$, so the rotor will not rotate when the friction is too high.
For this reason low friction is a necessary requirement with the the chosen magnet configuration. In the design of the magnets the following aspects have to be considered:

- the expected friction torque;
- the position at which the torque caused by the magnets gives a stable equilibrium;
- the slope of the torque-versus-angular-position curve at the stable point.

We are still experimenting with a view to finding solutions that would allow a load with a relatively high friction. This involves studying the influence of the dimensions, position and the direction of the magnetization of the magnets.

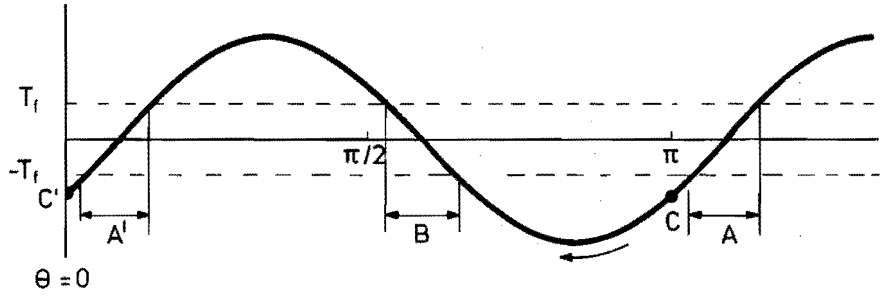

Fig. 6.2.3. A solution leading to a good starting position when the coulomb friction is given between T_f or $-T_f$ (depending on the direction of rotation).

A magnet configuration leading to the torque-angle relation given in fig. 6.2.3 is one possibility. The rotor position at standstill will be in area A or B when the coulomb friction torque is given between T_f and $-T_f$. It should be in area B to obtain the right initial direction of rotation at the start. To ensure that the rotor is at this position at the start, a limited current should be carried by the main coil. The rotor will be attracted in line with the stator poles ($\theta = \pi$ or $\theta = 0$) and subsequently the current should be switched off by the control. The torque caused by the field of the magnets will force the rotor to the required area B. The starting

procedure described in chapter 3 can be used when the rotor has arrived in area B. But, as mentioned before, this is still a subject of research.

Eddy current and hysteresis losses are introduced in the rotor and stator iron by the field of the magnets when the rotor rotates. This might diminish the efficiency of the motor compared with the motor without magnets. Furthermore since the field of the magnets is linked with the coils (see fig. 6.2.4), this leads to a change of the current through the coils as a function of time.

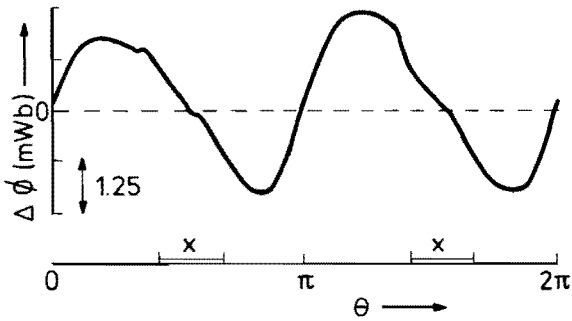

Fig. 6.2.4. Linkage between the field of the magnets and the main coil. X: closed switch (see fig. 6.2.6).

We have measured the torque and efficiency of the motor with the magnets for the two cases shown in fig. 6.2.5; the difference between the two cases is a reverse direction of the current in the coils. With an oscilloscope we measured the currents as a function of time for $\alpha = 0.22$ rad and $\beta = 1.01$ rad and a speed of 15 000 r.p.m. (see fig. 6.2.6). These curves show the influence of the flux linkage

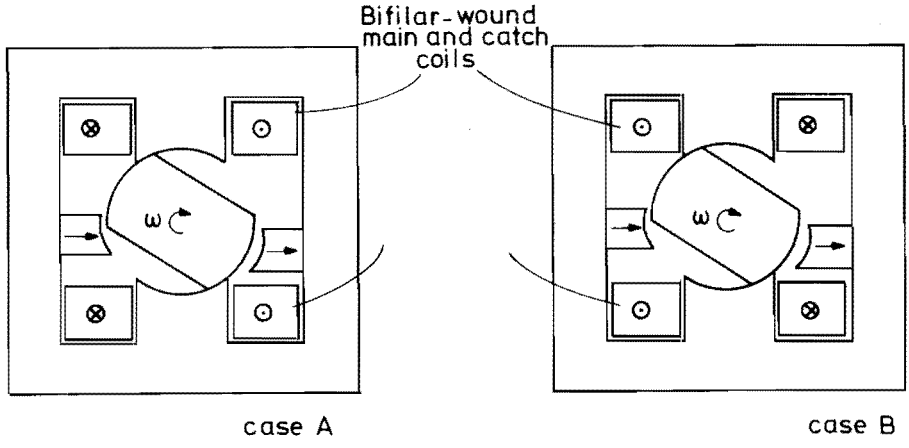

Fig. 6.2.5. Reversal of current direction.

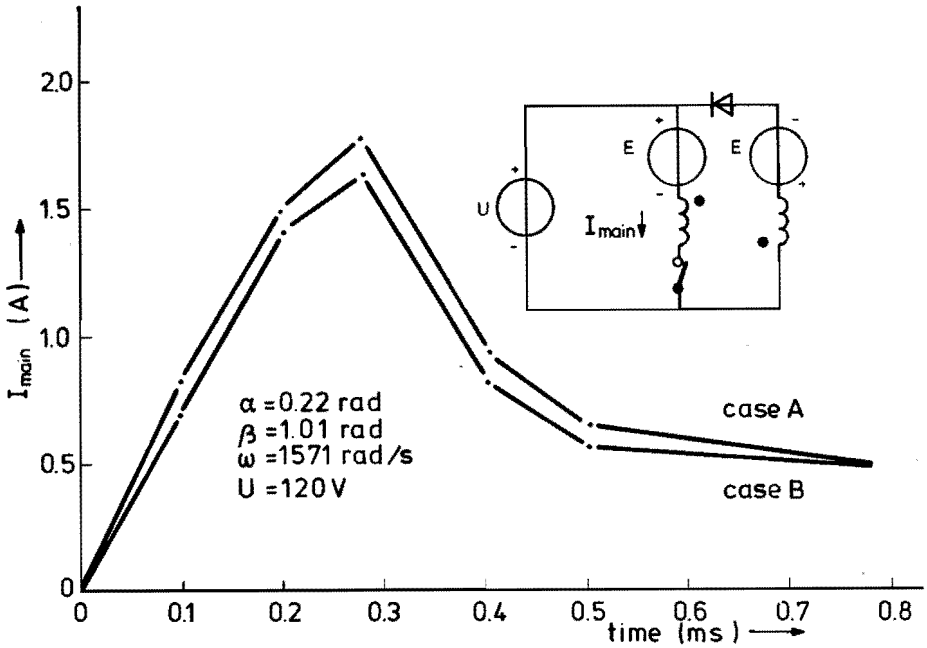

Fig. 6.2.6. Current versus time for the two situations given in fig. 6.2.5.

between the coils and the permanent magnets. The field of the magnets induces a voltage E in the coils, which is largely negative in case A and positive in case B when the rotor is in the region between $\pi/2$-0.22 rad and π-1.01 rad (see fig. 6.2.4). The maximum efficiencies obtained for a certain value of the torque produced by the experimental motor with a supply voltage of 120 V and a speed of 15 000 r.p.m. are shown in table 6.2.1.

case	**A**	**B**	**C**
torque	eff.	eff.	eff.
(Nm)	(%)	(%)	(%)
0.010	72	73	76
0.015	76	78	78
0.020	79	79	80
0.025	79	80	80
0.030	79	80	80
0.035	78	80	80
0.040	78	80	80

Table 6.2.1. Efficiencies found for a motor provided with magnets (the cases A and B) and without magnets (case C). Fig. 6.2.5 shows the difference between the cases A and B.

We emphasize that the results were obtained at different combinations of the control variables α and β. The table shows slightly higher efficiencies for case B. Column C gives the efficiencies for the case without magnets. Comparing case B with case C we see that the values of the efficiency are almost equal at torque values higher than 0.02 mNm.
A quantitative analysis of the observed phenomenon is hardly possible, due to the complex nature of the eddy current and hysteresis losses. It is nevertheless worth mentioning that the magnets do not lead to lower efficiencies in all circumstances.

6.3. The start

The single-phase reluctance motor is started by means of the two magnets mentioned in the previous section, and by a number of pulses given by the control program, as described in chapter 3. The first two pulses are especially important for the start, and for this reason we describe in this section the experiments that yield the optimum length of the first and second pulses and the optimum moment for triggering the second pulse.

We suppose that the rotor has the position given by the stable equilibrium in the torque-versus-angular-position relation, which is created by the permanent magnets (see fig. 6.2.2).
The start pulse is initiated by closing the switch, as discussed in chapter 3. The switch opens when the time interval of the start pulse has passed. The current will be taken over by the catch coil and disappear quickly. Our aim is to reach the highest possible speed after the start pulse.

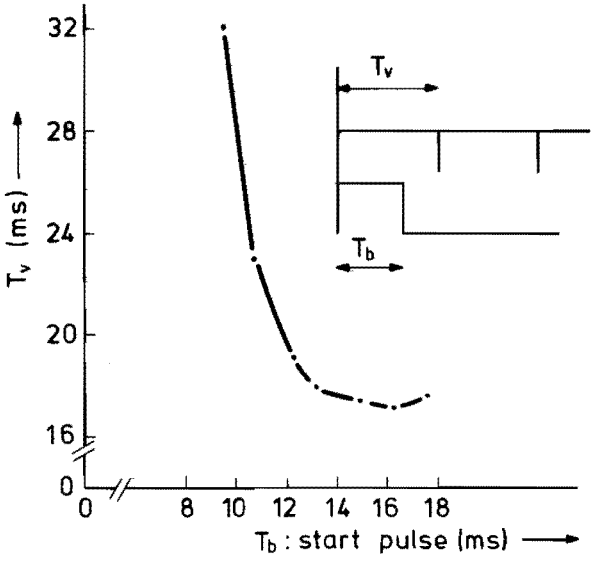

Fig. 6.3.1. Influence of the length of the start pulse.

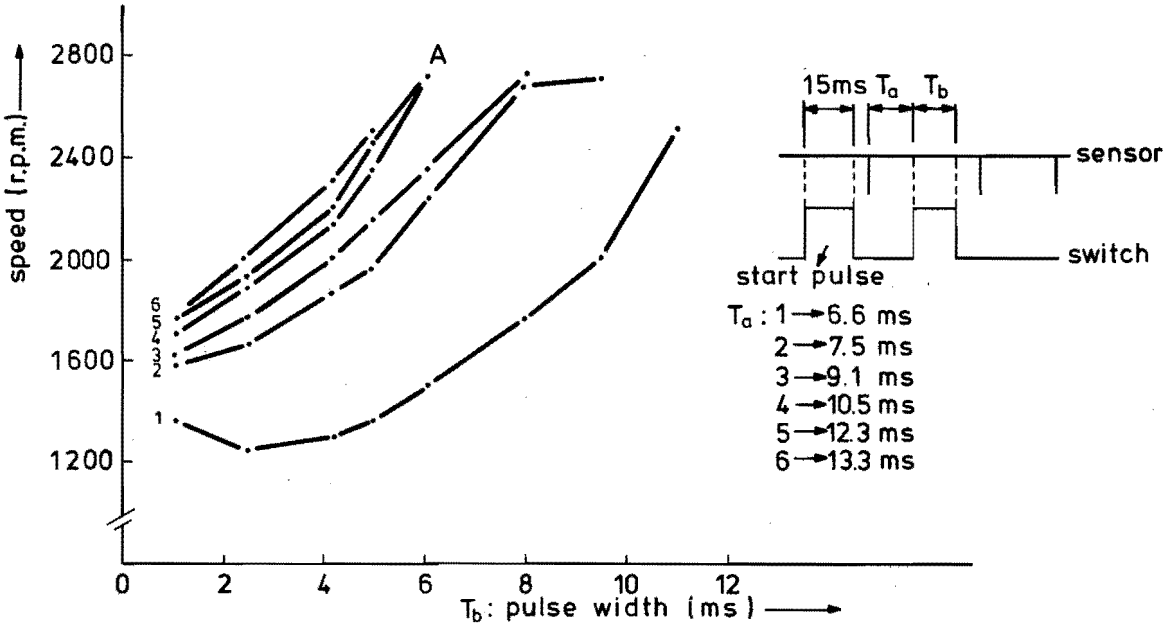

Fig. 6.3.2. Influence of the triggering moment and the length of the second pulse.

A numerical description of the system might be used to determine the optimum length of the start pulse. Calculations have shown a high sensitivity to the rotor position at standstill (see Appendix). A prediction of the rotor position at standstill is possible by means of the determination of the torque-versus-angular-position curve caused by the field of the magnets. The position at which the torque becomes negative has to be considered as the position at standstill. A measurement error of some degrees, however, will give a less appropriate length. For this reason we advise practical experiments directed to the determination of the optimum pulse length. In the following we give a procedure which we consider most applicable.
We tested the proposed procedure on an experimental motor without load, a supply voltage of 120 V and with the current overload protection adjusted to 3.2 A. Fig. 6.3.1 gives the relation between the length of the start pulse T_b and the time T_v between the beginning of the start pulse and the moment when the rotor attains the in-line position.
A higher value for T_b than 17.7 ms leads to the situation where the switch is still closed when the in-line position has been passed. In that case the torque reverses and the rotor speed decreases. To prevent this unwanted situation we have implemented a procedure in the control program that immediately cuts the pulse when the rotor attains the in-line position (see chapter 3). For this reason we stopped the measurements after $T_b = 17.7$ ms. A length of 15 ms gives a value for T_v near the minimum and we will use this length for further experiments.

The load torque in certain applications is not fixed, for example when the motor is used in a mixer. However the procedure mentioned above gave an optimum start pulse only for one load.
The earlier-mentioned procedure in the control program offers a solution for this problem. Let us suppose that we have followed the procedure to determine the optimum start pulse in combination with the highest expected load, and that a minimum for T_v is found at $T_b = 25$ ms. The rotor will attain the in-line position within the time of 25 ms when the load is small. The procedure mentioned above cuts the start pulse if the switch is still closed when the in-line position is reached. Thus the length of the start pulse is automatically adapted to the load.
However the control program described in chapter 3 has to be changed to allow the use of this mechanism.

For the second pulse we distinguish the triggering moment and the pulse width. The optimum values depend on the angular velocity which the rotor has reached. So the following experiment has to be carried out after settling the start pulse, which we gave a value of 15 ms.
Fig. 6.3.2 shows the speed of the motor after the second pulse as a function of the triggering moment and the length of the second pulse. The maximum value of the pulse width is limited by the coincidence of the ending of the second pulse and the reception of the sensor signal. If we require the highest acceleration we prefer the combination of T_a and T_b given by point A.

We conclude that simple experiments give the optimum values for the length of the first two pulses and the moment of triggering the second one for a well-known load. Experiments are in progress to find an appropriate procedure for the first pulses fitted for applications in which there is no well-defined load torque.

6.4. Higher ratings with the prototype.

In chapter 3 we gave figures representing the characteristics of the experimental motor (fig. 6.1.2) at a supply voltage of 120 V and a speed of 15 000 r.p.m. Figs. 2.3.3 and 2.3.4 show an efficiency of 80 % . . . 81 % at a mean torque of 0.025 Nm ($\alpha = 0.4$ rad, $\beta = 0.85$ rad). In this case the mechanical output power is near 40 W. In the same figures an efficiency of 78 % is found at 0.05 Nm, corresponding to 80 W ($\alpha = 0.8$ rad, $\beta = 0.8$ rad).
The temperature of the coils in the latter circumstances was appproximately 63° C at an ambient temperature of 30° C. Considering the temperature rise higher losses can be accepted, because the insulation is capable of withstanding higher temperatures. This fact allows experiments to see if higher ratings are possible.

To obtain an increased output power one could alter the control variables α and β in such a manner that the current carried by the coils becomes continuous as discussed at the end of section 2.2. However a considerable decrease of the efficiency has to be accepted in that case.
A better way is to increase the supply voltage. The circuit given in fig. 5.1.9 is designed for a supply voltage up to 310 V (behind the rectifier). We used this supply voltage and altered the values of the control variables α and β in our test rig (see chapter 4) to determine the ratings.

The current is limited to a value of 4.2 A to prevent an excessive temperature rise in the coil insulation. We measured a final temperature of more than 120°C at this latter current value under steady-state conditions. We found the ratings given in tables 6.4.1 and 6.4.2 by altering the control variables α and β. The power delivered by the 5 V and 15 V supply and the losses in the rectifier (see fig. 5.1.9) were not taken into account for determining the efficiency with the test rig.
Our experimental motor was not provided with forced cooling. We expect that the addition of forced cooling, allowing higher losses in the motor, would lead to a higher obtainable output power.

We conclude that a mechanical output power of more than 200 W is possible. It is the temperature rise of the coil insulation that limits the allowable losses and, related to these losses, the mechanical output power.

Speed (r.p.m.)	10 000	15 000	20 000
Torque (Nm)	0.176	0.162	0.110
Efficiency (%)	70	78	82
Output power (W)	184	255	230
Temperature of the coil-ends (°C)	105	110	80

Table 6.4.1. Measured maximum torque values, ambient temperature 35°C.

Speed (r.p.m.)	10 000	15 000	20 000
Torque (Nm)	0.122	0.131	0.077
Efficiency (%)	77.5	86	85
Output power (W)	128	206	161
Temperature of the coil-ends (°C)	74	76	54

Table 6.4.2. Measured maximum efficiency values, ambient temperature 35°C.

7. Conclusions

This study deals with the single-phase, electronically controlled reluctance motor. The single-phase reluctance motor may be considered as one of the simplest motors, because there are no windings of any type on the rotor, which consists only of iron laminations. This simple and robust rotor gives the motor a high speed capability.
Furthermore there is no need to provide for a current reversal during one revolution of the rotor. This characteristic allows the use of only one electronic switch to control the motor, which considerably reduces the costs of the electronic power circuitry.
In spite of its attractive points this single-phase motor has two major drawbacks. Its torque production is strongly pulsating, which makes it unsuitable for applications requiring a constant torque or speed, as for example in audio or video equipment.
Another drawback is the starting problem. It depends on the position of the rotor at standstill whether the motor will start rotating in the required direction or in the opposite direction. It is even possible that no rotation will occur. Provisions have to be made to prevent this unwanted behaviour.

The starting problem is solved by mounting two permanent magnets in the stator bore, which give the rotor a favourable starting position, and by an electronic control system featuring an appropriate start procedure.
The torque production and the efficiency of the motor are mainly determined by the rotor position reached at the moment the switch is closed and the position when the switch is opened. For every rotor speed and applied torque a combination of the switch-on and switch-off position can be found which gives an optimum efficiency.
The electronic switch is controlled by means of a microprocessor, which obtains the information required for the switching action by being supplied with the signal from a rotor position sensor.
The costs of the sensor are reduced by an adaptation of the control program to a sensor which gives only two pulses per revolution.
Within a wide range one or more torque versus speed relations can be selected by programming the processor in an appropriate manner.

Experiments with our prototype proved that a mechanical output power of 200 W can be obtained at 15 000 r.p.m. The efficiency under these circumstances was 78 %.

Considering applications of the single-phase reluctance motor in domestic appliances we have to compare our motor with the A.C. series motor. The stators of both motors are fairly equivalent. However, the rotor of the series motor is more complicated. Additional to the stack of laminated iron, as found in the reluctance motor, the series motor contains a commutator, brushes and a number

of coils. The consequences of the additions are higher production costs and a lower high-speed capability than we have found for the reluctance motor.
On the other hand the reluctance motor requires an electronic control system, the most important parts of which are the microprocessor, the position sensor and power electronic circuitry. The costs of the electronic control are mainly determined by the power electronic circuitry. The use of a microprocessor makes it possible to select one or more torque versus speed relations for the motor.

The solution of the starting problem with permanent magnets is suitable for applications with a low friction and load at standstill. Further research is needed to find a suitable solution for applications with a high friction and load at standstill, as well as to optimize the single-phase reluctance motor for specific applications.

References

[1] **Lawrenson, P.J. and J.M. Stephenson, P.T. Blenkinsop, J. Corda, N.N. Fulton**
Variable-speed switched reluctance motors.
IEE Proc. B, Vol. 127(1980), p. 253-265.

[2] **Davis, R.M. and W.F. Ray, R.J. Blake**
Inverter drive for switched reluctance motor: Circuits and component ratings.
IEE Proc. B, Vol. 128(1981), p. 126-136.

[3] **Unnewehr, L.E.**
Series-commutated SCR controllers for variable-speed reluctance motor drives.
In: PESC-73 Record: IEEE Power Electronics Specialists Conf., Pasadena, Calif., 11-13 June 1973.
New York: IEEE, 1973. P. 180-191.

[4] **Dahlquist, G. and A. Björck**
Numerical methods.
Englewood Cliffs, N.J.: Prentice-Hall, 1974.
Prentice-Hall series in automatic computation.

[5] **Woodson, H.H. and J.R. Melcher**
Electromechanical dynamics. Part 1: Discrete systems.
New York: Wiley, 1968.

[6] Mathematische Hilfsmittel des Ingenieurs. Teil 3.
Herausgegeben von **R. Sauer und I. Szabó.**
Berlin: Springer, 1968. P. 265-277.

[7] MCS-48 family of single chip microcomputers. User's manual.
Santa Clara, Calif.: Intel Corporation, 1978.

[8] **Marshall, J.E.**
Control of time-delay systems.
Stevenage: Peter Peregrinus, 1979.
IEE control engineering series, Vol. 10.

[9] Personality module PM 4321: User's manual.
Eindhoven (Netherlands): Philips (S&I).
Order No. 9499 620 01311. P. 5-13.

[10] **Dijken, R.H.**
Optimization of small AC series commutator motors.
Ph.D. Thesis. Eindhoven University of Technology, 1970.

[11] **Roters, H.C.**
Electromagnetic devices.
New York: Wiley, 1955.

[12] **Vogt, K. et al.**
Elektrische Maschinen: Berechnung rotierender elektrischer Maschinen.
Herausgegeben von **G. Müller.**
Berlin: VEB Verlag Technik, 1972. P. 275.

[13] **Beer, A. de and S.J. Polak, A.J.H. Wachters, J.S. van Wely**
MAGGY2 user manual.
Eindhoven (Netherlands): Philips (ISA), 1977.

[14] **Corda, J. and J.M. Stephenson**
An analytical estimation of the minimum and maximum inductance of a double-salient motor.
In: Proc. 3rd Int. Conf. on Stepping Motors and Systems, Leeds, 19-20 Sept. 1979. Ed. by **A. Hughes.**
Leeds: Department of Electrical and Electronic Engineering, University of Leeds, 1979. P. 50-59.

[15] **Beer, A. de and S.J. Polak, A.J.H. Wachters, J.S. van Wely**
PADDY user manual.
Eindhoven (Netherlands): Philips (ISA), 1981.
Order No. 4322 270 07371.

[16] **Harris, M.R. and A. Hughes, P.J. Lawrenson**
Static torque production in saturated doubly-salient machines.
IEE Proc., Vol. 122(1975), p. 1121-1127.

List of symbols

a	variable, referring to an open switch ($a=1$) or to a closed switch ($a=-1$)
b_c	width of the slots (m)
b_t	width of the stator pole (m)
g	ratio L_2/L_0
h_c	height of the coils (m)
h_s	height of the slots (m)
i_1	current carried by the main coil (A)
i_2	current carried by the catch coil (A)
i_{20}	current carried by the catch coil just before the switch is closed (A)
i_b	base current (A)
j_1	normalized current carried by the main coil
j_2	normalized current carried by the catch coil
l	length of rotor and stator (m)
r_1	normalized resistance of the main coil
r_2	normalized resistance of the catch coil
t_{on}	moment at which the switch is closed (s)
t_{off}	moment at which the switch is opened (s)
t	moment of time (s)
A_{cu}	copper cross-section of the main and catch coils together (m^2)
$A_{cu,c}$	copper cross-section of the catch coil (m^2)
$A_{cu,m}$	copper cross-section of the main coil (m^2)
B	flux density (Wb/m^2)

H	magnetic field strength (A/m)
I_i	current at t_i (A)
I_{20}	current carried by the catch coil just before the switch is closed (A)
I_c	effective current carried by the catch coil (A)
I_m	effective current carried by the main coil (A)
I_{sugg}	extrapolated value of the current (A)
$\Delta I_i\ t_i$	change of the current within a time interval starting with t_i (A)
L	coefficient of self-inductance of the motor coils (H)
L_0, L_2	coefficients related to L (H)
L_i'	$dL/d\theta$ at time t_i (H/rad)
L_i''	change of the $dL/d\theta$, defined by eq. 2.2.13 (H/rad)
N	number of turns of a coil
$P_{...}$	permeance (Wb/A)
P	power (W)
R_1	resistance of the main coil (Ω)
R_2	resistance of the catch coil (Ω)
R_a	represents R_1 and R_2, depending on the value of a (Ω)
R_s	radius of the stator bore (m)
T	torque (N m)
$\overline{T}$	average value of the torque (N m)
ΔT	small time interval (s)
T_a	time elapsed between the reception of an interrupt and the triggering of the preceding pulse (s)

T_b	pulse width (s)
T_c	time interval taken up by calculations (s)
T_i	time interval between two interrupts (s)
T_f	coulomb friction torque (N m)
T_v	time interval (s)
T_w	time interval in which the processor waits for an interrupt (s)
U	supply voltage (V)
U_d	voltage drop over the diode (V)
W	amount of energy (N m s)
α	angle related to the rotor position when the switch is closed (rad)
α	the ratio between the cross-sections of the main and catch coils in section 6.2
β	angle related to the rotor position when the switch is opened (rad)
ε	relative error in the energy balance, see eq. 2.2.31
ε	discrepancy between two values of the current, see eq. 2.3.28 (A)
γ	coefficient related to the linkage of the main and catch coils
η	efficiency
θ	rotor position (rad)
θ_0	start position of the rotor (rad)
θ_z	rotor position where i_2 becomes zero (rad)
μ_0	constant (H/m)
σ_1,σ_2	variable
τ_1,τ_2	variable

ω	angular velocity (rad/s)
Δ	infinitesimally small angle (rad)
Φ	flux linked with the coils of the motor (Wb)
Φ_0, Φ_2	coefficients related to Φ (Wb)
Φ_m	part of the flux (Wb)
Φ_σ	leakage flux (Wb)

Appendix

In section 6.3 we discussed the optimum length of the first pulse given by the control circuitry at the start. To determine the optimum length we have chosen a number of measurements with the experimental motor, because the length depends to a great extent on the starting position of the rotor. This appendix gives the results of a simplified numerical description of the start to show the influence of the starting position.

For the simplified model of the start we introduce a number of assumptions. We suppose that the current carried by main the coils arrives immediately after the electronic switch is closed at the value given by the current overload protection and it keeps this value until the rotor attains the in-line position. The current is assumed to be zero in the main and catch coils when this position is passed.
In practice a rise time of approximately 1 ms is found at a supply voltage of 120 V and a current overload protection adjusted to 3.2 A. The fall time found under the same circumstances was approximately 2 ms. We neglect these times, because they are small in comparison with the optimum length of approximately 15 ms which is found in section 6.3.

We use for the torque production of the motor with magnets (given in fig. 6.2.5, case B) the measured torque-versus-angular-position curve at a current of 3.2 A (see fig. A.1).
Only a coulomb friction (T_f) is assumed and the inertia of the rotor J has the value $1.48\ 10^{-5}$ kg.m^2.
To determine the angular position as a function of time we have to solve the following equation:

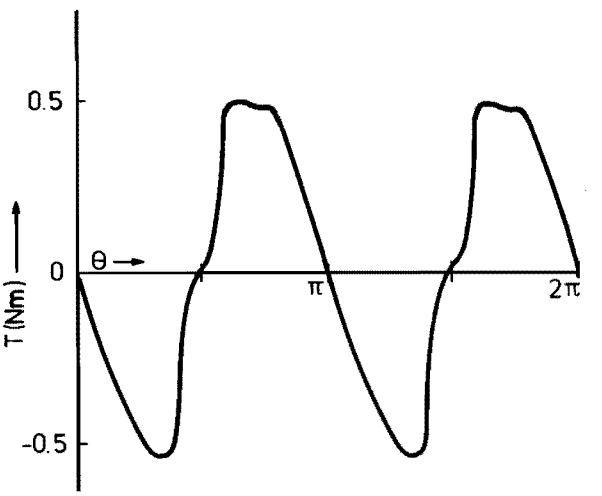

Fig. A.1 Torque production at 3.2 A.

$$T = J\frac{d^2\theta}{dt^2} + T_f \operatorname{sign}\left(\frac{d\theta}{dt}\right). \qquad \text{A.1}$$

We solved this equation by numerical means and fig. A.2 gives the time interval between the closing of the switch and the moment the rotor attains the in-line position as a function of the starting position of the rotor (θ_0). Furthermore this figure gives the speed at the in-line position. Case A deals with a situation without coulomb friction; in case B we introduced a friction of 0.02 Nm.
For both cases a minimum value of the elapsed time is found near 160°, but this is not an interesting minimum because the final speed at 180° is low compared with the obtainable speed at a start position in the range 90° . . . 110°.
The consequence of the introduced coulomb friction, however, is no acceleration if $90° < \theta < 92°$, because the generated torque is less than the coulomb friction of 0.02 Nm. One should use a starting position at which the generated torque is higher than the friction torque when coulomb friction occurs.
Fig. A.2 shows that the time between the ignition of the pulse and the arrival at the in-line position (and consequently the optimum length of the start pulse) depends to a great extent on the starting position when is this position is less than 100°. A small discrepancy between the assumed and the true starting position leads to a considerably different value for the optimum length of the first pulse. The high sensitivity of the optimum length to the starting position is caused by the low value of the torque production near $\theta = 90°$.

With a view to the speed at the in-line position we conclude that a favourable starting position is given by:

$$100° < \theta_0 < 110°. \qquad \text{A.2}$$

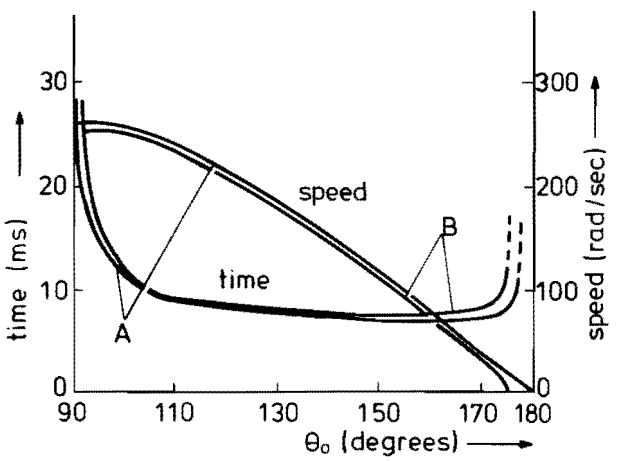

Fig. A.2

Summary

Compared with the A.C. series motor the single-phase reluctance motor is characterized by the simplicity of its construction. The rotor of the reluctance motor consists only of a stack of iron laminations, whereas the rotor of the series motor consists of a stack of laminated iron, a number of coils and a commutator. Furthermore there is no need to provide for a current reversal during one revolution of the rotor. This characteristic allows the use of only one electronic power switch. In view of these attractive aspects this study was started to investigate whether the single-phase reluctance motor could be considered as a potential replacement of the A.C. series motor.
The reluctance motor does, however, have some drawbacks. Special attention has to be paid to the conditions leading to a good start, which implies that the rotor must start rotating in the required direction with a high acceleration from the very first moment of the start. Furthermore the single-phase reluctance motor has a strongly pulsating torque production and for this reason it is less suited for applications that require a constant torque or speed as for example in video and audio equipment.

It is shown that the motor can be described by means of analytical equations when a large number of assumptions are accepted. Due to the complexity of the solution of the analytical equations a computer has to be used to obtain a numerical result. A more realistic description of the motor is obtained when the analytical equations are replaced by a set of difference equations, which can be solved easily by a computer. The aim of the model is to predict the torque production and efficiency of the motor. The results of calculations and measurements show a fair agreement as far as the torque is concerned. A considerable discrepancy, however, exists between the measured and calculated efficiency, and we ascribe this fact to hysteresis and eddy current losses, which are difficult to describe by analytical or numerical methods.

The mean value of the torque and the efficiency of the motor depend critically on the angular position of the rotor at the moments the switch is opened and closed. For every applied torque and rotor speed a combination of the switch-on and switch-off position can be found which gives an optimum efficiency.

This study shows that a microprocessor is very well suited to act as motor controller. With an adequate program the optimum switch-on and switch-off positions in relation to the speed can be selected. Furthermore the torque-versus-speed relation of the motor can be altered by modifications of the program.
The motor controller requires information about the rotor position, and this is provided by a simple sensor which gives two pulses per revolution of the rotor. We chose this simple sensor for reasons of economy and adapted the program accordingly.

The combination of a suitable program and two permanent magnets in the stator bore was chosen to solve the starting problem. This combination is well suited for applications with a low friction and load torque at the start. Further research is required to solve the starting problem in the case of a high friction or high load torque.

Measurements on the prototype (which was not optimized) yielded a mechanical output power of approximately 200 W with an efficiency of 78 % at a speed of 15 000 r.p.m.
A number of aspects related to the optimization are discussed, but we consider the optimization as a separate study in itself, due to the close relation between the optimum design and the application.

Summarizing we conclude that the single-phase reluctance motor in combination with the proposed control circuitry using a microprocessor should be considered as a potential replacement of the A.C. series motor. Attractive aspects of this motor are the simplicity of the motor and the required power electronics and further the selectable torque-versus-speed relation, achieved by the use of a microprocessor. However certain applications require careful attention to the starting problem of this motor.

Samenvatting

Ten opzichte van de wisselstroom-serie-motor wordt de eenfase-reluctantie-motor gekenmerkt door zijn grote eenvoud. De rotor van de reluctantie-motor bestaat slechts uit een blikpakket, terwijl bij de serie-motor de rotor bestaat uit een blikpakket, een aantal spoelen en een commutator.
Verder is de reluctantie-motor niet gevoelig voor de richting van de stroom in de spoelen, zodat het niet noodzakelijk is de stroomrichting binnen een omwenteling van de rotor om te keren. Door deze eigenschap is het mogelijk in de motorsturing slechts een elektronische vermogensschakelaar te gebruiken.

Met het oog op deze aantrekkelijk aspecten werd deze studie gestart om te onderzoeken of de eenfase-reluctantie-motor kon worden beschouwd als een mogelijke vervanger van de wisselstroom-serie-motor.
Naast de voordelen van de onderzochte motor dienen de bijzondere eisen genoemd te worden, waaraan voldaan moet zijn voor een goede start van de motor, waarbij een goede start inhoudt, dat de motor vanuit stilstand direct en met een hoge versnelling in de gewenste richting draait. Verder is het koppel van de eenfase-reluctantie-motor sterk pulserend, waardoor deze motor minder geschikt is voor toepassingen, die een constant koppel of toerental verlangen (bijvoorbeeld audio- of video-apparatuur).

De beschrijving van de motor met behulp van een analytische model blijkt mogelijk, indien een groot aantal vereenvoudigende veronderstellingen wordt gedaan. De complexiteit van de langs analytische weg gevonden oplossing dwingt ons echter om een rekenmachine te gebruiken om tot numerieke resultaten te komen.
Een realistischer model van de motor kan verkregen worden door het analytisch model te verlaten en te vervangen door een model, dat beschreven wordt door een aantal differentie vergelijkingen, waarvan de oplossing op eenvoudige wijze bepaald kan worden met een rekenmachine.
Het doel van het model is het koppel en rendement van een reluctantie-motor te kunnen voorspellen. Een vergelijking van de resultaten van metingen en berekeningen laat zien, dat het koppel goed berekend wordt met het numerieke model. Een aanzienlijk verschil blijkt echter te bestaan tussen het berekende en het gemeten rendement en wij schrijven dit toe aan wervelstroom- en hysteresisverliezen, die zich door hun complexe aard moeilijk lenen voor een numerieke of analytische beschrijving.

Het gemiddelde koppel en het rendement van de motor blijken sterk afhankelijk te zijn van de positie van de rotor op de moment, dat de elektronische schakelaar geopend of gesloten wordt. Voor ieder toegepast koppel is bij een zekere snelheid een combinatie van ontsteekhoek en doofhoek te vinden, die een optimaal rendement geeft.

Het onderzoek laat zien, dat een microprocessor zeer geschikt is om als centraal orgaan te dienen in de besturing van de motor. Met de juiste programmatuur kan de bovengenoemde afhankelijkheid van de motorsnelheid gerealiseerd worden. Door het wijzigen van de programmatuur is de koppel-toeren-kromme van de motor over een groot gebied beinvloedbaar. Het programma, beschreven in dit proefschrift, staat het gebruik toe van een eenvoudige en goedkope sensor, die slechts twee pulsen per omwenteling van de rotor geeft.

De gekozen oplossing om een goede start te bereiken, bestaat uit een combinatie van geschikte programmatuur en het plaatsen van twee magneten in de statorboring. Deze oplossing blijkt te voldoen voor toepassingen, waarin een lage waarde van het wrijvings- en belastingskoppel wordt gevonden bij de aanloop. Verder onderzoek is nodig om een oplossing te vinden voor het aanloopprobleem, indien de motor wordt gebruikt in een toepassing, waar een hoge waarde van het wrijvings- en/of belastingskoppel bij de aanloop optreedt.

Metingen aan het prototype laten zien dat een mechanisch vermogen van ongeveer 200 Watt bereikbaar is bij een rendement van 78 % en 15000 toeren per minuut. Wij merken op, dat het prototype niet geoptimaliseerd is. Een aantal aspecten, samenhangend met een optimalisatie, wordt besproken, maar gezien de nauwe samenhang tussen het optimale ontwerp en de toepassing, beschouwen wij een optimalisatie als deel van een nieuw onderzoek.

Samenvattend mogen wij stellen, dat de eenfase-reluctantie-motor met de voorgestelde besturing door een microprocessor beschouwd mag worden als een mogelijke opvolger van de wisselstroom-serie-motor. Sterke punten zijn de eenvoud van de motor en benodigde vermogenselektronica en verder de mogelijkheid de koppel-toeren-kromme van de motor te veranderen door het programma van de microprocessor aan te passen. Echter het gedrag van de reluctantie-motor tijdens het aanlopen wordt sterk bepaald door de aard van de belasting. Hieraan dient derhalve veel aandacht besteed te worden.

STELLINGEN

bij het proefschrift van J. C. Compter

4 mei 1984, Technische Hogeschool, Eindhoven

I

S.A. Nasar beoordeelt een geïdealiseerde reluctantie motor aan de hand van de verhouding tussen het mechanisch vermogen en het gewicht van de motor. Zijn stelling, dat deze verhouding niet veel toeneemt door het verhogen van de verhouding tussen de maximale en minimale zelfinductie, heeft geen algemene geldigheid.

Nasar, S. A.
The goodness of a reluctance machine.
Proc. IEE, Vol. 118 (1971), p. 796.

II

Voor het bepalen van het dynamische gedrag van kleine elektrische motoren kan met succes de techniek, die bekend staat als Laser-Doppler anemometrie, toegepast worden in die gevallen, waarin meer conventionele meettechnieken falen.

Welling, W. A.
De Laser-Doppler-methode voor het meten van snelheden.
PT/Werktuigbouw, 37 (1982), No. 12, p. 72-75.

III

Bij het ontwikkelen en testen van programmatuur, die bestemd is voor een motorregeling met een microprocessor, is het verstandig om een simulator te gebruiken voor de motor en zijn sturing.

IV

De nadruk, die gelegd wordt op het opgenomen vermogen van apparatuur, die bestemd is voor huishoudelijk gebruik, snijdt de weg af naar alternatieve oplossingen (bijv. een beter stofafscheidings-systeem in stofzuigers).

V

Elektrotechnische meetapparatuur (bijv. de oscilloscoop en de universeel meter) kan in vele gevallen vervangen worden door een microcomputer met adequate programmatuur en hardware. Het is derhalve verstandig de microcomputer als meetinstrument op te nemen in het praktische deel van de ingenieurs-opleiding.

VI

Vriendelijkheid is kostbaar als dit betrekking heeft op programmatuur voor computers en microprocessoren. Omdat niet-deskundige gebruikers met deze programmatuur gaan werken, dient men toch aan de vriendelijkheid de hoogste prioriteit te geven.

VII

De indeling van het QWERTY-toetsenbord is voor computergebruik voor verbetering vatbaar.

VIII

Het gebruik van personal computers voor technisch en wetenschappelijk rekenen dient afgewezen te worden, tenzij deze gekoppeld kunnen worden met een netwerk.

IX

Het zal van grote betekenis zijn voor aankomende computergebruikers, als er een onafhankelijke nederlandse organisatie komt, die de programma's van de vele software-leveranciers test en kwalificeert.

Dowdney, D. L.
Software testing: Evaluation by independent groups gives buyers an unbaised software standard.
Small Bus. Comput., Vol. 8 (1984), No. 1, p. 48-49.

X

Door het presenteren van hun telefoonnummers laten de omroepverenigingen zien dat men toch kan spreken over een verschil in identiteit.

4 mei 1984 J. C. Compter